LEVEL

6

Department of Earth and Planetary Sciences
Massachusetts Institute of Technology
Cambridge, Massachusetts 02139

RESEARCH IN SEISMOLOGY

Semi-Annual Technical Report No. 7

Period Covered: 1 July 1978 - 31 December 1978

ARPA Order No. 1827
Program Code No. 5F10
Name of Contractor - M.I.T.
Effective Date of Contract - 1 June 1975
Contract Expiration Date - 30 September 1979
Amount of Contract - $615,000
Contract No. - F44620-75-C-0064

Principal Investigators - M. Nafi Toksöz, 617/253-6382
Keiiti Aki, 617/253-6397
Sean C. Solomon, 617/253-3786
Program Manager - William J. Best, 202/694-5454

Short Title of Work - Research in Seismology

Sponsored by
Advanced Research Projects Agency
ARPA Order No. 1827

1. SUMMARY

The research completed under the contract F44620-75-C-0064 "Research in Seismology" during the period 1 July 1978 - 31 December 1978 falls within the two broad topics of (1) Seismic source mechanisms and (2) Seismic wave propagation. The specific research tasks within each category have broad applicability to the problem of discrimination of earthquakes from underground nuclear explosions, with particular emphasis on the Asian continent.

A major work on both source mechanisms and surface wave propagation was Patton's (1978) thesis research on the simultaneous determination of source moment tensor and propagation characteristics (phase velocity, Q) from a collection of sources in a small region observed by a set of common stations. Taylor and Toksöz (1978) applied the three-dimensional inversion technique of Aki and others to P wave data from the New England seismic network, demonstrating that the distinct velocity structure of major geologic units in an ancient continental collision zone extends to depths of 200 km. Johnston (1978) and Johnston and Toksöz (1979a,b) present laboratory data on attenuation in rocks at ultrasonic frequencies to investigate several possible loss mechanisms for the crust, including crack friction and fluid saturation.

Details of these studies are given in the preprints and abstracts in the following sections. A cumulative list of publications completed under the contract is also included.

Tifteon 1473
is right per Mr. Blore
at AFOSR
767-4912

DISCLAIMER NOTICE

THIS DOCUMENT IS BEST QUALITY PRACTICABLE. THE COPY FURNISHED TO DDC CONTAINED A SIGNIFICANT NUMBER OF PAGES WHICH DO NOT REPRODUCE LEGIBLY.

SECURITY CLASSIFICATION OF THIS PAGE (When Data Entered)

REPORT DOCUMENTATION PAGE	READ INSTRUCTIONS BEFORE COMPLETING FORM
1. REPORT NUMBER: AFOSR-TR-79-0687	2. GOVT ACCESSION NO. / 3. RECIPIENT'S CATALOG NUMBER
4. TITLE (and Subtitle): SOURCE AND PROPAGATION EFFECTS OF RAYLEIGH WAVES FROM CENTRAL ASIAN EARTHQUAKES .	5. TYPE OF REPORT & PERIOD COVERED: Interim
	6. PERFORMING ORG. REPORT NUMBER
7. AUTHOR(s): Howard Patton	8. CONTRACT OR GRANT NUMBER(s): F44620-75-C-0064, ARPA Order-1827
9. PERFORMING ORGANIZATION NAME AND ADDRESS: Department of Earth and Planetary Sciences, Massachusetts Institute of Technology, Cambridge, MA 02139	10. PROGRAM ELEMENT, PROJECT, TASK AREA & WORK UNIT NUMBERS: A.01827 5F10 61101E
11. CONTROLLING OFFICE NAME AND ADDRESS: ARPA, 1400 Wilson Boulevard, Arlington, VA 22209 (12) 193p.	12. REPORT DATE: (11) Apr 1979 13. NUMBER OF PAGES: 187
14. MONITORING AGENCY NAME & ADDRESS (if different from Controlling Office): AFOSR/NP, Bolling AFB/Bldg.#410, Wash DC 20332	15. SECURITY CLASS. (of this report): unclassified 15a. DECLASSIFICATION/DOWNGRADING SCHEDULE

16. DISTRIBUTION STATEMENT (of this Report)

Approved for public release;
distribution unlimited.

17. DISTRIBUTION STATEMENT (of the abstract entered in Block 20, if different from Report)

(9) Semi-annual technical rept. no. 7,
1 Jul - 31 Dec 78,

18. SUPPLEMENTARY NOTES

19. KEY WORDS (Continue on reverse side if necessary and identify by block number)

20. ABSTRACT (Continue on reverse side if necessary and identify by block number)

A reference point equalization method has been developed which enables the separation of source and propagation effects of surface waves. The method works on seismic events located in a small source region, which allows us to assume that all events share the same path effects to a given receiver. Two important steps in the method are initialization and iteration. Initialization obtains the first "reference events" in order to compute initial estimates of phase velocity and attenuation coefficient. Iteration simultaneously refines the propagation parameters and determines the source parameters of new earthquakes

DD FORM 1 JAN 73 1473 EDITION OF 1 NOV 65 IS OBSOLETE

UNCLASSIFIED

SECURITY CLASSIFICATION OF THIS PAGE (When Data Entered)

407 784

in the vicinity of the reference point. This method was applied to earthquakes in the Pamir mountains, Central Asia (reference point:39.58N, 73.55E). In the initialization step, the method of Weidner and Aki (1973) was applied to obtain focal depths and revise fault plane parameters of the first two earthquakes. The residuals obtained from fitting the observed amplitude ratios and phase differences indicate that the crust and upper mantle in Central Asia is more laterally heterogeneous than near the ocean rifts, the site of Weidner and Aki's experiment. We computed heterogenity quotients of .46 vs .80 x 10(-4Napier(2)/km and .93 vs 2.4 x 10(-4)radian(2)/km for ocean versus continent as a measure of the increasing scatter in amplitude and phase of 20-60sec Rayleigh waves due to lateral heterogeneities.

2. SEISMIC SOURCE MECHANISMS

SOURCE AND PROPAGATION EFFECTS OF RAYLEIGH WAVES FROM CENTRAL ASIAN EARTHQUAKES

BY HOWARD PATTON

Submitted to
the Department of Earth and Planetary Sciences
on April 28, 1978
in partial fulfillment of the requirements for the
degree of Doctor of Philosophy

ABSTRACT

A reference point equalization method has been developed which enables the separation of source and propagation effects of surface waves. The method works on seismic events located in a small source region, which allows us to assume that all events share the same path effects to a given receiver. Two important steps in the method are initialization and iteration. Initialization obtains the first "reference events" in order to compute initial estimates of phase velocity and attenuation coefficient. Iteration simultaneously refines the propagation parameters and determines the source parameters of new earthquakes in the vicinity of the reference point. This method was applied to earthquakes in the Pamir mountains, Central Asia (reference point: 39.58N, 73.55E).

In the initialization step, the method of Weidner and Aki (1973) was applied to obtain focal depths and revise fault plane parameters of the first two earthquakes. The residuals obtained from fitting the observed amplitude ratios and phase differences indicate that the crust and upper mantle in Central Asia is more laterally heterogeneous than near the ocean rifts, the site of Weidner and Aki's experiment. We computed heterogenity quotients of .46 vs .80 x 10^{-4}Napier^2/km and .93 vs 2.4 x 10^{-4}radian^2/km for ocean versus continent as a measure of the increasing scatter in amplitude and phase of 20-60sec Rayleigh waves due to lateral heterogeneities.

To determine source parameters in the iteration, we applied the linear moment tensor inversion on Rayleigh wave complex source spectra. The presence of random additive errors in the

complex spectra does not pose difficulties for recovering reliable source parameters using the linear inversion method. However, amplitude magnification errors in the complex spectra will lead to over-estimation of the moment tensor elements and phase incoherency will lead to under-estimation. In applying this method to our dataset, it was necessary to modify the straight least squares inversion method because of its sensitivity to even a few bad data points.

The residuals obtained from the repeated application of the moment tensor inversion over trial focal depth showed two minima: one minima at depths less than 20km and the other at depths greater than 70km. The values of the residuals at these minima were close enough to cast doubt on the determination of focal depth. One way to resolve this ambiguity is to compare the geometry of the moment tensor obtained for shallow and deep focus inversions with observed P-wave polarities.

The focal depths of eight out of the nine events in our dataset were found to be shallow, between 5-15km. Their principal compressive stress axes are aligned north-south and nearly horizontal, consistent with the interpretation of plate tectonics in Central Asia. The moment tensor inversion generally gives three-couple force systems having significant non-zero intermediate component. However, in light of errors in our data and the similarities of the double couple models to the three-couple models, it can not be established convincingly that these results are caused by departures of source from the double couple model.

We interpret the propagation parameters in terms of lateral variation of phase velocity and Q on the Eurasian continent. A phase velocity regionalization is proposed involving five continental provinces: Indian Shield, Northern Platforms, Coastal Plains, Tectonic and Plateau. Phase velocities on the Indian Shield are 20% higher than velocities on the Plateau province at 26sec period and 5% higher at 90sec period. Stable provinces in Eurasia are found to have significantly higher phase velocity than tectonic provinces out to 150sec period.

Interpretations of the phase velocities on the Indian Shield show a lithosphere thickness of about 120km, considerably thicker than the lithosphere under the Northern Platforms ($\sim$75km). The lowest shear velocity in the upper mantle is found under the Tectonic province with a value about 4.3km/sec over depths between 83-240km. The crustal thickness of the Plateau province is as great as 70km provided that shear velocity in the lower half of the crust is about 3.8km/sec. The upper mantle structure under this province is very similar to James' (1971) for the Andes mountains region.

Surface wave amplitudes on the Eurasian continent are strongly affected by horizontal refraction as well as intrinsic Q of the medium. Average Rayleigh wave Q has very different character on paths over northern platforms and tectonic provinces east and west of the reference point. Under platforms Q is found to increase with depth from a Q between 200-300 in the crust to

300-500 in the lid and asthenosphere. West of the reference point Q is low (∿60) in the bottom 20km of the crust and extending ∿35km into the mantle. East of the reference point Q appears to be ∿60 in a layer 35km thick at the base of the crust. Deeper in the mantle Q increases suggesting that the low Q zone is concentrated at shallow depths in the upper mantle under the tectonic provinces of Asia.

Thesis Supervisor: Keiiti Aki
Title: Professor of Geophysics

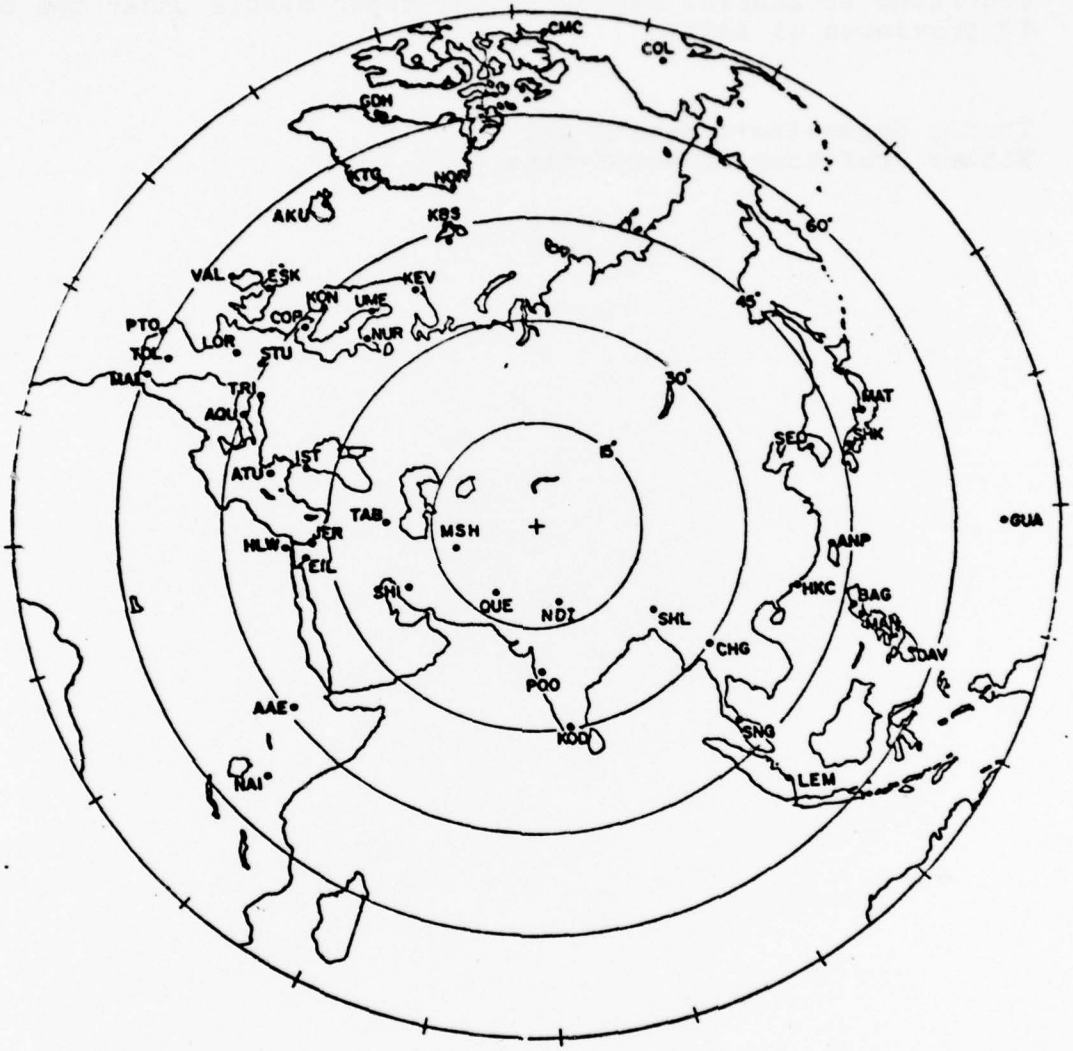

Fig.3-1.1: Azimuthal equidistance projection of Eurasia centered on the reference point in the Pamir Mountains. All stations used in this study are shown on this map.

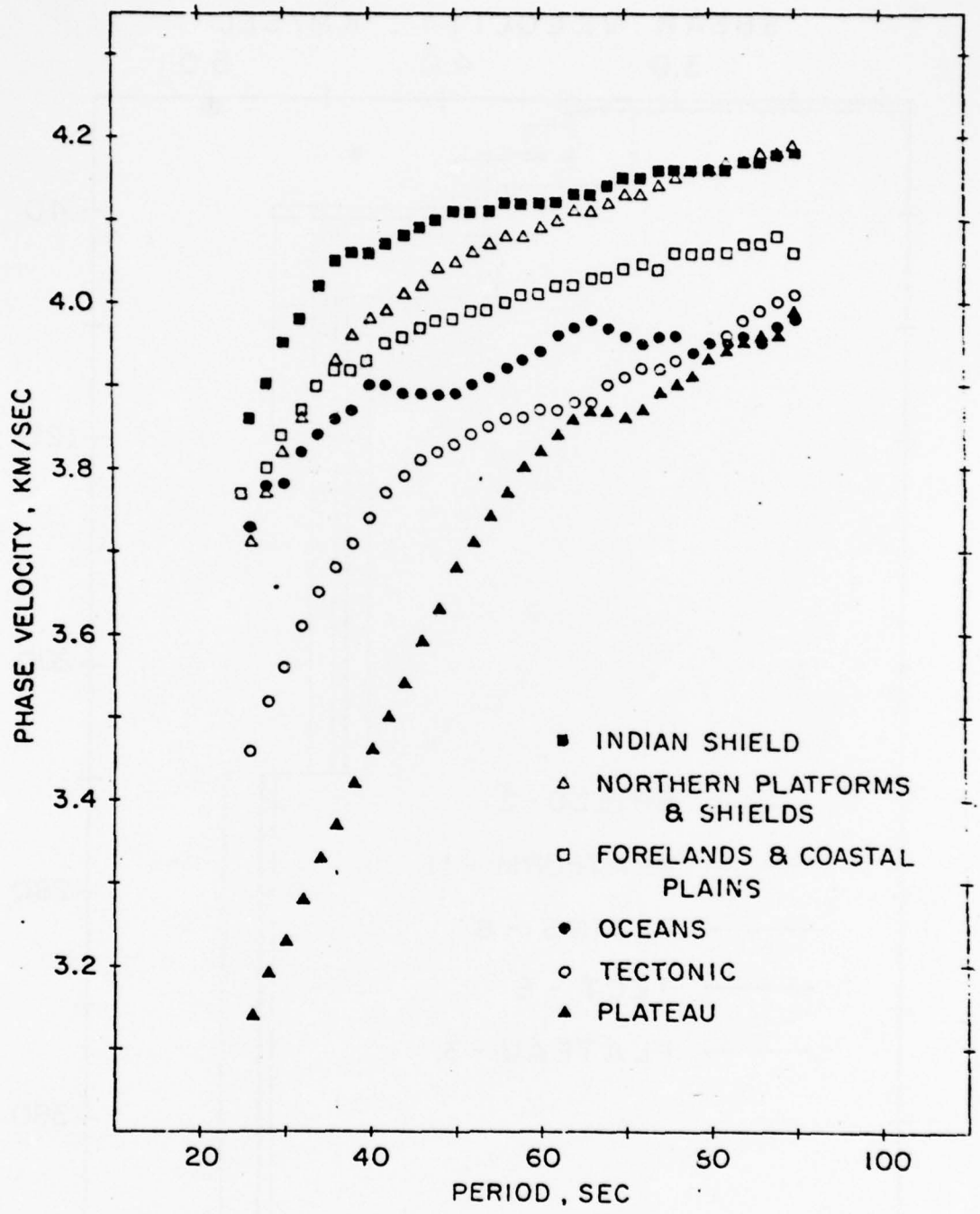

Fig. 5-2.3: Regionalized Rayleigh wave phase velocities.

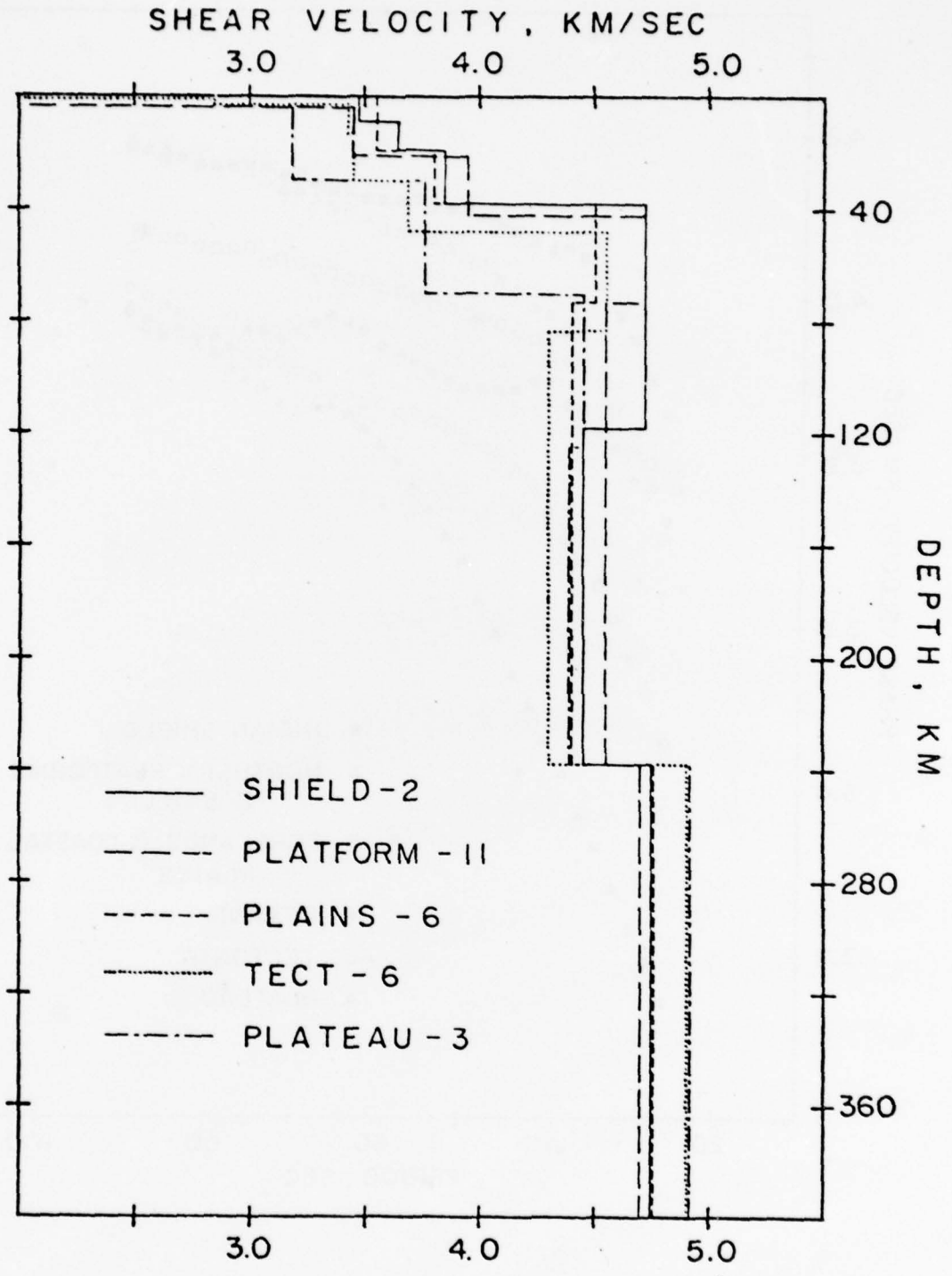

Fig. 5-3.4: Models of shear velocity structure of Eurasian provinces.

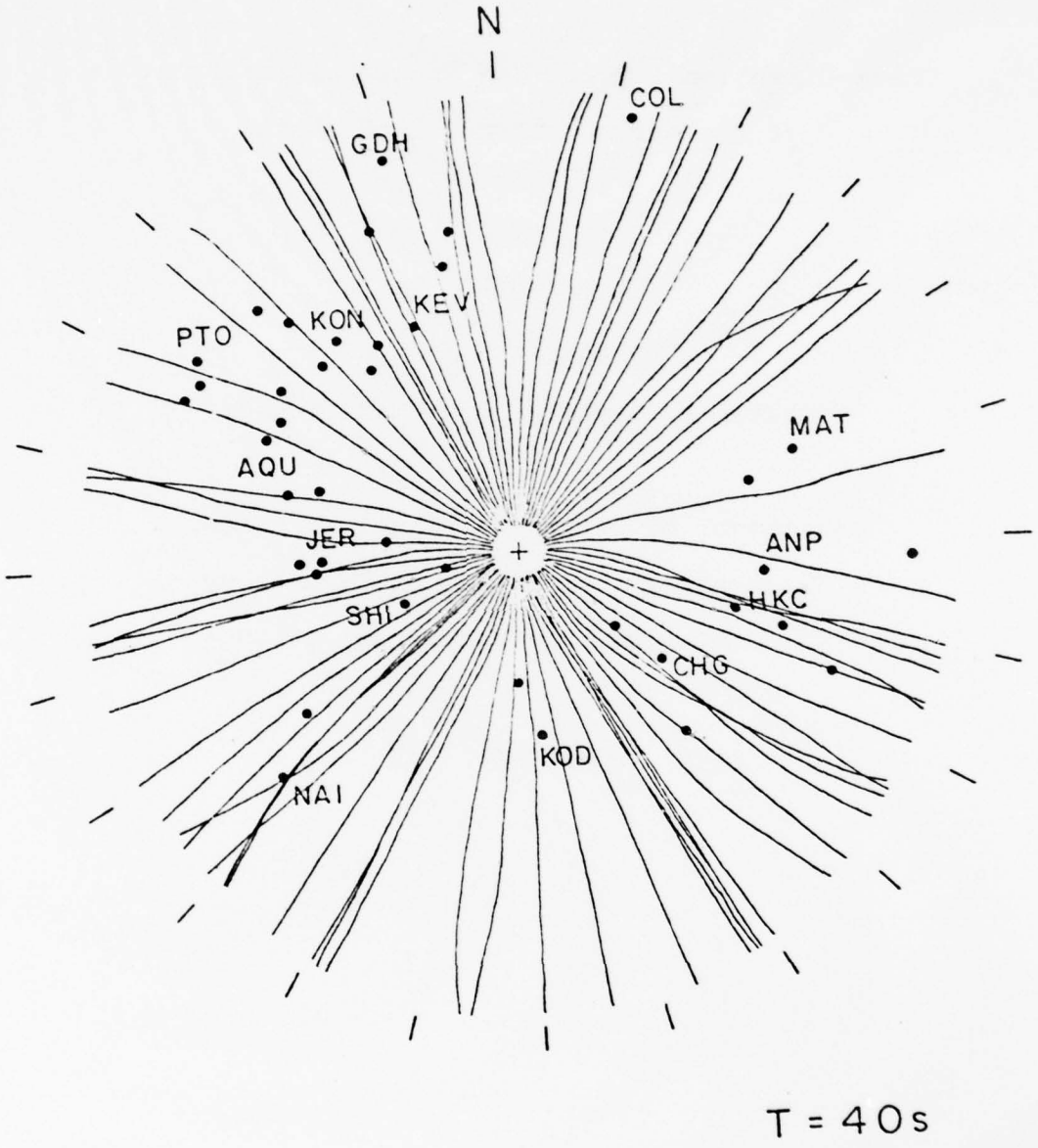

Fig. 5-4.1: Ray paths of 40sec period Rayleigh waves obtained from synthetic ray tracing experiment discussed in the text. Rays leave source (+) at 5° intervals of azimuth. Tick marks are given at 15° intervals.

3. SEISMIC WAVE PROPAGATION

Three-Dimensional Crust and Upper Mantle Structure of the Northeastern United States

Steven R. Taylor and M. Nafi Toksöz

Department of Earth and Planetary Sciences
Massachusetts Institute of Technology
Cambridge, Massachusetts 02139

November, 1978

Three-Dimensional Crust and Upper Mantle Structure of the Northeastern United States

Abstract

Teleseismic P wave arrival times recorded by the North-Eastern Seismic Network are used to invert for lateral crust and upper mantle structure to depths of 500 km. Three-dimensional inversion of the travel time data between two ancient orogenic provinces suggests that structures down to possibly 200 km and greater can be correlated with surficial geologic and tectonic features. This has the important implication that major orogenic belts have effects that reach well into the lithosphere which are stable for extended periods of time, perhaps as long as 1 billion years. The crust beneath the Paleozoic Appalachian Province is characterized by slightly greater thicknesses and lower average velocities than that of the Precambrian Grenville Province. The higher average velocities associated with the Grenville province extend to depths of 200 km and appear to be maximum beneath the Adirondack dome. A relatively low velocity anomaly extending to depths in excess of 200 km and dipping to the northwest shows a spatial correlation with the Bronson Hill - Boundary Mountains Anticlinorium in central New Hampshire and Maine. These structures occupy the sites of a complex series of island arc sequences last active in Early Devonian time prior to the Acadian orogeny. This low velocity region may represent subducted oceanic lithosphere which has undergone post-orogenic radioactive heating.

Introduction

This paper reports on the preliminary results of a study of teleseismic P wave arrival times recorded by the Northeastern Seismic Network. The inversion of teleseismic P wave travel time residuals is a commonly used method of extracting velocity information in the crust and upper mantle beneath an array. Notable studies include those in California (Bolt and Nuttli, 1966; Nuttli and Bolt, 1969; Steeples and Tyer, 1976) at LASA (Sheppard, 1966; Iyer and Healy, 1972; Greenfield and Sheppard, 1964), in Arizona (Johnson, 1967), in Japan (Zandt, 1975; Hirahara, 1977), at NORSAR (Aki, 1977), in Yellowstone National Park (Iyer, 1975; Zandt, 1978), in Hawaii (Ellsworth and Koyanagi, 1977), in New Madrid (Mitchell et al., 1977), and beneath the Tabela Array (Menke, 1977).

Many of the earlier studies consisted of determination of residual patterns and development of qualitative models to explain the observed trends. Recent models have utilized the techniques developed by Aki et al. (1977), for mapping the three-dimensional structure beneath an array.

To date, very little seismological work pertaining to crust and upper mantle structure has been done in the northeastern United States. Leet (1941), Lineham (1962), and Katz (1955) published refraction results using a small permanent array combined with some portable stations. More recently some refraction work has been reported by Chiburis and Graham (1978) and Aggarwal in Schnerk et al. (1976). Other relevant

studies include a surface wave analysis in New York (Dorman and Ewing, 1962), analysis of teleseismic PP residuals beneath Newfoundland (Stewart, 1978), and a study of teleseismic P-wave residuals across the eastern United States and Canada (Fletcher et al., 1978).

In this paper, a three-dimensional inversion of teleseismic P-wave residuals is presented using data collected from the Northeastern Seismic Network. The model is interpreted in conjunction with other geophysical and geological observations in an attempt to learn about the crust and upper mantle structure beneath two adjacent ancient orogenic belts, the Grenville and Appalachian Provinces. An effort is also made to interpret the models in light of, and to place constraints on a plate tectonics origin for both orogenic belts.

Geologic Setting and Tectonic Evolution

The northern Appalachians have undergone a long and extremely complex geological development. Dating and stratigraphic correlation between regions has been complicated by numerous orogenic episodes. The northern Appalachians can be divided into three major tectonic units (Bird and Dewey, 1970; Naylor, 1975): a western belt and an eastern belt possible representing the margins of two once convergent continental masses surround a central orogenic belt composed mainly of eugeoclinal lithologies (Figure 1). The western unit is mainly underlain by rocks of the Precambrian Grenville Province which are exposed in the Adirondacks and outlying massifs such as the Green Mountains, Berkshires, and the Hudson Highlands. Unconformably overlying the Grenville basement is an Eocambrian to Cambrian platform sequence which grades upward into a Lower Ordovician clastic sequence. Found above are the Taconic klippen which consist primarily of deep-water shales, sandstones, and graywackes. Paleontological evidence suggests that they were deposited contemporaneously with the shelf sediments (Zen, 1972).

The central orogenic belt consists of a number of broad structural warps. The Connecticut Valley Synclinorium (CVS) exists to the east of the previously discussed Precambrian massifs and can be traced from Connecticut through Quebec to the Gulf of St. Lawrence. The CVS contains a thick highly metamorphosed eugeoclinal sequence divided into two members

separated by a major Middle Ordovician unconformity. A linear serpentinite belt follows the western flanks of the CVS.

East of the CVS lies the Bronson Hill Anticlinorium (BHA) which consists of a chain of elliptical gneissic domes (Oliveran Plutonic series in New Hampshire). The structure can be traced from Connecticut through northern New Hampshire and is probably continuous with the Boundary Mountains Anticlinorium in Maine. Mantling the domes is a series of mafic metavolcanics associated with felsic metavolcanics and metasediments (Ammonoosic Volcanics in New Hampshire) of Middle Ordovician age or older (440±30 m.y.; Naylor, 1975). Unconformably overlying the Ammonoosics is a series of Silurian to Lower Devonian highly metamorphosed clastics with some carbonates and volcanics.

Eastward of the BHA lies the Merrimack Synclinorium (MS) which is a major northeast-trending tectonic feature extending from eastern Connecticut through Maine and into New Brunswick. It is the site of thick accumulations of Ordovician to Lower Devonian metasediments typically metamorphosed to sillimanite grade. These metasediments (Devonian Littleton Formation) can be correlated with Devonian strata at the top of the BHA. The MS also contains large volumes of intrusives belonging to the Middle Devonian New Hampshire Plutonic Series and the Mesozoic White Mountain magma series.

On the eastern flank of the MS is a major northeast-trending thrust belt (Clinton-Newbury, Bloody Bluff, and Lake Char Faults) extending from southern Connecticut through eastern Massachusetts (Skehan, 1969). Magnetic anomalies

associated with the formations in the thrust belt suggest that the faults continue offshore in an east-northeast direction into the Gulf of Maine (Weston Geophysical, 1976; Alvord et al., 1976) and possibly into New Brunswick (Nelson, 1976). In eastern Massachusetts the northwest dipping thrusts greatly offset metamorphic isograds and no stratigraphic units can be traced across them (Pat Barosh, personal commun.). Deformation and metamorphism in the MS probably delineates a zone of maximum intensity of the Middle Devonian Acadian Orogeny (Rodgers, 1970).

The Eastern Basement is exposed to the east of the above described thrust belt. These units are probably correlative with rocks of the Avalon Zone in Newfoundland and southeastern New Brunswick (Bird and Dewey, 1970; Nelson, 1976). The region in eastern Massachusetts is characterized by plutonic, metasedimentary and metavolcanic rocks metamorphosed mainly to chlorite grade ranging in age from late Precambrian to Carboniferous. Unfossiliferous strata and scattered age dating has made geologic interpretations enigmatic (Naylor, 1975; Zarrow et al., 1978). However, according to Naylor (1975), no rocks have been assigned an age greater than 650 m.y. which is significantly younger than the Grenville age rocks (∿1,100 m.y.) in the western belt.

A possible scenario for the evolution of the northern Appalachians will be outlined below. It must be emphasized that this is an over-simplified first order model, based on often poorly defined, conflicting geology. However, many of the

large scale features are correlative with observed velocity anomalies described in a later section.

The oldest rocks in the study area are exposed in the Adirondacks and the Precambrian outliers of the Green Mountains, Berkshires, and Hudson Highlands. On the basis of petrological and structural arguments Dewey and Burke (1973) suggested that the Adirondacks represent deep erosional levels of part of an ancient Tibetan-type plateau formed behind a continental collision zone during the Grenville Orogeny (∿1,100 m.y.). Doming in the southern Adirondacks may be due to intersection of regional fold structures affecting Precambrian rocks (McLelland, 1977). Since the late Precambrian, the Adirondacks have apparently remained a regional high, as suggested by the onlap of Paleozoic sediments (Rodgers, 1970).

It is currently thought that continental rifting stage initiated approximately 820 m.y. ago leading to the formation of the Iapetus Ocean (proto-Atlantic) (Rankin, 1976). The late Precambrian and Cambrian geology of the western belt is characterized by the establishment of an Atlantic-type stable continental margin.

Late Precambrian lithologies on the eastern belt also indicate a rifting stage with the development of an active continental margin (Kennedy, 1976). Geochemical, paleomagnetic, and paleontological evidence suggests that the western and eastern belts were located on opposite sides of the Iapetus Ocean (Strong et al., 1974; McKerrow and Cocks, 1976; Kent and Opdyke, 1978).

Early or Mid-Ordovician through Permian times are

characterized by the episodic closing of the Iapetus Ocean. The BHA was a site of major volcanic activity in this time period as evidenced by the presence of thick volcanic sequences. Major deformation occurring in Middle and Late Ordovician time marked the climax of the Taconic Orogeny which affected rocks within and west of the BHA. The Taconic klippe were thrust at this time and later deep seated thrusts involved Grenville basement resulting in the emplacement of the Precambrian massifs. The linear belt of ultramafics found to the east of the massifs were emplaced at this time, and probably represent highly altered, Cambrian to Lower Ordovician (Chidester, 1968) obducted oceanic crust of the Iapetus Ocean or of a marginal sea behind the volcanic arcs of the central mobile belt. The sequence of tectonic and metamorphic events are indicative of effects due to long-term heating, increased ductility and basement reactivation due to induced convection above subducted lithosphere. This effect is observed in continent-continent convergence zones (Toksöz and Bird, 1975) as well as on active continental margins involving only subductive oceanic lithosphere and arc-continent collisions (Burchfiel and Davis, 1975).

Evidence based on styles of deformation and metamorphism indicate that the Taconic Orogeny in New England probably was an episode of arc-continent collision. Numerous island arc segments and inner-arc basins now located within the central mobile belt were probably involved in the deformation. The lack of any major unconformity and Ordovician deformation in

the MS (Moench and Zartman, 1976) indicates that oceanic terrain continued to separate continental crust of the eastern belt from North America. However, the amount and type of volcanism in the central mobile belt following the Taconic Orogeny indicate that closure of the Iapetus was nearly complete. It may have been the close approach of the eastern belt and possibly the attempted subduction of an oceanic ridge which caused the island arcs to converge onto North America.

The Silurian to Early Devonian time was a period of relative quiescence and erosion of the Taconic highlands (Boucot, 1968). In the Early Devonian era there is evidence of increased tectonic activity as indicated by the deposition of vast thicknesses of turbidite sequences across the major synclinoria (Littleton Formation of New Hampshire) and renewed volcanism along arcs in the central mobile belt. This episode of major deformation is called the Acadian Orogeny and appears to have spanned a period of approximately 30 m.y. (Naylor, 1971) which is similar to the duration of the main collisional stages of the Himalayas (Toksöz and Bird, 1977).

The Acadian orogeny is typified by the following overlapping sequence of events: 1) high grade metamorphism in southeastern New England, 2) intrusion of granitic plutons, 3) large scale westward recumbent folding of many of the plutons, and 4) brittle deformation and development of large thrust belts. These styles of deformation show many parallels

with those documented in other continental convergence zones (Dewey, 1977). The period of metamorphism, intrusion, and ductile deformation are deep crustal processes characteristic of a major thermal event associated with initial heating of the crust from below due to asthenospheric convection prior to collision and post-collisional radioactive heat generation (Toksöz and Bird, 1977). The binary granites of the New Hampshire Plutonic Series (dated around 360 m.y.; Naylor, 1975) are indicative of extensive crustal heating and partial fusion of crustal sediments and are similar to those found throughout much of the Himalayas (Bird, 1976).

Three major events following the Acadian Orogeny are recorded in New England. Alleghenian deformation in Pennsylvanian to Permian times strongly affected rocks in southeastern New England. The Allegheny Orogeny probably represents the final closure of the Iapetus Ocean by the collision of Africa with North America. It has been suggested (Dewey and Kidd, 1974) that the Alleghenian deformational belt truncates the Appalachian-Caledonian belt in southern Connecticut and Rhode Island and is correlative with the Hercynian belt in central Europe.

In late Triassic time large rift-valley graben systems were developed along the trend of the Appalachians. These grabens were filled with thick accumulations of non-marine red beds. The rifting was accompanied by the fissure eruption of basaltic lavas and the intrusion of numerous diabase dikes, sills and stocks. This period of time represents the

initial opening of the modern Atlantic Ocean. The most recent major tectonic activity in New England was the emplacement of the White Mountain Magma Series, intruded over a 100 m.y. interval from Jurassic to Cretaceous time (Chapman, 1976).

The northeastern U.S. is presently an intraplate region adjacent to a stable continental margin, characterized by relatively low-level, diffuse seismicity. It is not clear at this time what structures control seismicity patterns. The region within and possibly east of the Grenville Province is characterized by a northeast trending maximum compressive stress and some earthquakes appear to be controlled by re-activated paleozoic faults (Sbar and Sykes, 1977). However, it is not known whether this stress pattern extends into New England.

Travel Time Residuals

Teleseismic P-wave arrival times were collected from 50 stations which are part of the Northeastern Seismic Network (Fig. 2). The stations were installed and are operated by research groups at Boston College (Weston Observatory), Lamont-Doherty Geological Observatory, and Massachusetts Institute of Technology. Station distribution is fairly uniform, although there are areas with large station spacing. Not all of the stations were in operation for the duration of this study. Because the network was not in full operation until February, 1976, events used in this study covered a time range between February, 1976, and December, 1977. Most stations are equipped with vertical component short period 1 or 2 Hz geophones. Signals are telemetered to central recording sites (located at each of the above institutions) and recorded on develocorder film.

The relative arrival times of teleseismic P-waves were read from enlarged copies of 16mm develocorder film. In general, strong scattering in the frequency bandwidth of the incident P waves is not observed as indicated by the coherency of the first few cycles across the network. The signals from each of the stations were visually correlated using an overlay of representative waveforms. Relative arrival measurements were taken from a prominent peak or trough early in the signal, and readings were taken to the nearest 0.1 sec. A misidentification of the peak or trough would cause a residual error of 0.5 to 1.0 sec. which is readily apparent

once the residuals are calculated.

1822 arrival times from 68 events were read from stations of the Northeast network. The epicentral distances range between 25° and 95° and azimuths were mainly from the northeast (from Eurasia), south and southwest (Central and South America), and the northwest (Aleutians, Kuriles), (Figure 3).

Elevation corrections were applied to the data and travel times were reduced to a datum elevation at sea-level. Absolute P-wave residuals were calculated using Herrin travel-time tables and are defined to be

$$R_{ij}^{H} = T_{ij}^{obs} - T_{ij}^{H} \qquad (1)$$

where R_{ij}^{H} is the absolute residual with respect to Herrin tables for station i, event j; T_{ij}^{obs} is the observed travel time using event locations and origin times from PDE bulletins; T_{ij}^{H} is the theoretical travel time through a Herrin earth. The residuals were further reduced by calculating relative residuals with respect to a mean residual computed for each event;

$$\bar{R}_{ij} = R_{ij}^{H} - \frac{1}{N} \sum_{i=1}^{N} R_{ij}^{H} \qquad (2)$$

where N is the number of stations reporting P arrivals for event j.

Using the above relationships, positive residuals represent late arrivals where the incident rays have been slowed in the crust or uppermantle beneath the network. It should be noted that no significant differences were observed in the values of the relative residuals when Jeffreys-Bullen travel

time tables were used instead of Herrin Tables. An error in the reported origin time or a source correction term will affect all stations similarly and will drop out when relative residuals are computed. The effects of the structure at the source, heterogeneities encountered along the major portion of the travel path, and structural variations beneath the array are major causes of the absolute residuals. Intuitively, the cone of rays from a teleseismic source to different stations in the network will sample nearly identical travel paths until they diverge in the upper mantle and crust beneath the array. Thus, it is reasonable to assume that the computed average residuals contain information regarding this common travel path up to the point where the rays diverge significantly. By subtracting off the average residual, effects due to mislocation errors or heterogeneities encountered along the common path are greatly reduced.

The above approximations which are reasonable when network aperture is small become progressively less valid as the network aperture is increased. If the apparent network aperture is large enough, the curvature (second derivative) of the travel time curve becomes significant. The problems involved in the analysis of relative P-wave residuals have been discussed by Engdahl et al. (1977). Using data from Alaskan-Aleutian stations, Engdahl concluded that the primary source of observed variations in relative residuals was from local structure beneath the network. For station separations comparable to the maximum diameter of the Northeastern U.S.

Network (600 km), scatter in relative residuals due to epicenter mislocations, source structure, earth models, etc. were at most0.2 sec, which is little more than our reading accuracy. Analysis of relative residuals recorded in the northeastern U.S. supports these conclusions. We found no systematic differences in relative residuals from various depths in the same epicentral regions where it is presumed rays would encounter different source structures.

Two additional sources of error remain to be discussed. Because of down-time for some stations, and of other stations that became operational during the period of this study, slightly different station subsets are available for each earthquake, and the mean residual subtracted off from a given source region may vary for different events. However, this problem is greatly reduced by the large number of stations (typically 25-35) used to calculated the mean residual for each earthquake. The other problem results from the fact that each subnetwork records on a different time base. Each sub-network operates a temperature compensated crystal oscillator clock and timing corrections are generally less than 20 ms/day. To assure accuracy tests were made by comparing signals from a common station recorded on more than one sub-network. The analysis of travel time residuals were carried out using relative residuals. The distribution of average relative residuals, $\bar{R}$, for each station is shown in Figure 4. The relative residuals as a function of azimuth and incidence angle show significant variations across the network (Figure 5).

These trends suggest the presence of large scale lateral heterogeneities in the crust and upper mantle, and considerable effort is required to separate the factors causing the observed patterns.

Average relative residuals for each station were calculated with ten or more readings from well-distributed azimuths. Large positive residuals (late arrivals) occur throughout central and northern New Hampshire, southern Maine and eastern Vermont. As was observed by Fletcher et al. (1978) these contrast sharply with large negative residuals in western Vermont, northern New York, southeastern New York, and southeastern Connecticut. Shallow, localized structural differences would result in rapidly varying trends between adjacent stations. However, the slowly varying distribution of residuals suggests that the observed variations are probably due to deep, regional structures such as differences in crustal thickness and upper mantle velocity.

As a first step we compare the residuals with surface geologic and other geophysical data. Figure 7 illustrates the relationship between average relative station residuals, $\bar{R}$, and the regional Bouguer gravity taken from each station site (Kane et al. (1972), Simmons, (1964), and Diment et al. (1972)). Because the long wavelength (≈100 km) regional gravity anomalies probably reflect variations in Moho topography, (Simmons, 1964), the inverse correlation between gravity and average residuals suggests that for many stations, the average residuals depend partly on crustal thickness variations. It is also interesting to note the dependence of average residuals on the age of the basement

beneath each station. The two sets of symbols in the figure correspond to the inferred age of the basement for each station site. Stations in New York and New Jersey are located above Precambrian (>1.0 b.y.) Grenville basement, while most New England stations are atop younger (<1.0 b.y.) Paleozoic basement of the Appalachian province (the central mobile belt, and eastern belt described earlier). Clearly, the stations within the older Grenville Province see early arrivals relative to those in the younger Appalachian Province. However, because of the relationship between Bouguer gravity anomalies and station elevation it is difficult to attribute this separation totally to crustal thickness variations (Figure 8). In isostatically compensated regions, crustal thickness should be correlated with surface elevations (Woolard, 1954; Tseng, 1975). Figure 8 illustrates that there exists a correlation between gravity and elevation although there is no obvious separation between the two regions. To explain the behavior of both Figures 7 and 8 it is necessary to invoke velocity changes in addition to any possible variations in crustal thickness. This idea is supported by refraction profiles constructed in the northeastern U.S. Although little detailed refraction work has been done in this region, existing studies indicate slightly higher average crustal velocities in the Grenville Province, as opposed to the Appalachian Province. Table I shows MIT and Weston Geophysical Co. (Ron Street, personal comm.) refraction models collected from measured quarry blasts for eastern Massachusetts, southern and central New Hampshire, and

southern Maine. Also shown is a model published by Aggarwal in Schnerk et al. (1976) for northern New York and the Adirondacks. Comparison of the refraction models indicates that the crust beneath this part of the Appalachian Province is on the average slightly thicker and slower, and it is possible to account for a large part of the almost one second difference in relative residuals between the two regions.

The dependence of average relative residuals on crustal properties is also supported by the results of a time-term analysis which indicated a positive correlation between P_n residuals and teleseismic P-wave residuals (Taylor and Toksöz, 1978). However, these observations cannot fully explain Figures 7 and 8 and as indicated by three-dimensional models presented in the next section, structural differences between the two regions extend into the upper mantle.

In addition to distinct patterns in the distribution of average residuals across network, most stations show a strong dependence in residuals with azimuth and incidence angle. Polar plots of relative residuals as a function of azimuth and incidence angle for many northeastern stations are shown in Figure 5. Moving from south to north we see a number of interesting residual trends. In Connecticut, for arrivals from the northeast, the residuals become increasingly less positive (arrive earlier) as the incidence angle decreases until in southwest Connecticut and northern New Jersey residuals are largely negative. Rapidly varying structure is observed to the south which will be reflected in the three-dimensional models presented in th e next section. In Massachusetts,

arrivals are late to the northwest and small to the south and northeast while New Hampshire and southern Maine observe late arrivals from all azimuths. Negative residuals are observed in the Grenville Province across most of New York, particularly in the northern regions, where large negative residuals are observed from the northwest.

The residual patterns indicate that between the Grenville and Appalachian orogenic belts structural differences exist in the crust, and into the upper mantle. It appears that a large region of relatively low velocities occurs in the upper mantle beneath central new England and that velocities become increasingly higher beneath the older Grenville Province to the west. From Figure 4 it is evident that most stations in close proximity to one another show a similar distribution in residual values implying that lateral variations are not a clear surface effect. Since the incidence angles are small for the teleseismic P-waves ($15^\circ - 30^\circ$), lateral variations in crustal velocities cannot account for the observed effects. For example, teleseismic rays of equal slowness and incident from opposite azimuths, enter the crust with a maximum separation of 50 km. Azimuthal variations of one second and greater would require unreasonably large lateral velocity differences.

The possibility of a dipping Moho as a cause of azimuthal variations in residuals was investigated. To the first order in the dip, α, the maximum differential travel time for teleseismic ray approaching from opposite azimuths perpendicular to the strike of a dipping layer is given by

$$T = 2hp\left(1 - \frac{\cos\theta}{V_m^2\sqrt{\eta_c^2 - p^2}}\right)\alpha \qquad (3)$$

where h is the depth to the interface beneath a given station; α is the dip of the interface; $\theta = \sin^{-1}(pV_m)$ represents the incident angle at the interface; and $\eta_c = \frac{1}{V_c}$. Substitution into equation (3) implies that unreasonably large regional dips of the Moho (20-30°) are required to satisfy the observations. Thus, it is reasonable to assume that laterally varying structures in the upper mantle beneath the network are required to explain the pronounced residual versus azimuth and incident angle variations.

Three-Dimensional Inversion

Qualitative description of residual patterns as in the previous section is a useful but inadequate means of estimating the structural disturbances an incident ray encounters beneath the network. In this section we present results from a three-dimensional inversion of the teleseismic travel time data following the techniques illustrated by Aki, et al (1977). The initial model used in the inversion consists of a plane-layered medium where each layer is sub-divided into a series of right rectangular blocks. Using relative teleseismic P wave residuals, individual slowness ($\frac{\delta V}{V}$) perturbations are computed for each block relative to a layer average. Aki et al. (1977) has shown that for the ith station and jth event, relative residuals (with respect to a mean) can be represented by

$$r_{ij} = \sum_{k=1}^{a} T'_{ijk} D_{ijk} \qquad (4)$$

where $T'_{ijk} = T_{ijk} - \frac{1}{N} \sum_{k=1}^{n} T_{ijk}$, reduced travel times

T_{ijk} - travel time through kth block

D_{ijk} - $-\frac{\delta V}{V_k}$, percent perturbation in slowness relative to the layer average $(1/V_k)$

N - number of observations for event j

a - number of layers

In matrix form

$$\underline{r} = A\underline{m} \qquad (5)$$

where $\underline{r}$ - n-length vector containing relative residuals

$\underline{m}$ - k-length vector containing unknown velocity perturbations

A - n x k symmetric matrix with reduced travel times

Solution of the system (5) by classical least squares fails because there exist two sources of non-uniqueness. The first source can be caused by insufficient data and results in vertical "coupling" of inadequately sampled blocks in separate layers which share a common ray path. The other source of non-uniqueness is inherent to the formulation of the problem and results from the removal of the average residual from the data. This implies that within a given layer, the velocity perturbations are determinant only to within a constant and no information regarding absolute velocities is attained. Thus, the system (5) is solved by using a damped least squares technique where a positive constant is added to the diagonal elements of A^TA which reduces the effect of zero-eigenvalues on the generalized inverse solution. The solution to (5) is given by

$$\underline{\hat{m}} = (A^TA + \theta^2 I)^{-1} A^T\underline{r} \qquad (6)$$

where θ^2 is the damping parameter and I is the identity matrix. The resolution and covariance matrices are, respectively

$$R = (A^TA + \theta^2 I)^{-1} A^TA \qquad (7)$$

$$C = S^2 (A^TA + \theta^2 I)^{-1} R \qquad (8)$$

where S^2 is the estimate of the data variance, σ_d^2. Because

addition of the damping parameter has the effect of reducing the number of degrees of freedom, the trade-off between resolution and standard-error should be examined in order to select a proper choice for θ^2. For this study we chose $\theta^2 = 0.1$ (sec/%) .

Selection of the initial model geometry requires experimentation with different configurations in order to derive a well-resolved solution with small standard errors. The blocksize depends on the station distribution, and the number of observations. Because it is desirable to have a minimum of ten rays sample each block, we chose our blocks to be one degree on a side. The inversion should be carried to a depth of at least one array diameter which we selected to be 500 km. As suggested by Ellworth (1977), a suitable height to width ratio is 1.5:1 which we found to be satisfactory. Experimentation with displaced layers (in an effort to decouple blocks) and rotated coordinate systems showed little, if any, improvement on the final model.

The initial model used for the ray tracing was a layered spherical model with constant velocities in each layer. Velocity differences of up to 10% do not substantially alter the sampling of the blocks. We average velocities from a Herrin earth model to derive the layer velocities (Table 2).

The velocity perturbations and the number of observations for blocks in each layer of the final model are shown in Figure 9. In these figures, negative velocity perturbations represent relatively lower velocities. We only included blocks which were sampled by a minimum of ten rays which mainly eliminated the outermost elements.

Modeling of the crust is probably one of the most crucial results we wish to obtain. Unfortunately, because of small incidence angles, most rays pass through the crustal block and the block lying directly underneath. This makes it difficult to decouple the effects of the two superposed blocks. Resolution could be improved if the thickness of the surface layer were increased. However, the surface blocks would then contain a large and important velocity discontinuity (the Moho) and information regarding crustal structure would be lost.

Problems may also arise because of the uneven station distribution. If rectangular prisms are used to model the crust, a number of stations located in areas with potentially different structures may be included within the same element. To remedy this problem we compute velocity perturbations for each individual station rather than for a given block configuration. It was found that using this approach had little effect on the upper mantle layers and it facilitated a means to compute a three-dimensional crustal thickness model which is described below.

Although resolution is poor and standard errors are large, the velocity perturbations show a good inverse correlation with the average station residuals (Figure 10). This further supports previous conclusions that the average station residuals are mainly dependent on crustal structure, and may reflect crustal thicknesss and velocity variations. Iyer and Healy (1972) successfully used a general relationship to model crustal thickness at LASA from the distribution of average station residuals. They made the assumption of a homo-

geneous crust beneath the array which may be a reasonable assumption for a first order crustal model in the particular region they were modeling. However, in the previous section, we concluded that the two orogenic belts in the northeastern U.S. show regional differences in average crustal velocities and thicknesses. This implies that we must account for lateral velocity variations in order to use the average residuals for crustal thickness. Combination of the velocity perturbations with the average station residuals allows us to construct a crustal thickness model. Although there is a trade-off between crustal thickness and lateral velocity differences we feel that the method is justified because independent geophysical data suggests the dependence of average station residuals on crustal thickness and lateral velocity variations.

We assumed that the velocity perturbations, $\frac{\delta V}{V}$, represent differences from an average crustal velocity, V_c. It should be stressed that any information regarding absolute velocities in the three dimensional inversion is lost and the technique we are using is therefore an approximation and represents only a first order crustal model. The average crustal velocity, V_i, beneath each station i is then

$$V_i = V_c((\frac{\delta V}{V})_i/100) + V_c \qquad (9)$$

and the crustal thickness is

$$h_i = V_i \bar{R}_i + h_o \qquad (10)$$

where h_o is some average crustal thickness to be varied. We chose V_c = 6.5 km/s and h_o = 38 km and calculated the crustal thickness and average crustal velocity maps shown in Figure 11. Overall, the crust beneath the Appalachian province appears to be 3 km thicker than that of the Grenville. Average crustal velocities differ very little but may be slightly lower in many parts of the Appalachians. There is a region of greater crustal thickness beneath eastern Vermont, New Hampshire, and southern Maine. In western Vermont, and western Connecticut there are high thickness gradients where the crust thins to the west. These features are located just to the east of the Taconic thrust belt and in western Vermont, the gradients show an impressive correlation with the serpentinite belt. Slight crustal thinning is observed in eastern Massachusetts, and it is not clear if this represents a trend which may continue eastward towards the outer edge of the continental margin. Alternatively, it may represent the contact between the central orogenic belt and the eastern belt described earlier. The average crustal thickness of 36 km in northern New York agrees very well with refraction models of Katz (1955) and those of Aggarwal in Schnerk et al (1976).

The upper mantle (layer 2) between 35 and 200 km (Figure 9b) depth is characterized by a northeast trending region of low velocities beneath Massachusetts, New Hampshire and southern Maine. The trend of this zone has an interesting parallel with the "grain" of the Appalachian surface structure. The velocities appear to increase to the west and northwest be-

neath the Precambrian Grenville Province. This suggests that structural differences between the two orogenic belts extends into the upper mantle. The resolution in the upper mantle layer increases markedly relative to that of the crustal elements. Because the block configuration in layer 2 is better suited for sampling incident waves, each element, particularly the central elements, observe a good cross-fire of rays. Resolution degrades somewhat towards the outer edges of the model because the number of observations decreases, and the azimuths are limited to a small sector. The overall resolution and standard errors are best for this particular layer.

In layer 3 (200-350 km) the region of lower velocities is shifted west and northwest and is found beneath Vermont and central Maine. There is still some evidence of higher velocities in the western-most blocks in the model.

The deepest layer (layer 4; 350-500 km) shows little resemblance to the overlying layers. The overall trends appear to be of shorter wavelength and, not surprisingly, there is little, if any distinction between the two geologic provinces observed at the surface.

Discussion

Three-dimensional inversion of travel time data illustrates that structures down to perhaps 200 km and greater can be correlated with surface geology. This has the important implication that major orogenic belts have effects that reach well into the lithosphere which are stable for extended periods of time, perhaps as long as 1 billion years.

In addition to the regional differences existing between the two structural provinces in the northeastern U.S., we see smaller scale features that are related to specific segments of each orogenic belt and to the intervening suture zone. As discussed previously, the Taconite belt, the eastward-lying Precambrian uplifts (The Berkshire Highlands and Green Mountains), and serpentinite belt are Lower Ordovician structures related to the closure of an inner-arc basin and a continent-island arc collision. This region is not only a site of large scale geologic deformation but it is also characterized by geophysical anomalies such as apparent crustal thinning, high crustal velocities, and large positive Bouguer gravity anomalies (Figure 6). It is possible that these effects are related to deep-seated thrusts emplaced near the end of the Taconic orogeny which carried oceanic crust and upper mantle material to higher levels within the crust. This material would have high velocities and densities relative to the surrounding eugeoclinal lithologies and would provide a model consistent with the observed geophysical and geological anomalies. There are at least two objections to

this model. The first is that higher crustal velocities are observed just to the west of the Taconic thrust belt at stations PNY and WNY. Secondly, we see that geophysical anomalies are not observed along the entire Taconide belt, although the geologic structures are fairly uniform. This gap in the zone of high crustal thickness and velocity gradients east of and parallel to the thrust belt in southwestern Vermont and western Massachusetts may simply be an effect of poor station coverage in the region. As pointed out by Fletcher et al. (1978), the anomalous residuals beneath PNY may be related to buried mafic or ultramafic bodies whose presence is indicated by local gravity highs (anomaly 22 of Simmons, 1964). However, it is readily apparent that all of the stations in northern New York record very early arrivals from the northwest. This implies the existence of regional, deep-seated effects extending to the northwest beneath the Adirondack dome and is supported by the three-dimensional inversion (Figure 9). Interestingly, the large negative residuals from the northwest are not observed at stations further south which suggests that the zone of relatively high upper mantle velocities is controlled by a structure unique to the Adirondacks. It has been postulated that the Adirondacks and associated Grenville basement represent deeper levels of an ancient "Tibetan Plateau" characterized by crustal thickening and shortening behind a continental collision zone (Dewey and Burke, 1973; Toksöz and Bird, 1977). It is not clear when the Adirondack dome was elevated, and

the cause of relatively high velocities found in the upper mantle beneath the region remains problematical. If the Grenville belt does represent an analog of a Tibetan Plateau, and crustal thicknesses presently average 36 km, then possibly another 15-35 km of crust has been eroded away since the late Precambrian. This implies that the presently exposed surface geologic features of the Adirondacks represent lithologies deformed, metamorphosed, and intruded at great crustal depths.

Another prominent feature in the crustal model is the apparent crustal thickening beneath central New Hampshire and southern Maine. Topographically, these are the regions of highest elevations in New England and are therefore isostatically compensated highland areas. The Lower Devonian Acadian orogeny had a severe impact on the structure as evidenced by high grade metamorphism, intrusion of granitic plutons, and large scale westward recumbent folding of many of these plutons (Naylor, 1968). Many lines of evidence suggest the uplift of a significant mountain belt. Early Devonian miogeoclinal sediments in eastern New York are overlain by a thick clastic Middle Devonian sequence of the Catskill Delta - a thick clastic wedge derived from the uplifted landmass in central New England (Rodgers, 1970). The crustal thinning towards central and northern Maine is correlated with the drop-off in the grade of metamorphism (Thompson, 1968). This implies that the continental collision of Acadian orogeny was particularly severe in southeastern and central New England and we would expect to see greater crustal

thicknesses in these regions.

In eastern Massachusetts we again see an apparent crustal thinning over much of the eastern belt described in an earlier section. These contours conform very well with the position of the middle Paleozoic thrust belt and the abrupt falloff in metamorphic isograds from sillimanite to chlorite (Thompson, 1968).

The low velocity anomalies in the upper mantle (35-200 km) beneath Massachusetts, New Hampshire, and southcentral Maine strike northeast parallel to the structural grain of the Appalachian orogenic belt. There is some evidence that this feature dips to the northwest to depths greater than 200 km. Because of the geometry of the initial model, the vertical extent of this structure is only constrained to lie somewhere between 200 and 350 km. It is interesting to note the spatial correlation of this low velocity trend with the Bronson Hill - Boundary Mountains anticlinorium. As discussed previously, these structures probably occupy the sites of a complex series of island arc sequences last active in the Early Devonian time prior to the Acadian orogeny. If it is true that subduction occurred east-southeast of the Bronson Hill in a west-northwest direction, we may expect to observe some anomalous feature at these depths.

Assuming that a subducted oceanic slab can produce such a long-term anomaly, the existence of velocities that are lower than the surrounding mantle material is surprising, yet not necessarily inconsistent with its possible thermal evolution. Thermal models of downgoing oceanic lithosphere

(Toksöz et al., 1973) illustrate that in the early stages of subduction, the slab is cold and dense relative to its surroundings to a depth of at least 600 km. At approximately 100 m.y. from the cessation of subduction, the slab reaches thermal equilibrium. Thermal models suggest that beyond about 100 m.y. the subducted oceanic lithosphere starts to heat up because of its higher radioactivity relative to the surroundings. The anomaly is not necessarily thermally-induced and other explanations related to the compositional changes of the descending lithosphere may be constructed. If we assume the velocity anomalies are produced by temperature changes, and take temperature coefficient of velocity for dunite, a 1% velocity decrease corresponds to a temperature increase of about 100-200° C. These observations are consistent with preliminary unpublished heat flow measurements in central New England corrected for radioacitivity which show regions of highest heat flow in central and southeastern New Hampshire relative to northern New Hampshire and southeastern Massachusetts (Jaupart, pers. comm.). Geomagnetic data from the northeastern United States suggests a 200° C temperature anomaly in the lower crust beneath central New Hampshire and southern Maine (Bailey et al., 1978).

It is also interesting to note that similar trends in teleseismic PP residuals are observed beneath Newfoundland (Stewart, 1978). Newfoundland is a northward extension of the Appalachian orogenic belt and it is not inconsistent that the crust and upper mantle structures appear to be similar to our observations in New England.

Figure Captions

Figure 1a. Generalized geologic map of northeastern United States. Modified from King (1969).

Figure 1b. Major tectonic structures in northeastern United States. Shaded regions correspond to sillimanite-grade metamorphic zones.

Figure 2. Seismograph stations used for three-dimensional inversion of teleseismic P wave residuals. Labeled stations correspond to those referred to in the text or shown in Figure 5.

Figure 3. Epicenters of earthquakes and explosions used as P wave sources.

Figure 4. Map of average relative travel time residuals in seconds for seismograph stations in northeastern United States.

Figure 5. Station focal sphere projection plots. Relative residuals plotted as a function of azimuth to the source and incidence angle.

Figure 6. Bouguer gravity in northeastern United States. Areas with positive gravity anomalies are shaded. Modified from Kane et al., (1972).

Figure 7. Mean relative teleseismic travel time residual in seconds relative to Bouguer gravity for northeastern United States stations. Open circles correspond to stations located in the Grenville Province above Precambrian basement. Closed circles correspond to stations mainly in the Appalachian Province located above Paleozoic basement.

In summary, we have presented geophysical data which suggests that structural differences between two juxtaposed orogenic belts exist to depths of 200 km and greater. This indicates that major collisional episodes have very long lasting deep-seated effects as well as large areal extents. Crustal thickness and velocity variations are correlative with many surficial geologic and tectonic features. The Paleozoic Appalachian province appears to have a slightly thicker crust with lower average velocities than the Precambrian Grenville province. The higher average velocities associated with the Grenville province are evident to depths of 200 km particularly beneath the Adirondack dome. A relatively low velocity anomaly extending to depths of at least 200 km and dipping to the northwest shows a spatial correlation with the Bronson Hill - Boundary Mountains Anticlinorium. This may be due to effects of post-Acadian radioactive heating of subducted oceanic lithosphere.

References

Aki, K., A. Christoffersson, and E.S. Husebye, Determination of the three-dimensional seismic structure of the lithosphere, J. Geophys. Res., 82, 277-296, 1977.

Alvord, D.C., K. Bell, M. Pease, and P. Barosh, The areomagnetic expression of bedrock geology between the Clinton-Newbury and Bloody Bluff fault zones, northeastern Massachusetts, J. Res. U.S. Geol. Surv., 4, 601-604, 1976.

Bailey, R.C., R.N. Edwards, G.D. Garland, and J.P. Greenhouse, Geomagnetic sounding of eastern North America and the White Mountain heat flow anomaly, Geophys. J. R. Astr. Soc., 55, 499-502, 1978.

Bird, G.P., Thermal and mechanical evolution of continental convergence zones: Augros and Himalayas, unpublished Ph.D. Thesis, Massachusetts Institute of Technology, 1976.

Bird, J.M., and J.F. Dewey, Lithosphere plate-continental margin tectonics and the evolution of the Appalachian orogen, Geol. Soc. America Bull., 81, 1031-1060, 1970.

Bolt, B.A., and O.W. Nuttli, P wave residuals as a function of azimuth, J. Geophys. Res., 71, 5977-5985, 1966.

Boucot, A.J., Silurian and Devonian of the northern Appalachians, in Studies of Appalachian Geology - Northern and Maritime, E. Zen, ed., Interscience, New York, 83-94, 1968.

Chapman, C.A., Structural evolution of the White Mountain magma series, GSA mem 146, 281-300, 1976.

Burchfiel, B.C., and G.A. Davis, Nature and controls of Cordilleran orogenesis, western United States: extensions of an earlier synthesis, Am. J. of Sci., 275-A, 363-396, 1975.

Figure 8. Bouguer gravity relative to station elevation for northeastern United States stations.

Figure 9. Percent velocity variations for crust and upper mantle layers beneath northeastern United States. Numbers in parentheses correspond to the number of observations in each element used in the inversion.

Figure 10. Percent velocity variations for the crustal layer plotted against mean relative travel time residual for the northeastern United States seismic stations.

Figure 11. Lateral average velocity (Km/sec) and crustal thickness (Km) variations across the northeastern United States.

Chiburis, E.F. and R.O. Ahner, Seismicity of the Northeastern U.S., Northeastern U.S. Seismic Network Bull. 6, 1977.

Chiburis, E.F. and T. Graham, Seismic networks in New England, (abstract), Northeastern Sec. G.S.A., 10, 36, 1978

Chidester, A.H., Evolution of the ultramafic complexes of northwestern New England, in Studies of Appalachian Geology - Northern and Maritime, E. Zen, ed., Interscience, New York, 343-354, 1968.

Dewey, J.F., Suture zone complexities: a review, Tectonophysics, 40, 53-67, 1977.

Dewey, J.F. and K. C.A. Burke, Tibetan, variscan, and Precambrian basement reactivation: products of continental collision, J. Geol., 81, 683-692, 1973.

Dewey, J.F., and W.S. Kidd, Continental collisions in the Appalachian Caledonian Orogenic belt. Variations related to complete and incomplete suturing, Geology, 2, 543-546, 1974.

Diment, W.H., T.C. Urban, and F.A. Revetta, Some geophysical anomalies in the eastern United States, in Nature of the Solid Earth, E.C. Robertson, ed., McGraw-Hill, 1972.

Dorman, I. and M. Ewing, Numerical Inversion of seismic surface wave dispersion data and crust-mantle structure in the New York - Pennsylvania area, J. Geophys. Res., 67, 5227-5241, 1962.

Ellsworth, W.L., Three-dimensional structure of the crust and mantle beneath the island of Hawaii, unpublished Ph.D. thesis, Massachusetts Institute of Technology, 1977.

Ellsworth, W.L. and R.Y. Koyanagi, Three-dimensional crust and mantle structure of Kilauea Volcano, Hawaii, J. Geophys. Res., 82, 5379-5394, 1977.

Engdahl, E.R., J.G. Sindorf, and R.A. Eppley, Interpretation of relative teleseismic P wave residuals, J. Geophys. Res., 82, 5671-5682, 1977.

Fletcher, J.B., M.L. Sbar, and L.R. Sykes, Seismic trends and travel-time residuals in eastern North America and their tectonic implications, Bull. Geol. Soc. Am., 89, 1656-1676, 1978.

Greenfield, R.J. and R.M. Sheppard, The Moho depth variations under the LASA and their effect on dT/dΔ measurements, Bull. Seism. Soc. Am., 59, 409-420, 1969.

Hirahara, K., A large-scale three-dimensional seismic structure under the Japan Islands and the Sea of Japan, J. Phys. Earth, 25, 393-417, 1977.

Iyer, H.M. and J.H. Healy, Teleseismic residuals at the LASA-USGS extended array and their interpretation in terms of crust and upper mantle structure, J. Geophys. Res., 77, 1503-1527, 1972.

Iyer, H.M., Anomalous delays of Teleseismic P waves in Yellowstone National Park, Nature, 253, 425-427, 1974.

Johnson, L.R., Array measurements of P velocities in the upper mantle, J. Geophys. Res., 72, 6309-6324, 1967.

Kane, M.F., G. Simmons, W. Diment, M. Fitzpatrick, W. Joyner, R. Bromery, Bouguer gravity and generalized geologic map of New England and adjoining areas, U.S. Geol. Survey

Geophys. Inv. Map, GP-839, 1972.

Katz, S., Seismic study of crustal structure in Pennsylvania and New York, Bull. Seism. Soc. Am., 45, 303-325, 1955.

Kent, D.V. and N.D. Opdyke, Paleomagnetism of the Devonian Catskill red beds: evidence for motion of the coastal New England - Canadian Maritime region relative to cratonic North America, J. Geophys. Res., 83, 1441-1450, 1978.

Kennedy, M.J., Southeastern margin of the Northeastern Appalachians: late Precambrian orogeny on a continental margin, Geol. Soc. America Bull., 87, 1317-1325, 1976.

King, P.B., Tectonic map of north America, scale 1:5,000,000, U.S. Geol., Surv., Washington, D.C., 1969.

Leet, D., Trial travel times for northeastern America, Bull. Seism. Soc. Am., 31, 325-334, 1941.

Lineham, S.J., New England seismic network, Semiannual technical report, V, 1962.

McKerrow, W.S., and L.R.M. Cocks, The location of the Iapetus Ocean suture in Newfoundland, Can. J. Earth Sci., 14, 488-495, 1977.

McLelland, J., The structural framework and stratigraphy of the southeastern Adirondacks, unpublished manuscript, 1977.

Menke, W.H., Lateral inhomogeneities in P velocity under the Tarbela Array of the Lesser Himalayas of Pakistan, Bull. Seism. Soc. Am., 67, 725-734, 1977.

Mitchell, B.J., C.C. Cheng, and W. Stauder, A three-dimensional velocity model of the lithosphere beneath the New Madrid seismic zone, Bull. Seism. Soc. Am., 67, 1061-1074, 1977.

Moench, R.H., and R.E. Zurtman, Chronology and styles of multiple deformation, plutonism, and polymetamorphism in the Merrimack Synclinorium of western Maine, Geol. Soc. of America, mem 146, 203-238, 1976.

Naylor, R.S., Origin and regional relationships of the core-rocks of the Oliverian domes, in Studies of Appalachian Geology - Northern and Maritime, E. Zen, ed., Interscience, New York, 231-239, 1968.

Naylor, R.S., Acadian orogeny: an abrupt and brief event, Science, 1972, 558-560, 1971.

Naylor, R.S., Age provinces in the Northern Appalachians, Ann. Rev. Earth and Planetary Sci., 3, 387-400, 1975.

Nelson, A.E., Structural elements and deformational history of rocks in eastern Massachusetts, Geol. Soc. America Bull., 87, 1377-1383, 1976.

Nuttli, O.W., and B.A. Bolt, P wave residuals as a function of azimuth, J. Geophys. Res., 74, 6594-6602, 1969.

Ratcliffe, N.M., Cross section of the Berkshire massif at 42°N: Profile of a basement reactivation zone, in N.E.I.G.C. Guidebook for field trips in western Massachusetts, northern Connecticut and adjacent areas of New York, N.M. Ratcliffe, ed., 1975.

Rankin, D.W., Volcanism related to tectonism in the Piscataquis volcanic belt, an island arc of Early Devonian age in north-central Maine, in Studies of Appalachian Geology -

Northern and Maritime, E. Zen, ed., Interscience, New York, 355-369, 1968.

Rankin, D.W., Appalachian salients and recesses: Late Precambrian continental breakup and the opening of the Iapetus Ocean, J. Geophys. Res., 81, 5605-5619, 1976.

Rodgers, J., The Tectonics of the Appalachians, Wiley-Interscience, New York, 271 pages, 1970.

Sbar, M.L. and L.B. Sykes, Seismicity and lithospheric stress in New York and adjacent areas, J. Geophys. Res., 82, 5771-5786, 1977.

Scheiddegger,A.E. and P.L. Willmore, The rise of a least squares method for the interpretation of data from seismic surveys, Geophys., 22, 9-22, 1957.

Schnerk, R., Y.P. Aggarwal, M. Golisomo, F. England, Regional seismicity bulletin of the Lamont-Doherty Network, 1976.

Sheppard, R.M., Values of LASA time station residuals, velocity and azimuth errors, Lincoln Lab tech. note, 90 pages, 1967.

Simmons, G., Gravity survey and geological interpretation, northern New York, Geol. Soc. Am. Bull., 75, 81-98, 1964.

Skehan, J.W., Fracture tectonics of southeastern New England as illustrated by the Wachusett-Marlborough Tunnel, Studies in Appalachian Geology: Northern and Maritime, New York, Interscience Publs, 281-290, 1968.

Steeples, D.W. and H.M. Iyer, Low-velocity zone under Long Valley as determined from teleseismic events, J. Geophys. Res., 81, 849-860, 1976.

Stewart, I.C.F., Teleseismic reflections and the Newfoundland lithosphere, Can. J. of Earth Sci., 15, 175-180, 1978.

Strong, D.F., Dickson, W.F., O'Driscoll, L.F., Kean, B.F., and R.K. Stevens, Geochemical evidence for an east-dipping Appalachian subduction zone in Newfoundland, Nature, 248, 37-39, 1974.

Taylor, S.R. and M.N. Toksöz, Crustal structure in New England (abstract), Earthquake Notes, 49, 81, 1978.

Thompson, M., Paleozoic regional metamorphism in New England and adjacent areas, in Studies in Appalachian Geology: Northern and Maritime, E. Zen, ed., Interscience, New York, 319-326, 1968.

Toksöz, M.N., N.H. Sleep, A.T. Smith, Evolution of the downgoing lithosphere and the mechanisms of deep focus earthquakes, Geophys. J. R. Astron. Soc., 35, 285-310, 1973.

Toksöz, M.N., and P. Bird, Modeling of temperatures in continental convergence zones, Tectonophysics, 41, 181-193, 1977.

Tseng, J., Gravity compensation of the Mohorovicic discontinuity and the basic model of crustal structure, Acta Geophysica Sinica, 16, 1-5, 1973.

Weston Geophysical Research, Inc., Areomagnetic map of southeastern New England and the Western Gulf of Maine, Pl. 26-1, 1976.

Woollard, G.P., Crustal structure from gravity and seismic measurements, J. Geophys. Res., 64, 1521-1544, 1959.

Zandt, G., Study of three-dimensional heterogeneity beneath seismic arrays in central California and Yellowstone, Wyoming, unpublished Massachusetts Instute of Technology Ph.D. Thesis, 1978.

Zandt, G., Three-dimensional seismic velocity anomalies in the crust and upper mantle under southwest Japan, (abstract), Trans. Am. Geop. Un., 56, 344, 1975.

Zarrow, L., Naylor, R.S., and F.A. Frey, Precambrian age of the Lynn Volcanics at Pine Hill in the Middlesex Fells Reservation, North Boston Quadrangle, Massachusetts, (abstract), N.E. Geol. Soc. of America, 10, 91, 1978.

Zen, E -An, The Taconide zone and the Taconic Orogeny in the western part of the northern Appalachian Orogen, Geol. Soc. Am. S.P. 135, 1972.

Table 1

Comparison of refraction models for eastern Massachusetts and southern New Hampshire (M.I.T.), central New Hampshire (Weston Geophysical), and northern New York and Adirondacks (Lamont-Doherty Geological Observatory, LDGO).

M.I.T.		Weston Geophysical		L.D.G.O.	
Depth(km)	P-velocity(km/s)	Depth	P-velocity	Depth	P-velocity
0-7.3	5.68	0-2.5	5.76	0-4.0	6.1
7.3-26.1	6.20	2.5-26.0	6.40	4.0-35.0	6.6
26.1-39.0	7.33	26.0-42.1	7.47	Moho	8.1
Moho	8.13	Moho	8.13		

Table 2

Initial Layered Velocity Model For Three-Dimensional Inversion

Layer No.	Velocity(km/s)	Thickness(km)	Block Length
1	6.4	35.0	(see text)
2	8.2	165.0	1°
3	8.6	150.0	1°
4	9.2	150.0	1°

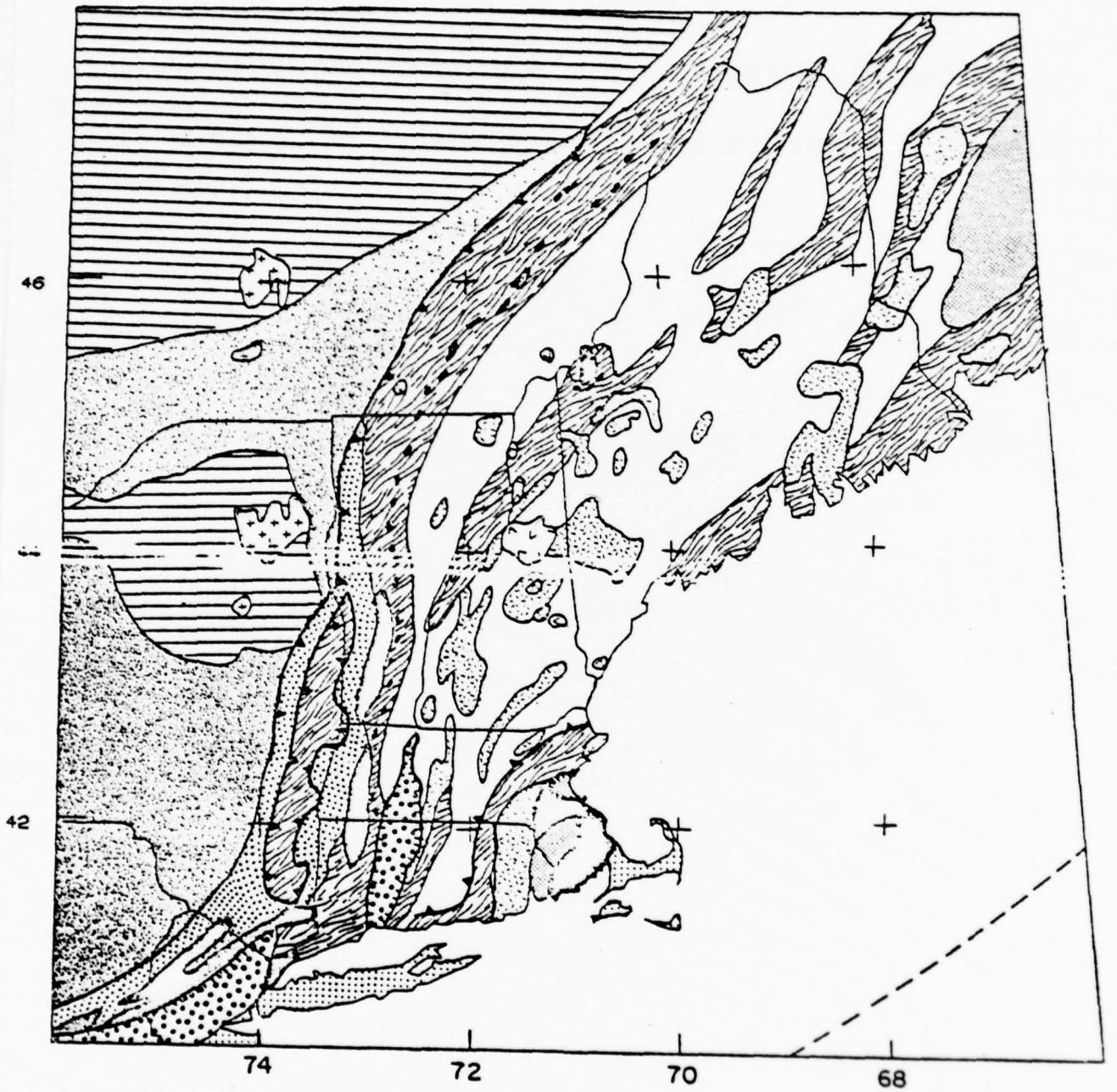

Figure 1a

Thrust fault, barbs on upper block

Normal fault, hachures on downthrown side

STRATIFIED ROCKS

Cenezoic glacial deposits

Triassic red beds

Carboniferous

Silurian - Devonian eugeoclinal rocks

Cambrian - Ordovician foreland rocks

Cambrian - Ordovician deformed miogeoclinal rocks

Cambrian - Ordovician eugeoclinal rocks

Precambrian rocks of the eastern block

Precambrian uplifts, Grenville basement

Precambrian Grenville basement

IGNEOUS ROCKS

Mesozoic White Mountain Plutonic Series

Devonian New Hampshire Plutonic Series

Cambrian - Ordovician serpentinites, ultramafics

Precambrian anorthosites

Figure 1a

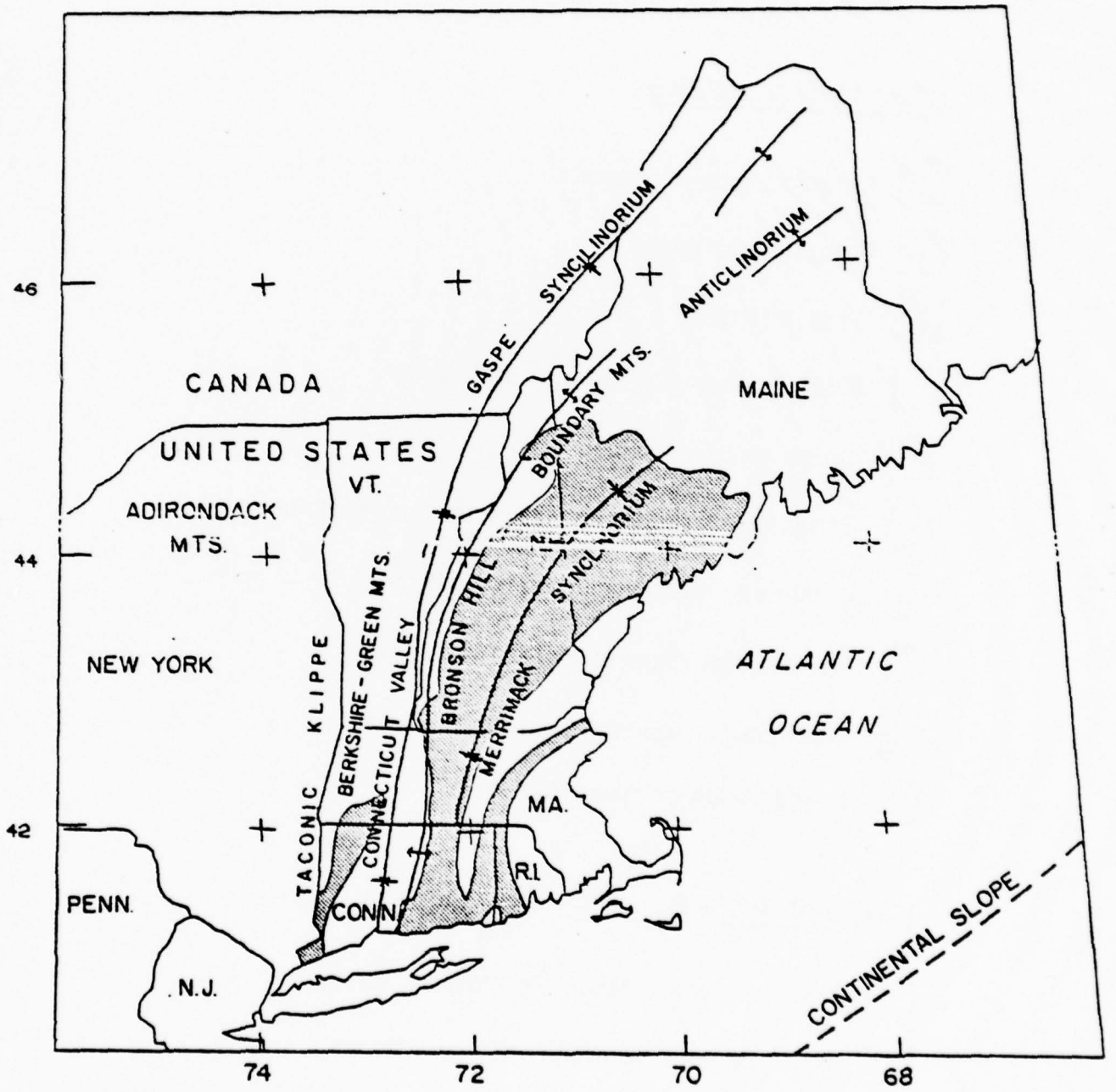
46
44
42
74
72
70
68
CANADA
UNITED STATES
VT.
ADIRONDACK
MTS.
NEW YORK
PENN.
N.J.
CONN.
MA.
RI
MAINE
ATLANTIC
OCEAN
GASPE SYNCLINORIUM
ANTICLINORIUM
BOUNDARY MTS.
SYNCLINORIUM
BRONSON HILL
MERRIMACK
CONNECTICUT VALLEY
BERKSHIRE - GREEN MTS.
KLIPPE
TACONIC
CONTINENTAL SLOPE

Figure 1b

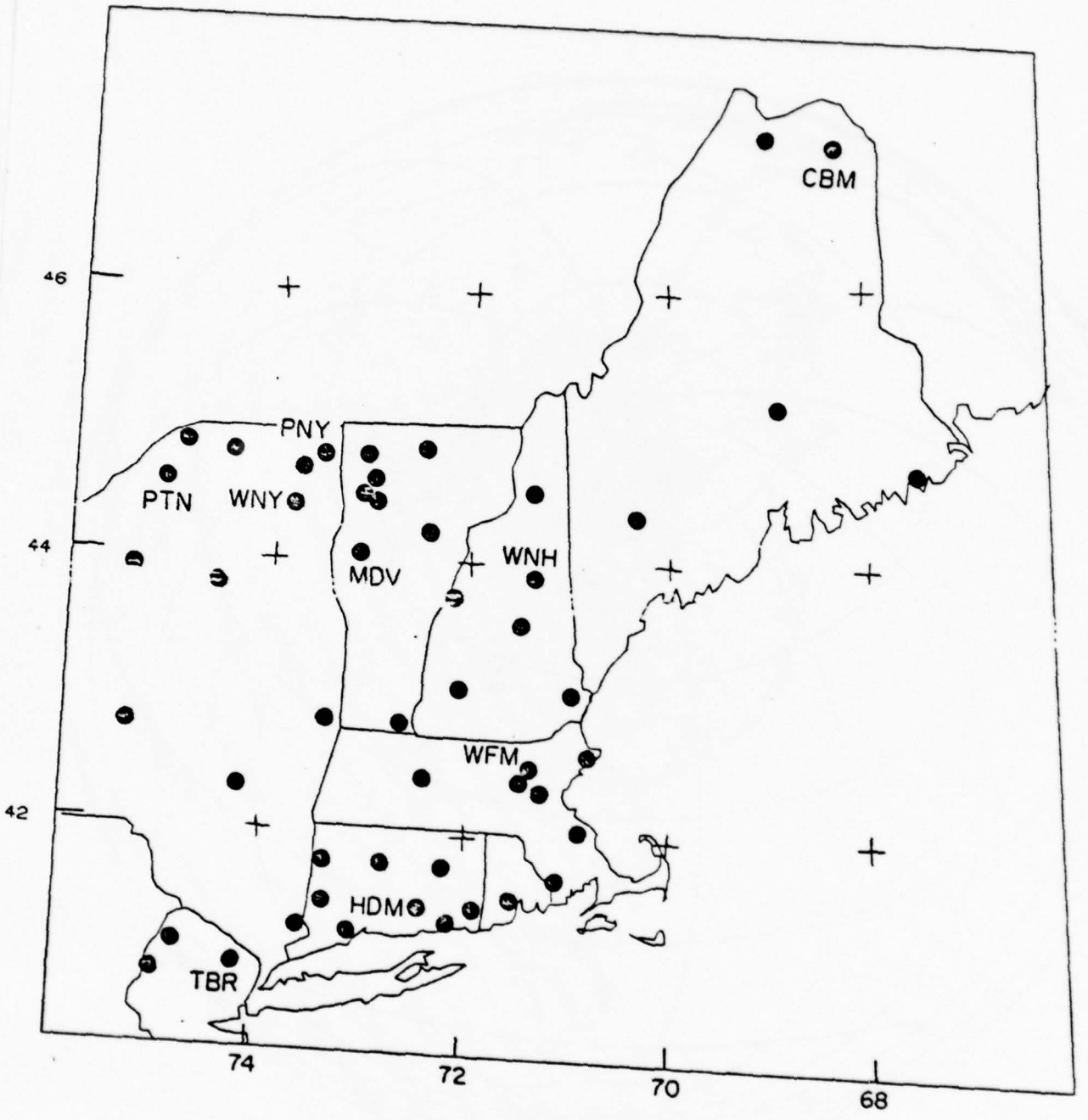

Figure 2

Figure 3

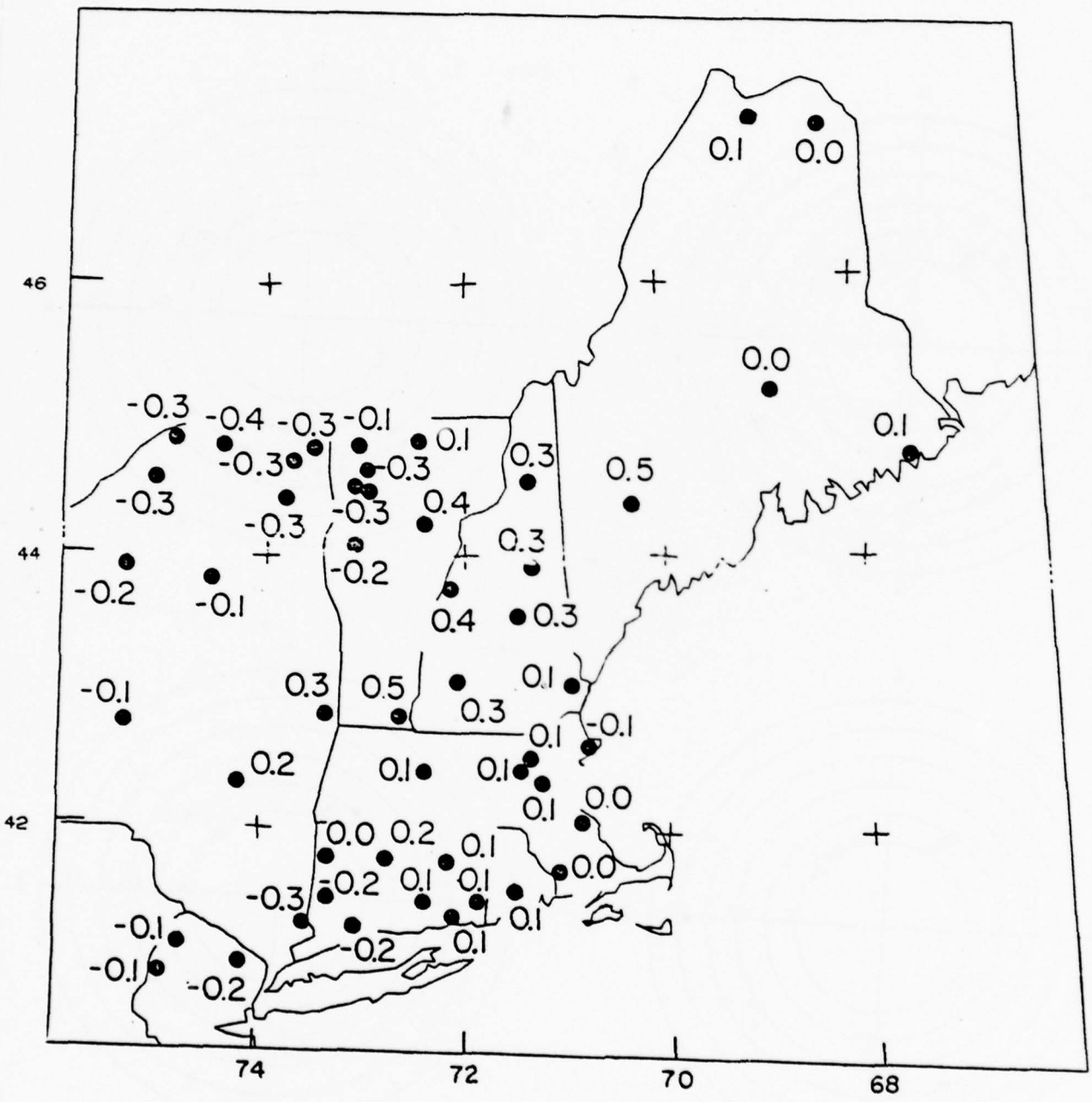
46
44
42
74
72
70
68
0.1
0.0
0.0
0.1
0.5
-0.3
-0.4
-0.3
-0.1
0.1
0.3
-0.3
-0.3
-0.3
-0.3
0.4
-0.3
-0.2
-0.2
-0.1
0.3
0.4
0.3
-0.1
0.3
0.5
0.3
0.1
0.1
-0.1
0.2
0.1
0.1
0.1
0.0
0.0
0.2
0.1
0.0
-0.2
0.1
0.1
-0.3
0.1
-0.1
-0.2
0.1
-0.1
-0.2

Figure 4

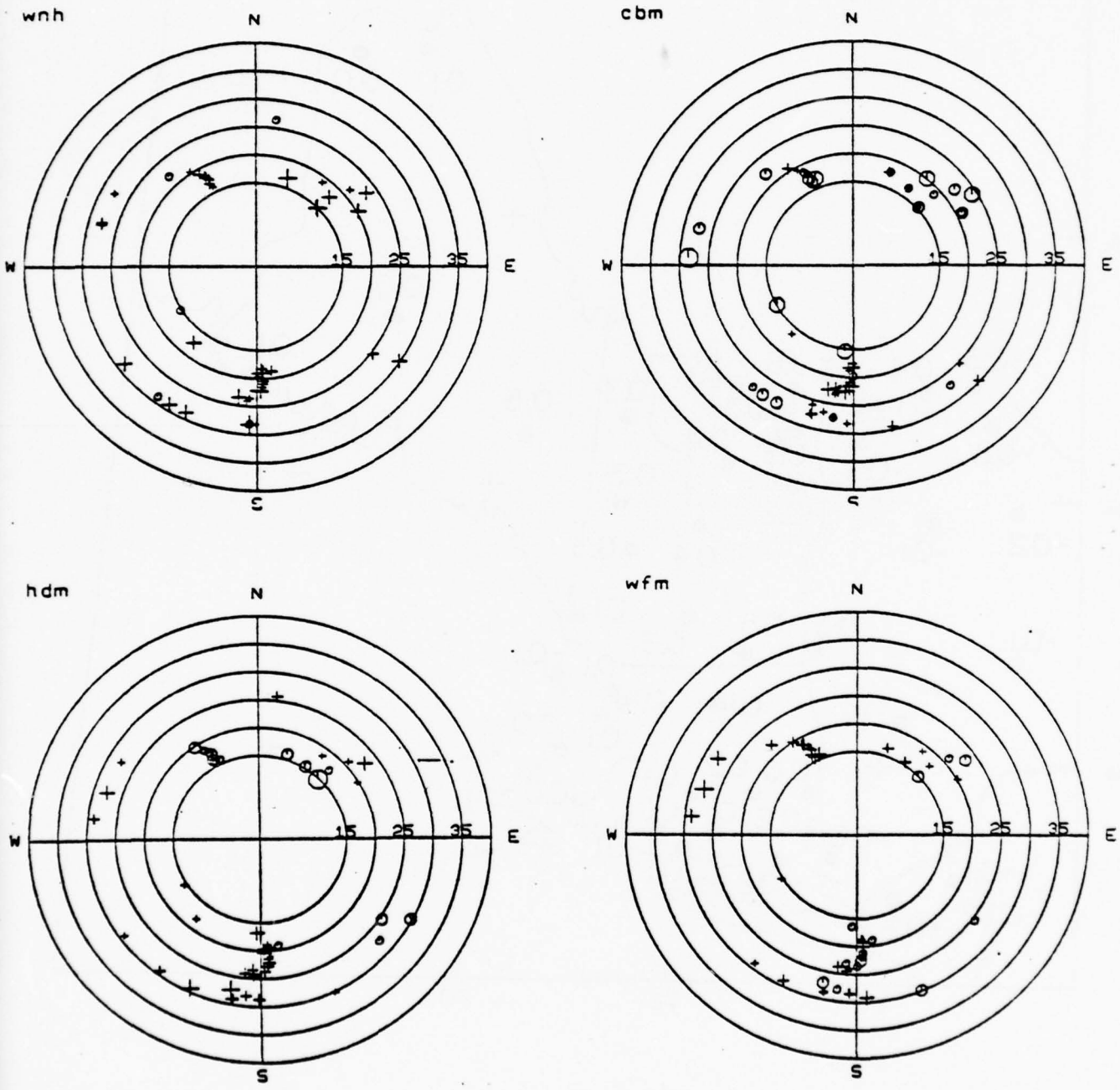
wnh
N
W
E
S
15
25
35
cbm
N
W
E
S
15
25
35
hdm
N
W
E
S
15
25
35
wfm
N
W
E
S
15
25
35

Figure 5

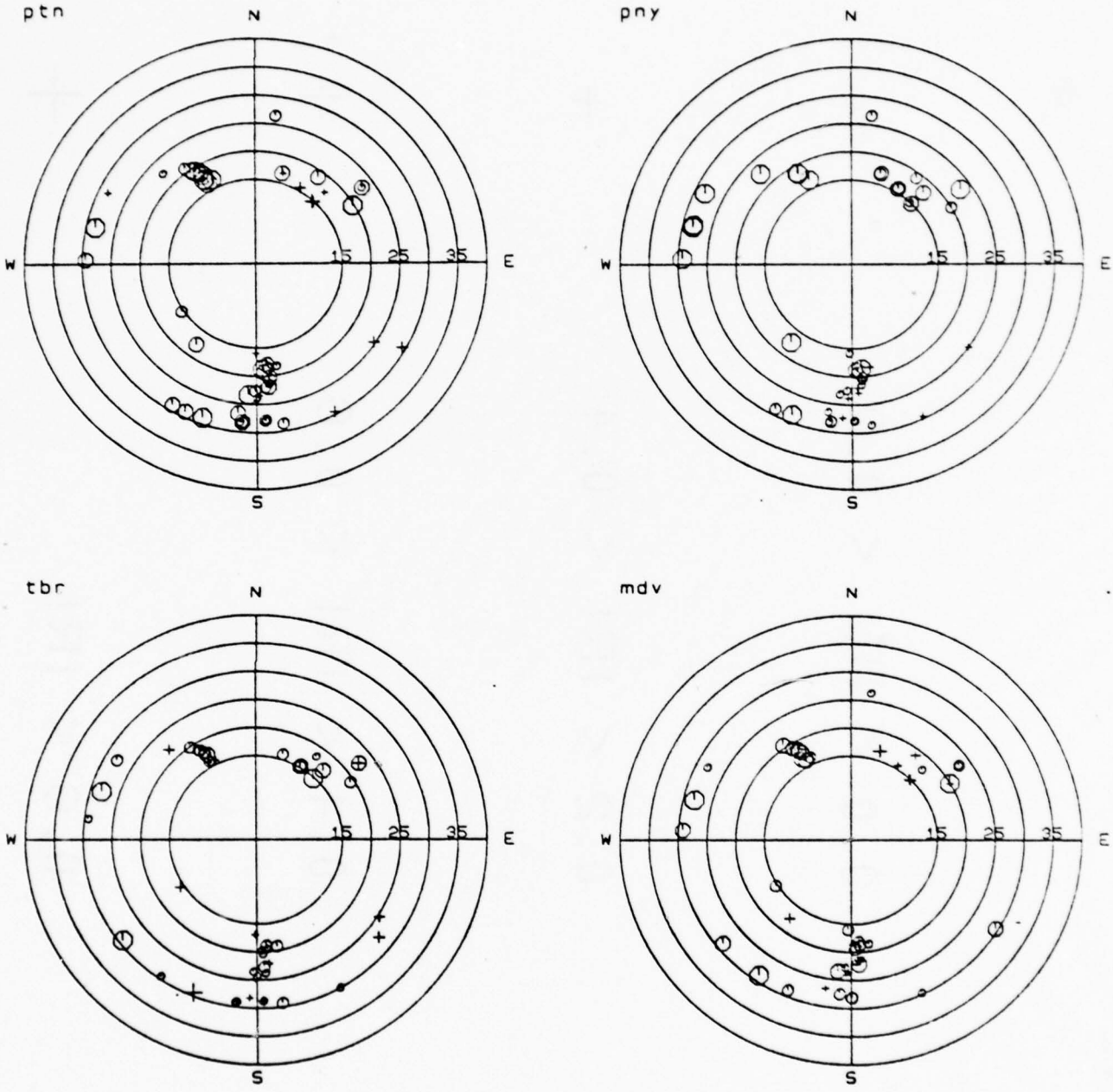
ptn
N
W
E
S
15
25
35
pny
N
W
E
S
15
25
35
tbr
N
W
E
S
15
25
35
mdv
N
W
E
S
15
25
35

Figure 5

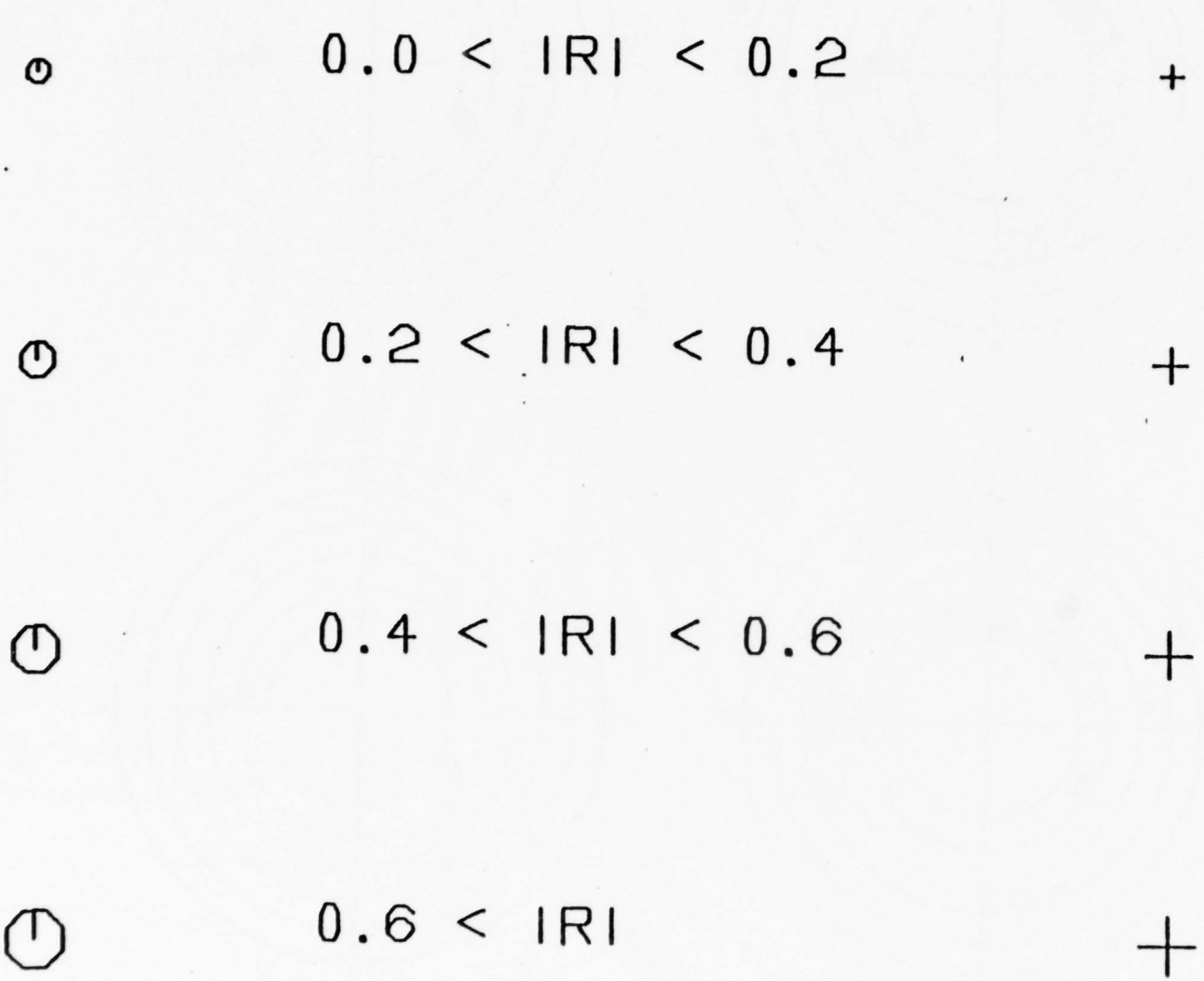

Figure 5

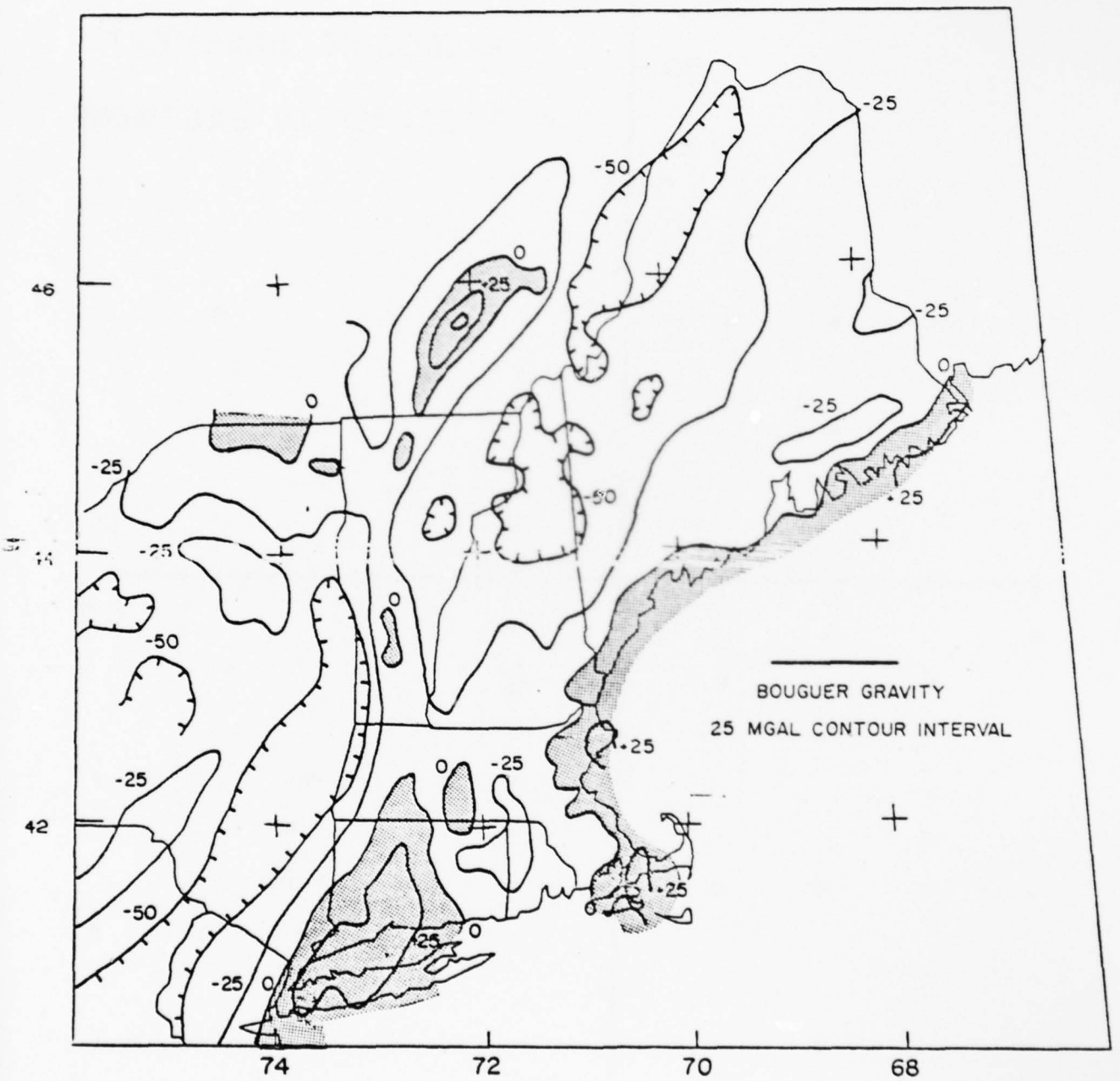
46
42
74
72
70
68
-25
-50
0
BOUGUER GRAVITY
25 MGAL CONTOUR INTERVAL

Figure 6

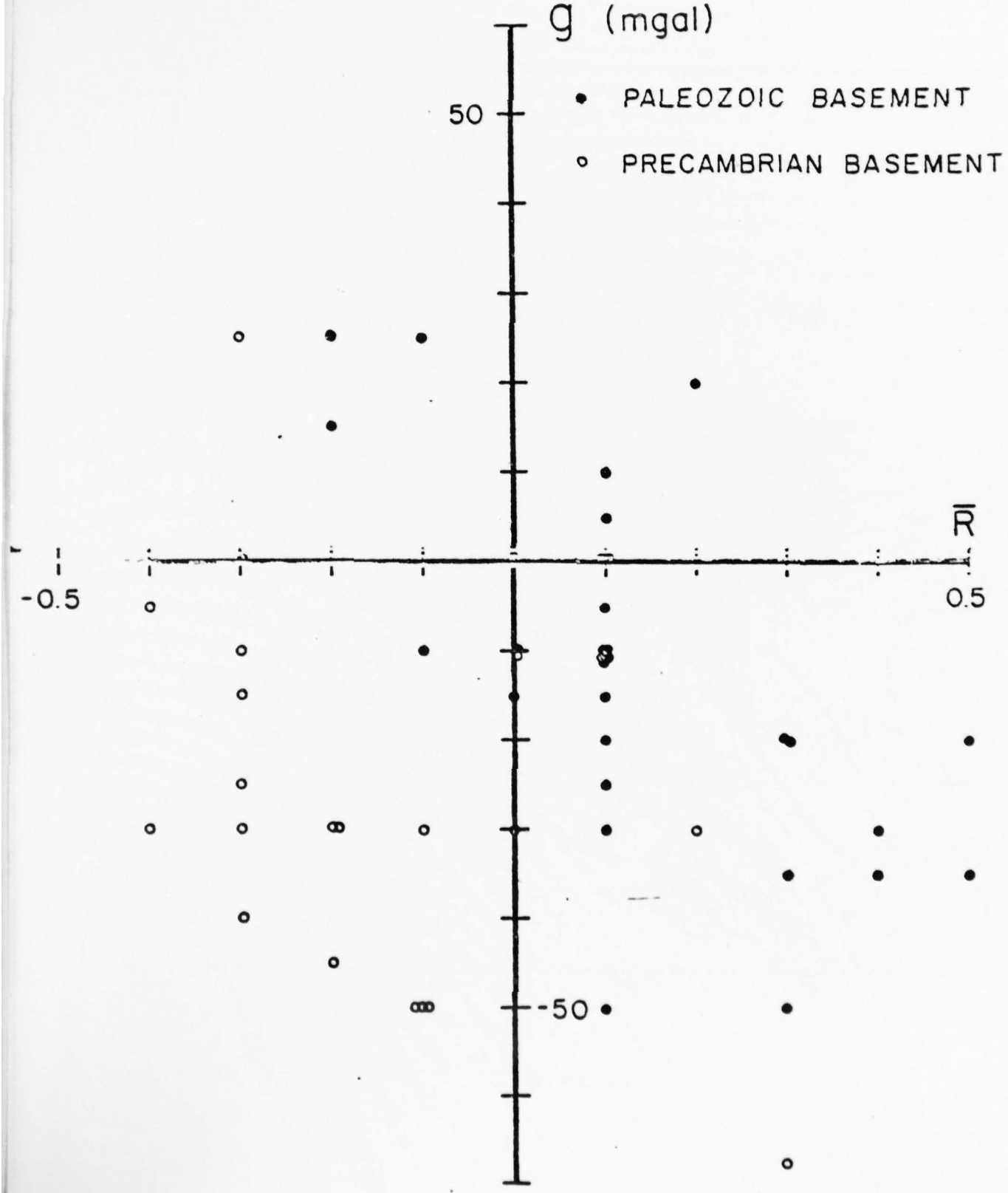
g (mgal)
PALEOZOIC BASEMENT
PRECAMBRIAN BASEMENT
50
-50
R̄
-0.5
0.5

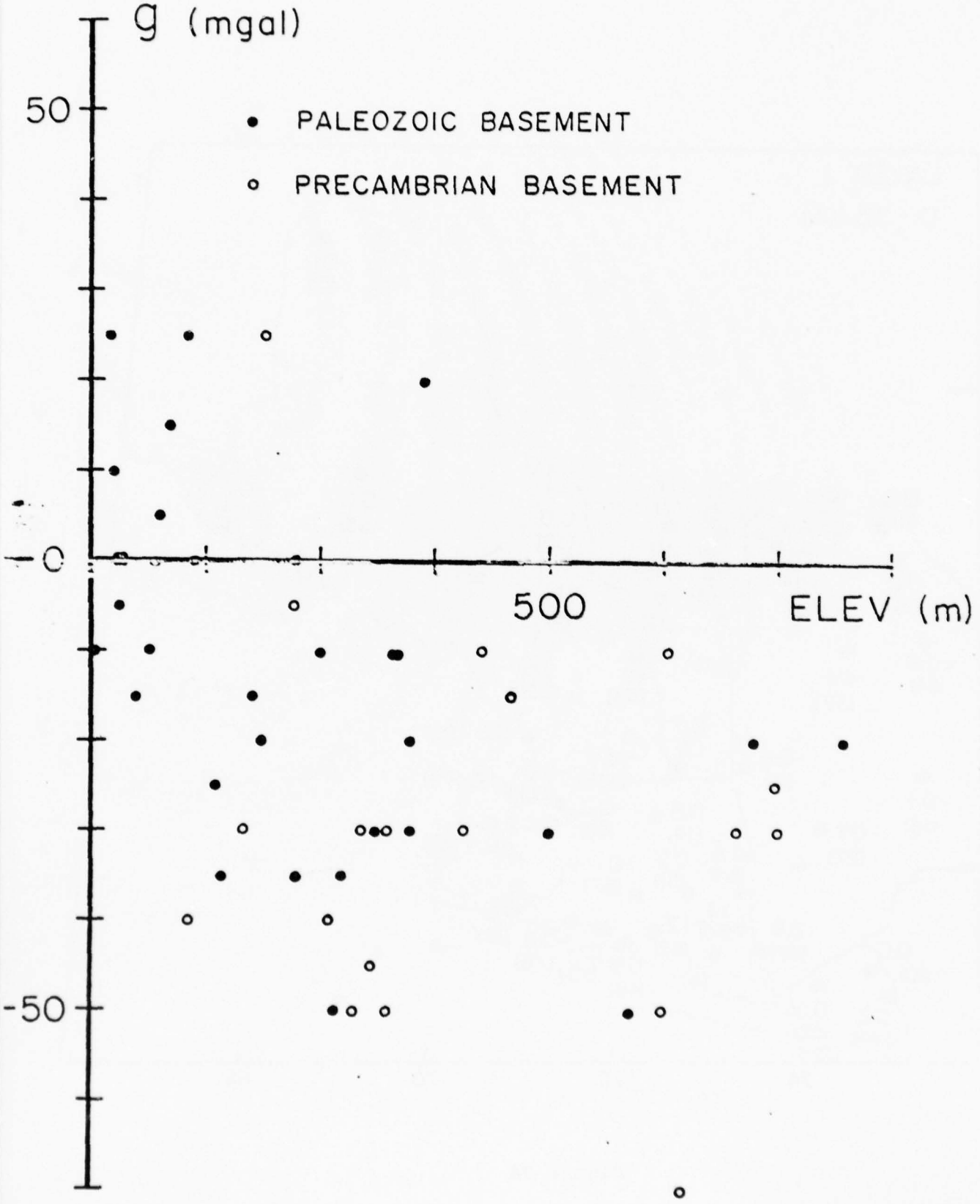
g (mgal)
50
PALEOZOIC BASEMENT
PRECAMBRIAN BASEMENT
0
500
ELEV (m)
-50

Figure 8

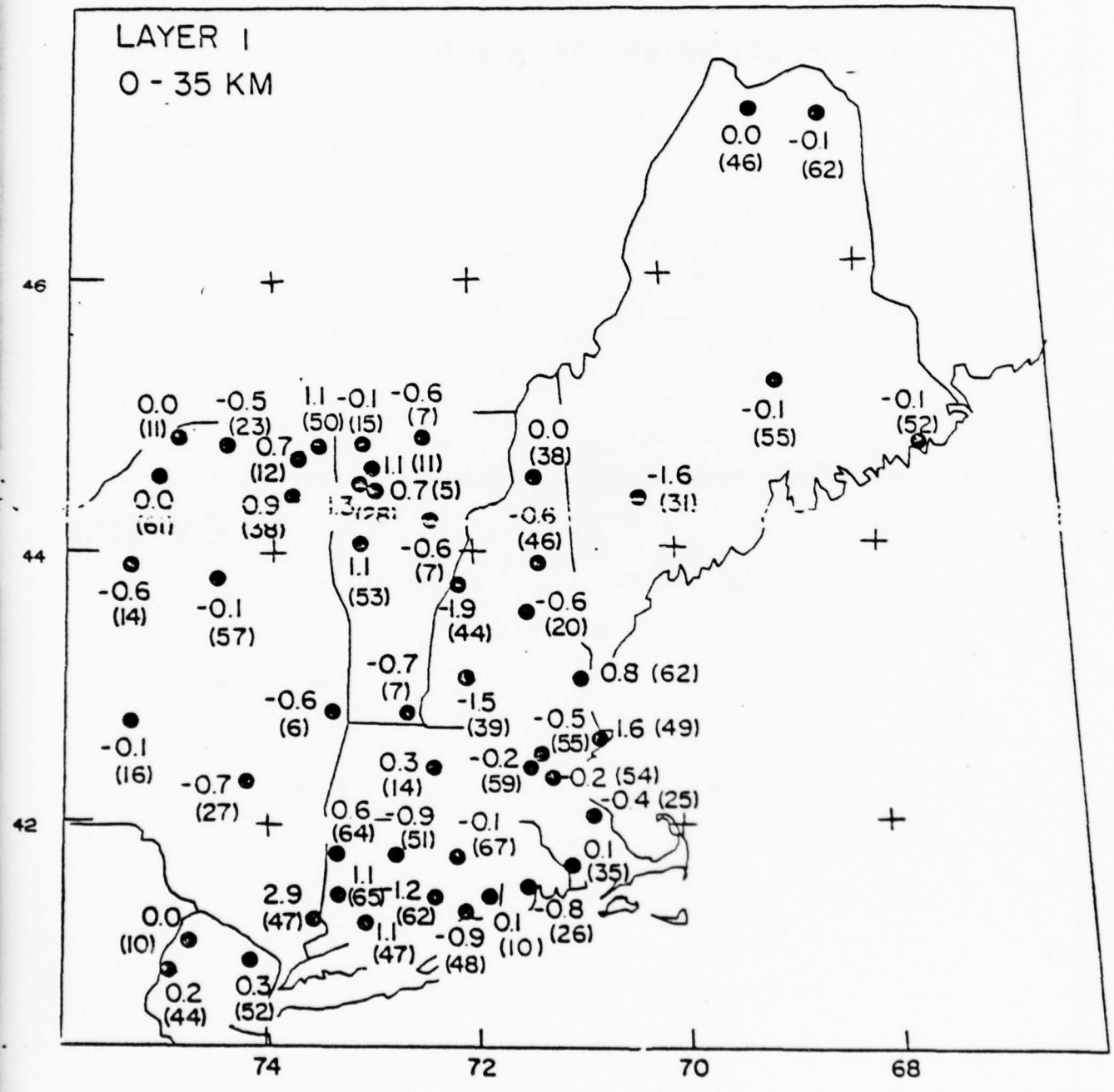
LAYER 1
0 - 35 KM
46
44
42
74
72
70
68
0.0 (46)
-0.1 (62)
-0.1 (55)
-0.1 (52)
0.0 (38)
-1.6 (31)
-0.6 (46)
0.0 (11)
-0.5 (23)
1.1 (50)
-0.1 (15)
-0.6 (7)
0.7 (12)
1.1 (11)
0.7 (5)
0.0 (61)
0.9 (38)
-0.6 (7)
1.1 (53)
-0.6 (14)
-0.1 (57)
-1.9 (44)
-0.6 (20)
-0.7 (7)
0.8 (62)
-0.6 (6)
-1.5 (39)
-0.5 (55)
1.6 (49)
-0.1 (16)
0.3 (14)
-0.2 (59)
0.2 (54)
-0.7 (27)
-0.4 (25)
0.6 (64)
-0.9 (51)
-0.1 (67)
0.1 (35)
1.1 (65)
2.9 (47)
1.2 (62)
-0.8 (26)
0.0 (10)
1.1 (47)
0.1 (10)
-0.9 (48)
0.2 (44)
0.3 (52)

Figure 9a

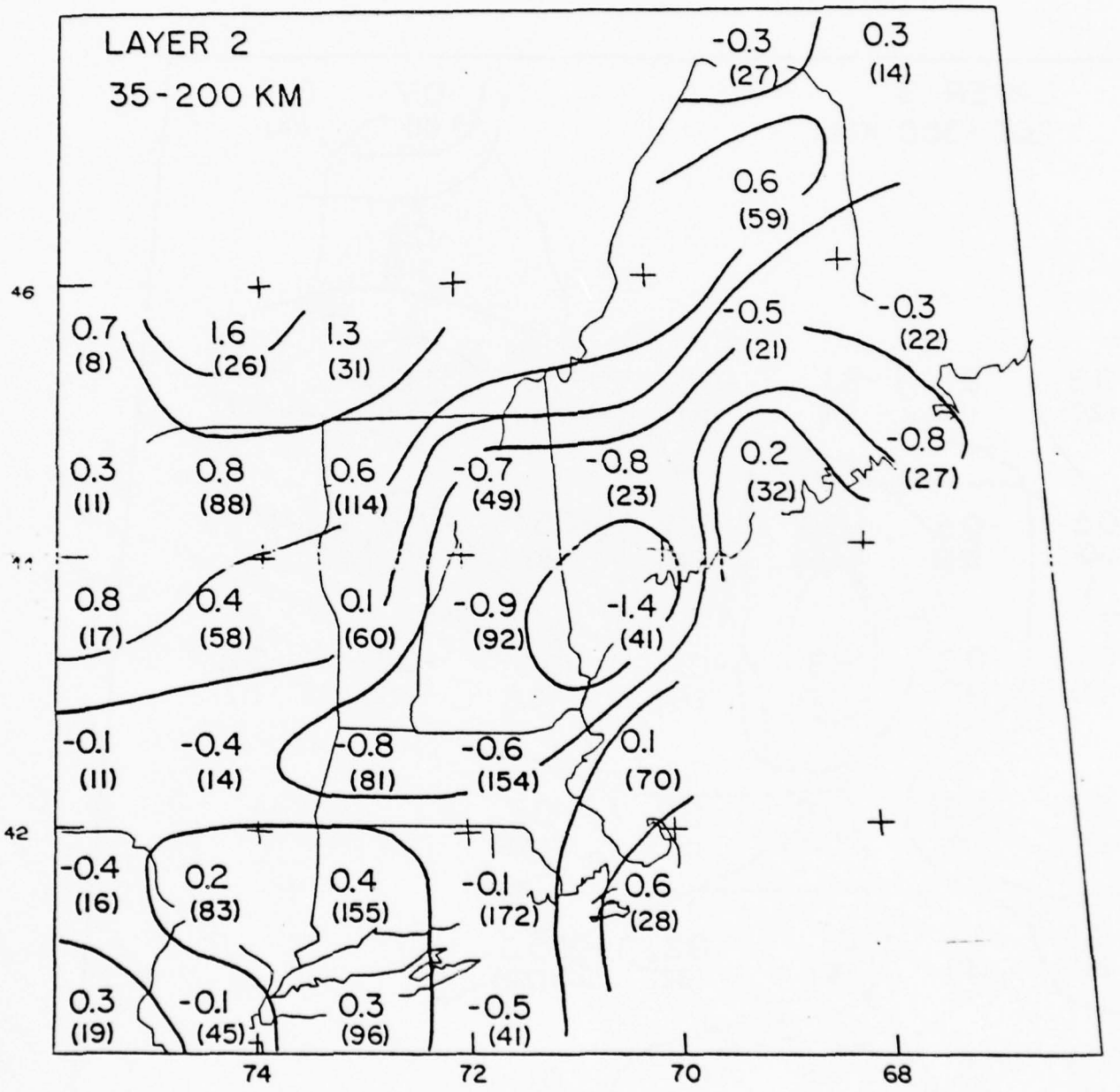
LAYER 2
35-200 KM
-0.3
(27)
0.3
(14)
0.6
(59)
-0.5
(21)
-0.3
(22)
0.7
(8)
1.6
(26)
1.3
(31)
0.3
(11)
0.8
(88)
0.6
(114)
-0.7
(49)
-0.8
(23)
0.2
(32)
-0.8
(27)
0.8
(17)
0.4
(58)
0.1
(60)
-0.9
(92)
-1.4
(41)
-0.1
(11)
-0.4
(14)
-0.8
(81)
-0.6
(154)
0.1
(70)
-0.4
(16)
0.2
(83)
0.4
(155)
-0.1
(172)
0.6
(28)
0.3
(19)
-0.1
(45)
0.3
(96)
-0.5
(41)
46
44
42
74
72
70
68

Figure 9b

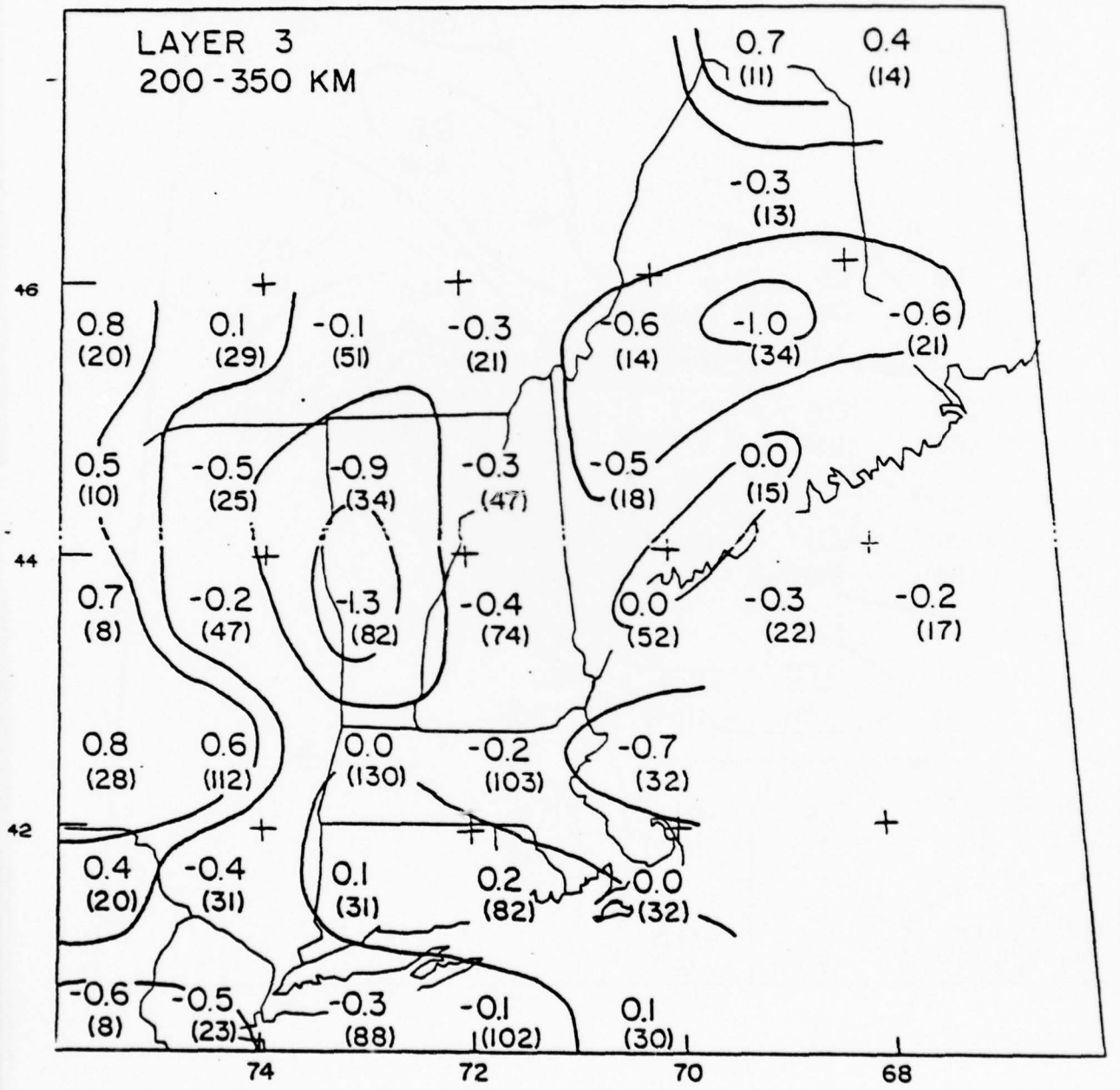
LAYER 3
200-350 KM
0.7 (11)
0.4 (14)
-0.3 (13)
0.8 (20)
0.1 (29)
-0.1 (51)
-0.3 (21)
-0.6 (14)
-1.0 (34)
-0.6 (21)
0.5 (10)
-0.5 (25)
-0.9 (34)
-0.3 (47)
-0.5 (18)
0.0 (15)
0.7 (8)
-0.2 (47)
-1.3 (82)
-0.4 (74)
0.0 (52)
-0.3 (22)
-0.2 (17)
0.8 (28)
0.6 (112)
0.0 (130)
-0.2 (103)
-0.7 (32)
0.4 (20)
-0.4 (31)
0.1 (31)
0.2 (82)
0.0 (32)
-0.6 (8)
-0.5 (23)
-0.3 (88)
-0.1 (102)
0.1 (30)
46
44
42
74
72
70
68

Figure 9c

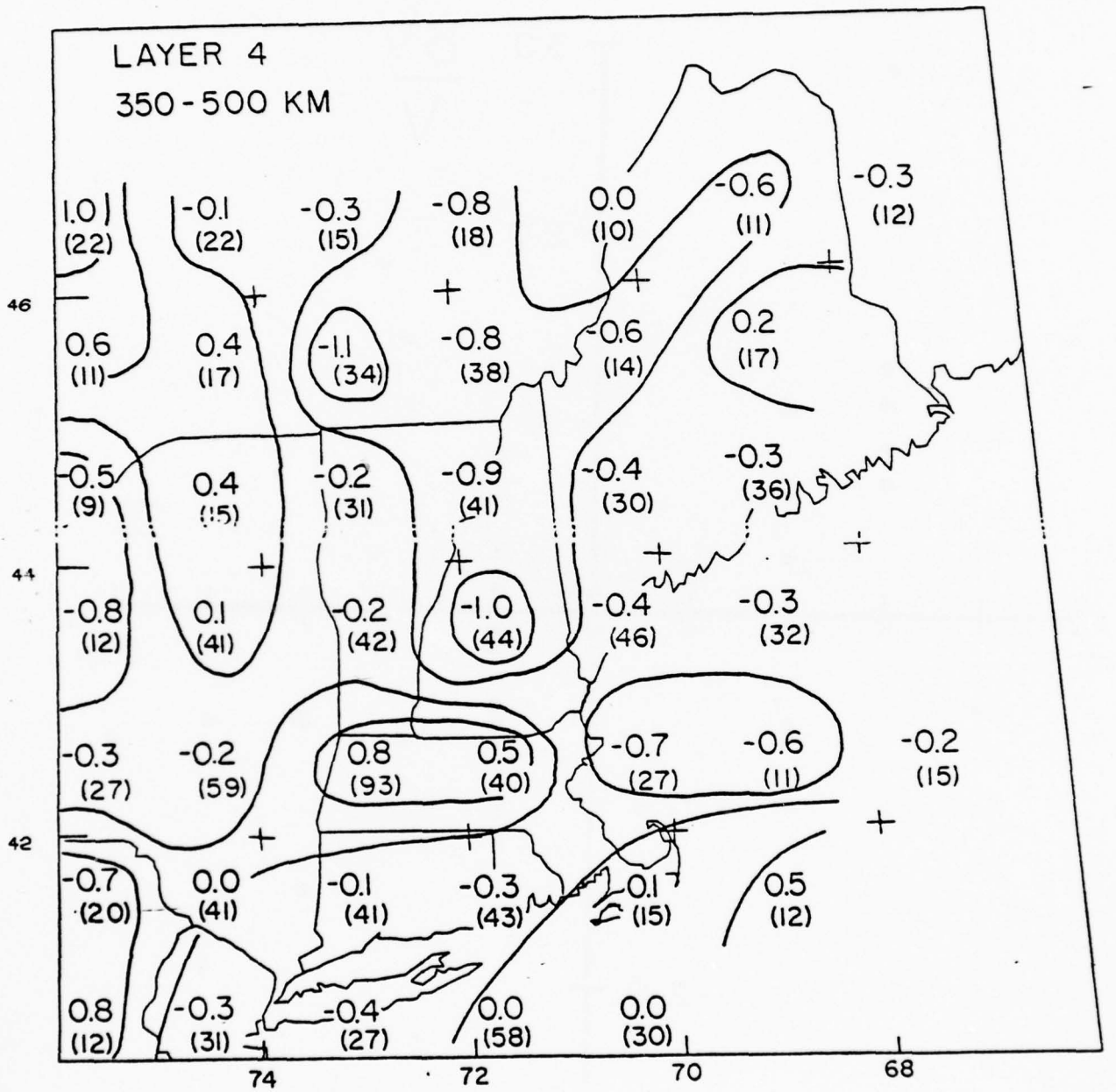
LAYER 4
350 - 500 KM
1.0 (22)
-0.1 (22)
-0.3 (15)
-0.8 (18)
0.0 (10)
-0.6 (11)
-0.3 (12)
0.6 (11)
0.4 (17)
-1.1 (34)
-0.8 (38)
-0.6 (14)
0.2 (17)
-0.5 (9)
0.4 (15)
-0.2 (31)
-0.9 (41)
-0.4 (30)
-0.3 (36)
-0.8 (12)
0.1 (41)
-0.2 (42)
-1.0 (44)
-0.4 (46)
-0.3 (32)
-0.3 (27)
-0.2 (59)
0.8 (93)
0.5 (40)
-0.7 (27)
-0.6 (11)
-0.2 (15)
-0.7 (20)
0.0 (41)
-0.1 (41)
-0.3 (43)
0.1 (15)
0.5 (12)
0.8 (12)
-0.3 (31)
-0.4 (27)
0.0 (58)
0.0 (30)
46
44
42
74
72
70
68

Figure 9d

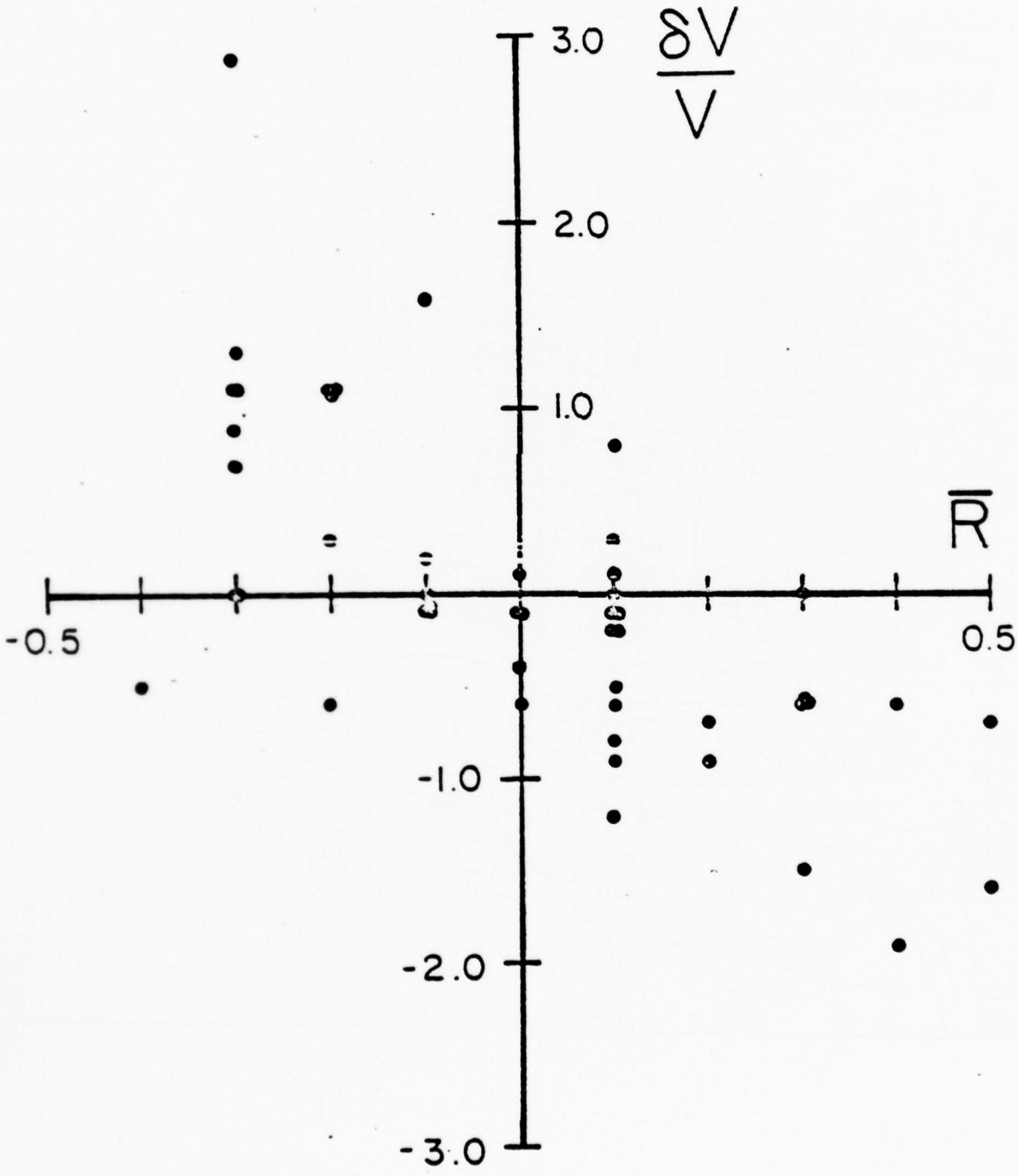

Figure 10

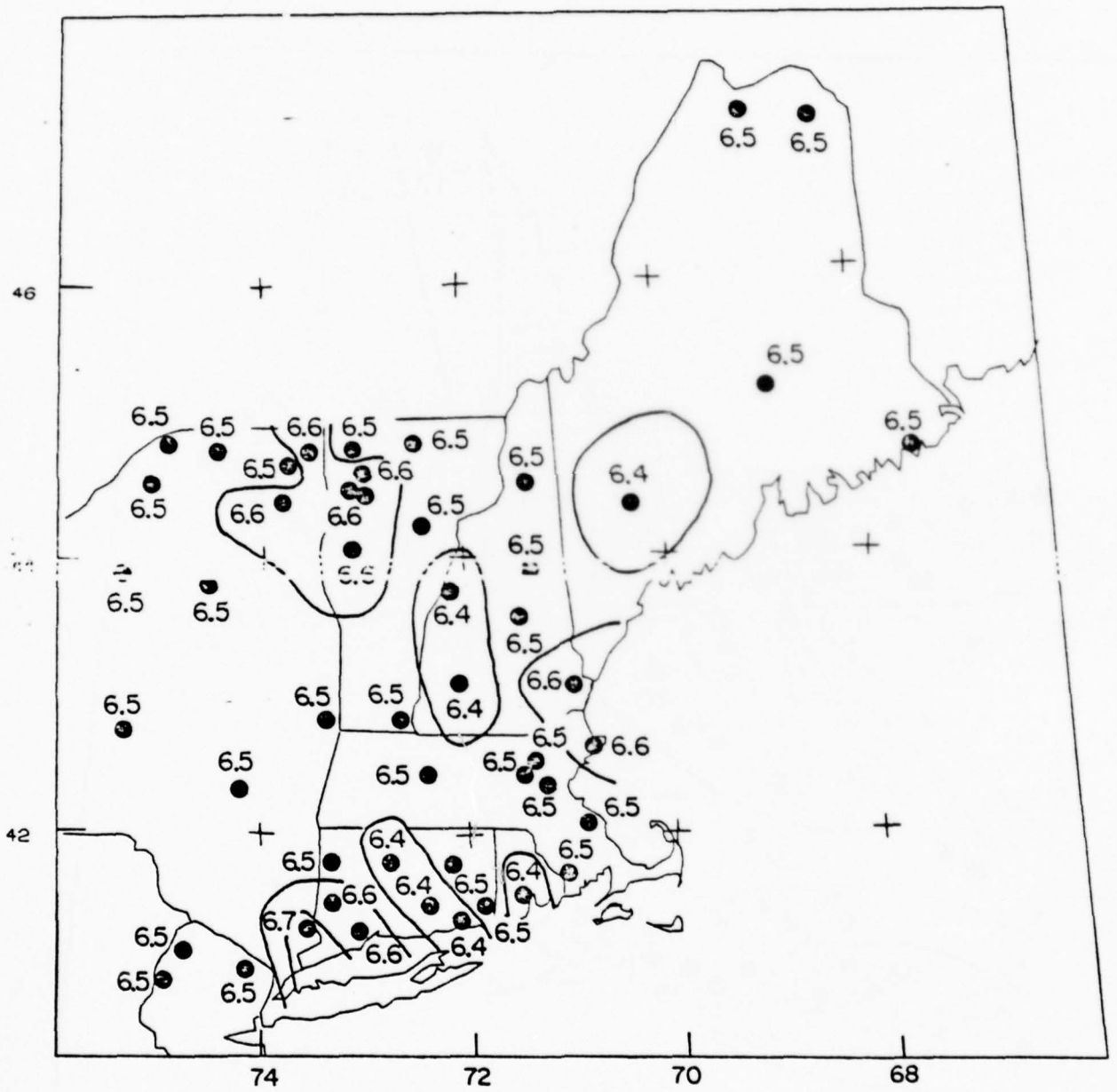

Figure 11a

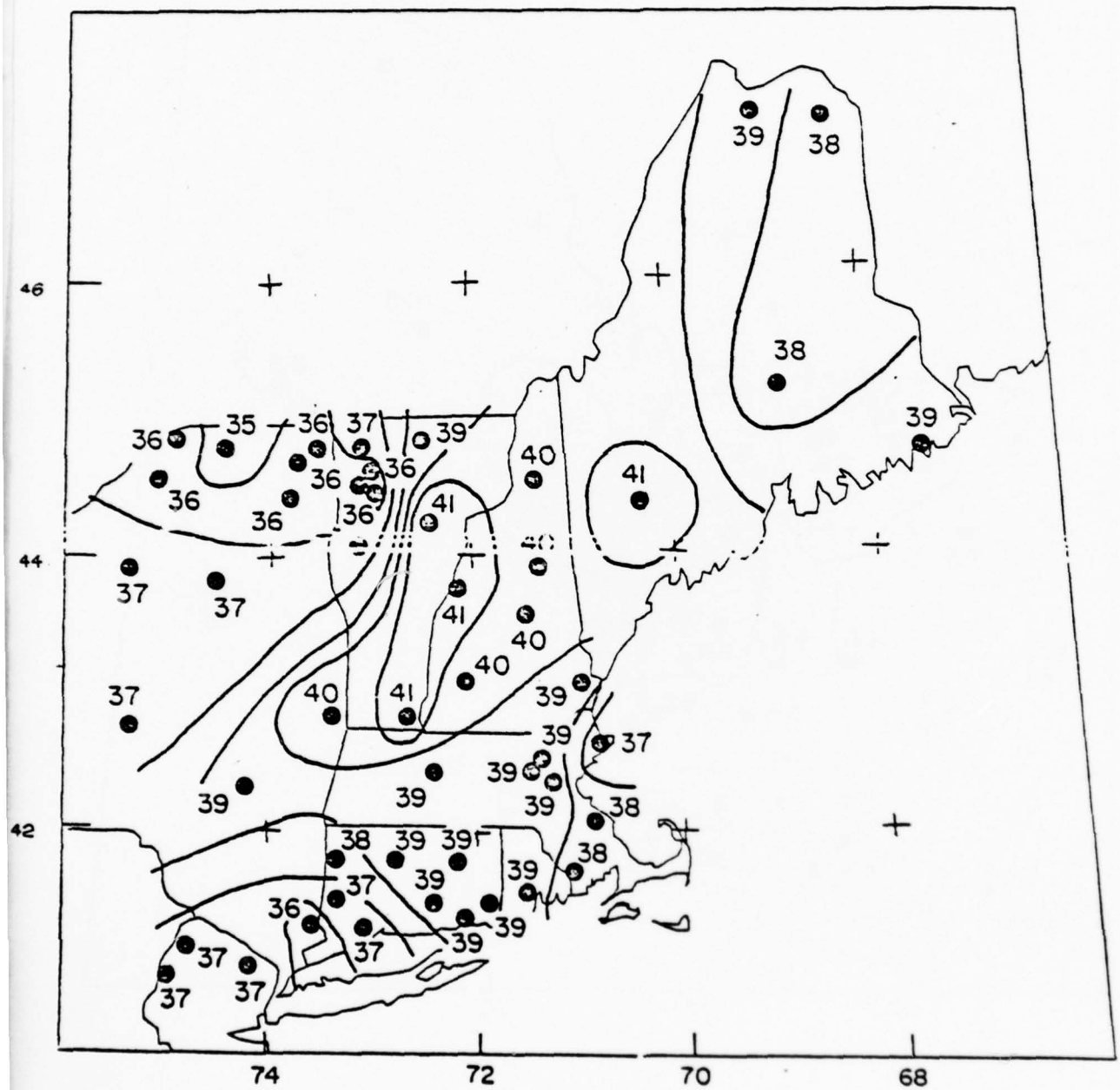
46
44
42
74
72
70
68
39
38
38
39
36
35
36
37
39
36
36
36
36
36
40
41
41
41
40
40
40
37
37
37
40
41
39
39
37
39
39
39
38
38
39
39
38
39
37
39
36
37
39
37
37
37

Figure 11b

THE ATTENUATION OF SEISMIC WAVES IN DRY AND SATURATED ROCKS

by

DAVID H. JOHNSTON

S.B., Massachusetts Institute of Technology (1973)

SUBMITTED IN PARTIAL FULFILLMENT

OF THE REQUIREMENTS FOR THE

DEGREE OF

DOCTOR OF PHILOSOPHY

at the

 MASSACHUSETTS INSTITUTE OF TECHNOLOGY

October 19, 1978

Signature of Author David H. Johnston
Department of Earth and Planetary Sciences, October 19, 1978

Certified by ..... Thesis Supervisor

Accepted by ..... Chairman, Departmental Committee on Graduate Students

THE ATTENUATION OF SEISMIC WAVES IN DRY AND SATURATED ROCKS

by

David H. Johnston

Submitted to the Department of Earth and Planetary Sciences on October 19, 1978, in partial fulfillment of the requirements for the degree of Doctor of Philosophy.

ABSTRACT

The attenuation of seismic waves in upper crustal rocks is studied from both experimental data and theoretical models of specific attenuation mechanisms. The attenuation, or anelasticity may be used in conjunction with the compressional (P) and shear (S) wave velocities to infer the microstructure of the rock and the physical conditions encountered in the subsurface environment. Generally, the attenuation varies much more than velocity with accompanying changes in the physical state making this measurement a particularly valuable tool. Unfortunately, systematic studies of the behavior of attenuation with parameters such as pressure and saturation conditions are deficient. Nor has the development of new experimental techniques and theoretical models kept pace with the methods for elastic properties.

It is shown in this thesis that previous experimental data suggest one or more of several proposed mechanisms may be contributing to the overall attenuation observed in crustal rocks. These include crack and grain boundary sliding friction; fluid associated mechanisms such as crack lubrication, fluid flow through porous and permeable rock, squirting flow from thin cracks to larger pores, and viscous shear relaxation in the void spaces; losses associated with gas bubble resonances; and a host of geometrical effects with scattering from pores in the rock being most important from an experimental point of view. Mathematical models of all these mechanisms in terms of their frequency and pressure dependences are developed.

The attenuation or Q values (inverse proportional to

the energy loss) for P and S waves are determined for a suite of upper crustal rocks as functions of pressure and saturation using an ultrasonic pulse transmission technique with the goal of interpreting these results in terms of the theoretical models of the mechanisms. In general, it is found that Q for both P and S waves increases (attenuation decreases) as a function of pressure for dry and water saturated rocks. Q values for saturated and partially saturated rocks are less than for dry rocks and while not conclusive, the experiments suggest that Q_p for low gas saturations is slightly lower compared to the fully water saturated case. The major controlling factor in determining the differences in Q for individual rocks is the nature and concentration of thin cracks - the exceptions studied being shales and tuffs. Rocks with a higher density of fine cracks exhibit lower Q values and the rate of change of Q with pressure may be correlated with the crack width distribution inferred from static stress-strain measurements.

Modeling of the Q data obtained for dry and water saturated samples of Berea sandstone imply that friction is the dominant mechanism for attenuation. Increasing pressure decreases the number of sliding surfaces and thus Q increases. The major effect of fluid is to lubricate these surfaces thus facilitating sliding. Attenuation due to fluid flow plays a secondary role. At ultrasonic frequencies and moderate pressures, flow is, however, important in porous and permeable rock like the sandstone. Scattering is dominant only at very high frequency or, as with the tuffs, when the grain or pore sizes are large compared to the wavelength. Attenuation in shales may be due to relative shear motion between the rock matrix and clay or kerogen. Bubble associated losses in partially saturated rocks may be important only in limited cases.

The phenomenon of frictional attenuation is further examined using a resonance bar experimental technique. It is found that Q in dry rocks is dependent on amplitude, constant at low strains but decreasing rapidly at strains greater than about 10^{-6}, explaining differences in Q observed between resonance and ultrasonic methods. The amplitude dependence is also a function of the types of cracks existing in the rock. This is investigated for samples that have been thermally cycled in order to induce cracking. It is found that rocks cycled at low heating rates show an increase in Q up to a cycled temperature of about 400°C which is accompanied by a migration of the amplitude transition to lower strains. These data are interpreted in terms of the widening of thin cracks thus reducing the contact area of frictional sliding - both

increasing Q and allowing the surfaces to slide at lower amplitudes. Some of the effect observed may also be due to outgassing of volatiles from the crack surfaces.

The results obtained in this thesis may be used to evaluate the difficulties involved in extrapolating laboratory data to insitu measurements of attenuation. Theoretical models such as those used to describe the anelastic behavior of the Berea sandstone, provide the best method at the present time. However, field measurements must be corrected for other factors that affect seismic wave amplitude. Furthermore, the contributions of mechanisms that may be important at low frequencies and not easily established from ultrasonic data plus the amplitude dependence of attenuation must be considered before any meaningful comparisons can be made.

Thesis Supervisor: M. Nafi Toksöz
Title: Professor of Geophysics

THERMAL CRACKING AND AMPLITUDE DEPENDENT ATTENUATION

by

David H. Johnston and M. Nafi Toksöz
Department of Earth and Planetary Sciences
Massachusetts Institute of Technology
Cambridge, Massachusetts 02139

December 1978

Copies: 4

MS Pages: 49

Figures: 16

Tables: 2

Address correspondence to: M.N. Toksöz, M.I.T. 54-518
Cambridge, MA 02139

ABSTRACT

The role of crack and grain boundary contacts in determining seismic wave attenuation in rock is investigated by examining Q as a function of thermal cycling (cracking) and wave strain amplitude. Q values are obtained using a longitudinal resonant bar technique in the 10-20 kHz range for maximum strain amplitudes varying from roughly 10^{-8} to 10^{-5}. The samples studied include the Berea and Navajo sandstones, Plexiglas, westerly granite, Solenhofen limestone and Frederick diabase, the latter two relatively crack free in their virgin state. Measurements were made at room temperature and pressure in air.

Q values for both sandstones are constant at low strains ($<10^{-6}$) but decrease rapidly with amplitude at higher strains. There is no hysteresis of Q with amplitude. Q values for Plexiglas show no indication of amplitude dependent behavior.

The granite, limestone and diabase are thermally cycled at both fast and slow heating rates in order to induce cracking. Samples slowly cycled to 400°C show a marked increase in Q that cannot be entirely explained by outgassing of volatiles. Cycling widens thin cracks and grain boundaries,

reducing contact areas. Rapidly heated samples exhibit completely different behavior. Amplitude dependence of Q is found to be coupled to the effects of thermal cycling. The transition from low to high strain amplitude behavior occurs at lower strains for thermally cycled rocks.

INTRODUCTION

The presence of fine, thin cracks and grain boundary contacts has been shown to have an important role in determining many of the elastic and anelastic properties of rock. In particular, they control the velocity and attenuation behavior at moderate confining pressures (Walsh, 1965 and 1966; Toksöz et al., 1976; Johnston and Toksöz, 1979). Increases in both velocity and Q with pressure at all frequencies and under a variety of saturation and strain amplitude conditions may be attributed to the closing of these cracks and grain boundary contacts. The pressure dependence of Q, however, provides only a general indication as to the importance of cracks. As will be seen, attenuation does not depend simply on parameters like crack density but rather in more complicated ways on distributions, shapes, sizes, and contacts.

The variation of Q with wave strain amplitude also proves to be an important diagnostic for the understanding of contact related attenuation. It is almost invariably assumed in the literature that attenuation is independent of strain amplitude. While this may indeed be true for strains associated with teleseismic waves ($\varepsilon < 10^{-6}$) numerous experimental studies have shown amplitude dependent behavior at higher strains ($\varepsilon > 10^{-6}$). Gordon and Davis (1968) examined Q as a function of amplitude ranging from 10^{-9} to about 10^{-4} using a resonant bar at 90 kHz. The samples studied included granite, basalt, dunite, quartzite, and others. Q was observed to be constant at low strains,

decreasing sharply for strain amplitudes greater than about 10^{-6}. Other studies by Peselnick and Outerbridge (1961) on Solenhofen limestone under torsional vibrations at 1 Hz and Gordon and Rader (1971) for the Chester granite and Winkler and Nur (1978) for the Massilon sandstone produce similar results.

As will be shown, the observation of amplitude dependence at strains of about 10^{-6} and greater may also explain many of the discrepancies reported between Q measurements obtained by dynamic resonance and ultrasonic pulse techniques although a frequency dependent attenuation mechanism cannot be ruled out.

To investigate the nature of amplitude dependent Q, we carried out two sets of experiments. In the first, the amplitude dependence of Q was investigated for two sandstones and Plexiglas. In the second, the behavior of attenuation was examined as a function of cracks induced by temperature cycling of the rock. For this case, the effects of both increasing crack density and outgassing of volatiles from crack surfaces must be considered. Furthermore, it was observed that amplitude dependence is coupled to the effects of thermal cycling.

EXPERIMENTAL RESULTS

Q values for all the experiments reported in this paper were determined using a longitudinal resonant bar method, driven as a composite oscillator (Quimby, 1925) by high Q PZT-4 transducers cemented to the sample ends. The samples were about 15 cm long by 0.635 cm in diameter producing fundamental mode frequencies in the 10-20 kHz range. Several runs were done with a sample diameter of 1.27 cm. Bar velocity and Q

are found from the resonance frequency and half power bandwidth. These values are corrected for the loading effects and mechanical Q of the transducers (Bozorth et al., 1951; Marx, 1951).

All of the measurements were made under room conditions with unjacketed samples. Maximum strain amplitude at resonance was varied from roughly 10^{-8} to 10^{-5} by increasing the peak voltage to the driving transducer.

The samples studied include the Berea and Navajo sandstones, Plexiglas, Westerly granite, Frederick diabase, and Solenhofen limestone. The latter two were chosen for their low crack porosity in the virgin state. Descriptions of the sandstones may be found in Johnston and Toksöz (1979), the granite and diabase in Brace (1965) and the limestone in Birch (1960).

As mentioned in the introduction, attenuation values for dry rocks obtained by dynamic resonace and ultrasonic techniques differ, the former yielding higher Q's. Since these measurements are generally made at different frequencies, one might possibly hypothesize a frequency dependent mechanism. However, no data support this. Q dependent of strain amplitude though, may provide an explanation. Most resonance experiments are carried out at low strains relative to those associated with ultrasonic pulses. If Q for low strains is higher than for high strains, the apparent discrepancy in the data may be resolved. This behavior is indeed observed for the dry Berea sandstone as shown in Figure 1 where Q and bar velocity are plotted as a function of maximum strain amplitude. Also shown for comparison

is Q for amorphous Plexiglas over the same amplitude range. Behaving similarly to data reported by Winkler and Nur (1978) for the Massilon sandstone, Q for the Berea rapidly decreases from a value of 75 to a value of 30 at a strain amplitude of about 10^{-5}. This corresponds to a 60% decrease in Q. Velocity decreases by only 1%. Also note that both velocity and Q appear to level off at higher amplitudes.

Comparison of the increasing amplitude curve versus decreasing amplitude shows nearly complete recovery of the initial Q value. As will be seen, this lack of hysteresis is observed for all the rocks studied and implies that little or no damage to the sliding surfaces (assuming that attenuation is due to frictional sliding) occurs at the higher strains.

For the same range of strain amplitude, Q of the Plexiglas remains relatively constant and if anything, increases slightly. This fact strongly suggests that the presence of grain boundaries and cracks in the rock is the controlling factor in producing amplitude dependent behavior.

In Figure 2, Q is plotted as a function of strain amplitude for the Navajo sandstone. The same behavior as seen for the Berea - constant Q at low amplitudes with a sharp decrease at a strain amplitude of 10^{-6} is observed, although the transition from low to high amplitude behavior does seem to occur at slightly lower amplitudes in the Navajo.

Does the amplitude dependence explain the difference between reported resonance and ultrasonic measurements? For the most part - yes. Q_p values at low pressure reported by Toksöz et al. (1979) and Johnston and Toksöz (1979) using ultrasonic

pulses are compared to the results just described for the dry Berea and Navajo sandstones in Table 1. Here, low and high amplitude resonant bar Q values are listed along with the ultrasonic P wave values. Clearly the high amplitude results from the resonance technique are comparable to the ultrasonic data. The data, however, are limited and it would be premature to rule out other mechanisms- even frequency dependent dry friction - as supplements to amplitude dependence in interpreting the discrepancy between the two experimental methods. It is inescapable, however, that amplitude dependence must be considered if any comparison is to be made between not only different experimental techniques but also between laboratory and field data.

The preceding data strongly suggest that cracks in the rock are important in determining the amplitude dependent behavior of Q. Thermal cycling presents a unique opportunity to form cracks in rock. Thus, if information on the induced crack porosity is available, the change in Q might be quantified in terms of crack density. Intuitively, one would expect that Q would decrease with increasing thermal cycling. As will be seen, this is not always the case. In fact, one of the more interesting results is what can be said about the nature of thermal cracking mechanisms.

Samples of Frederick diabase, Solenhofen limestone, and Westerly granite, 0.635 cm in diameter, were thermally cycled up to a maximum temperature of 600°C at room pressure in order to induce cracking. Second samples of each rock were cycled in separate runs in order to check reproducibility.

The heating and cooling rates were kept under 2 °C/minute. The samples were exposed to the maximum temperature for at least one hour. Data from Johnson et al. (1978) suggest that this time is required for the decay of acoustic emissions (and thus cracking) in a rock at constant temperature.

Other samples of each rock were slowly cycled to maximum temperatures of 400° and 800 °C. These were used for static stress-strain measurements to obtain a handle on the induced crack density. Finally, samples of Solenhofen limestone and Frederick diabase, 1.27 cm in diamater, were subjected to thermal cycling at high heating rates of about 20 °C/minute. The samples were maintained at the maximum temperature for at least an hour to equalize outgassing effects compared to the slow heating rate experiments. Westerly granite did not remain coherent during these runs and was thus not used.

In both procedures, after cooling the samples were left in laboratory air for several days. Again note that all attenuation measurements were made at room temperature and pressure in air. The relative humidity in the laboratory varied during the course of the experiments from 45 to 75%. This appeared to have had no bearing on the Q measurements. In fact, several samples were saturated with water and then allowed to dry with little change in the results.

Thermally induced crack porosity may be characterized using static stress-strain analysis. Linear strain as a function of hydrostatic confining pressure is shown for virgin and thermally cycled samples of diabase, limestone, and granite in Figures 3 through 7. For Westerly granite,

data is shown for two orientations: the stiff (parallel) and soft (perpendicular) directions. The induced crack porosities for cycling to 400 and 800° are found using the method described by Walsh (1965) and the results are listed in Table 2. The increase in porosity is generally proportionally greater for the samples cycled to 800° than those heated to 400°. The shapes of the thermally induced cracks seem also to depend on the temperature achieved during cycling. In the diabase, for the 400°curve, the cracks appear to be of fairly high aspect ratio. The closure pressure is relatively high (>1000 bars) and there is little curvature at low pressures. The case for higher aspect ratio cracks in the 400°cycled Westerly samples is not nearly as clear as for the diabase. The effect is masked by preexisting low aspect ratio cracks. However, evidence to be presented later suggests relatively higher concentrations of wide cracks compared to thin ones produced by thermal cycling to temperatures no greater than 400°C. In both the diabase and granite, heat treatment to 800° not only produces a dramatic increase in crack porosity but also, these cracks seem to be of lower aspect ratio. In both cases, the curvature of the stress-strain curve at low pressures is strikingly high compared to the other runs. For the Solenhofen limestone, however, a rapid change in crack porosity is not observed after heating to 800° nor are the induced cracks of particularly low aspect ratio.

Q values at low strain amplitude and bar velocity as functions of maximum temperature obtained in slow heating

and cooling cycles for the diabase and limestone are shown in Figures 8 and 9. Q and V for the two core directions of Westerly are shown in Figure 10. For all three rocks, two separate experiments were run to check reproducibility (with the exception of the "stiff" core of Westerly granite). These are denoted on the figures by different symbols. While the experiments were run under different humidity conditions, there is quite satisfactory agreement between the two runs for all three rocks.

The remarkable aspect of the data is the dramatic increase in Q for all the samples at maximum temperatures of 400° and less. Simultaneously, velocity decreases - quite substantially for the Westerly granite which contains more cracks initially. The changes in velocity seen for the granite are nearly identical to those reported by Johnson et al (1978) in a similar experiment on Westerly (Q values were not obtained). Anisotropy in Westerly is apparent, amounting to 10% for velocity and 25% for Q. The velocity changes in the diabase and limestone are low compared to the granite for temperatures below 400° followed by a rapid change above that point. This is reflected by the changes in crack porosity upon thermal cycling listed in Table 2. It is clear then, from all the data, that Q increases up to a point, even though crack porosity is also increasing. This change in Q is also apparently independent of orientation as shown for the Westerly granite in Figure 10.

Between 400 and 500°, however, the trend in Q reverses and in two of the three cases, Q decreases substantially.

These data are very similar to those reported by Todd et al. (1972) for Westerly granite and Fairfax diabase. The high temperature Q values of the limestone do not follow the form of the other two rocks, showing only a slight decrease. This difference might have been expected from the static measurements where the Solenhofen was the only sample not exhibiting a large increase in low aspect ratio cracks at 800°. It should be noted that the decrease in Q above 400° observed for the diabase and granite is not initially due to the α-β transition in quartz which does not occur until 573° C.

Q and bar velocity for the 1.27 cm diamater cores of rapidly heated limestone and diabase are shown in Figures 11 and 12. The behavior of Q as a function of maximum temperature for the limestone is clearly opposite that observed for low heating rates. For the diabase, there is an initial decrease in Q at 200° followed by a gradual rise to a maximum at 500° although the Q values at this point are far below those obtained by slow heating even though the sample here was kept at temperature for at least one hour as before. A sharp decrease in Q is noted between 500 and 600° C probably due to the phase transition in quartz. In cycling to 800° C, a marked change in the sample appearance was noted. This was accompanied by a further decrease in Q and a very rapid decrease in velocity.

These results imply that a different crack producing mechanism is operative for high heating rates. Compared to the slow rate, one might expect that finer (lower aspect

ratio) cracks are generated. The data are more conclusive for the limestone where not only Q decreases continuously but the decrease in velocity is larger than for the slow heating rate case. For a given volume concentration, lower aspect ratio cracks produce larger changes in the elastic moduli compared to high aspect ratio cracks (Toksöz et al., 1976). Apparently in the diabase, permanent outgassing of volatiles has a compensating effect on the generation of thin cracks at temperatures between 300 and 500° C. The minor contribution of this same effect may be observed in the limestone where Q levels off between 400 and 600°C.

Amplitude dependent behavior is also coupled to the nature of thermally induced cracks. Q as a function of maximum strain amplitude is shown for several temperatures each for the three slowly cycled rocks in Figures 13 through 15. Amplitude dependence not readily apparent in the virgin states of the diabase and limestone appears for thermally cycled samples. The important feature to note from the data is that while Q increases as a function of temperatures for low strains, the transition from low to high strain amplitude behavior migrates to lower amplitudes. It also appears that the Q values for high strains tend to converge. Once the maximum temperature exceeds 400 °C and the Q's at low strains decrease, the amplitude transition moves back to higher strains. The exception to this is the Solenhofen limestone. Again it is apparent in this case that the nature of the cracks obtained at high temperature

are different than in the granite or diabase.

Amplitude dependent behavior was also observed for the rapidly heated samples although for a given maximum obtained temperature, the transition seems to occur at a higher strain than for the slowly heated samples. This is shown in Figure I6 for the Frederick diabase where Q as a function of amplitude is plotted for the virgin rock and the two heat treated runs. The amplitude dependence for the 20° C/minute treated sample is not as clearly defined as for the other run. Either the transition does occur at higher strains or the amplitude dependence is smeared out or reduced somewhat.

The behavior of amplitude cycling on Q is nearly identical for all the rocks including the sandstones shown in Figures 1 and 2. Again, the lack of hysteresis implies little or no damage to contact surfaces at high strain amplitudes.

DISCUSSION AND CONCLUSIONS

The data presented in the preceding section may be interpreted in terms of the mechanisms for volatile outgassing from crack surfaces, thermally induced cracking and amplitude dependent attenuation. The theoretical basis for the latter is not well developed, the difficulty being that the specifics of such amplitude behavior is very model dependent. Thus, the discussion of this aspect must be qualitative. The increase in Q observed in slow thermal cycling may be due to one or both of the following mechanisms.

1) Outgassing of volatiles tied to mineral grains and crack contact surfaces. If attenuation is due to some kind

of friction mechanism, this has the effect of increasing the friction coefficient thus decreasing the attenuation (increasing Q). Tittmann et al. (1974 and 1976), in their exhaustive survey of the effects of volatiles on the acoustic properties of lunar rocks, have shown that very high Q values (>3000) can be obtained in the laboratory by repeated thermal cycling and the application of hard vacuum ($<10^{-7}$ torr). However, outgassed samples exposed for 30 minutes to saturated vapors of several volatiles, similar to water in their physical properties, at ambient pressure resulted in 40-60% decreases in Q (Tittmann et al., 1976).

Clearly, the major question at this point is whether exposure of the samples to air after cycling has resulted in substantial reabsorption of water vapor. It is probable that for the most part, it has. If the effect of outgassing is to lock contact surfaces, then the migration of the amplitude dependence to lower amplitudes would not be observed. Furthermore, if outgassing had a major effect on the Q, then this should be seen in the rapidly heated samples also. Rather, Q decreased or remained relatively constant with maximum temperature. The slight rise in Q observed for the diabase may, however, indicate that part of the overall effect is, in fact, due to volatile loss.

2) Changes in crack density and shape as a result of thermal cycling. The overall crack density must increase

during cycling, resulting in decreases in measured bar velocities. Thermal cracking for low temperature gradients, though, is due to thermal expansion coefficient mismatches across grains (Myklestad, 1942; Edwards, 1951; Eshelby, 1957). Stresses induced by this differential thermal expansion are concentrated between grains, the effect being to widen pre-existing crack contacts and grain boundaries. Thus, contact surfaces are reduced and attenuation decreases. At higher temperatures and high heating rates new cracks are formed and propagated.

There is some evidence to support the contention that expansion and contraction of grains at thermal equilibrium has the effect of opening cracks. Differential strain analysis of several rock types including Westerly granite and Frederick diabase (Cooper and Simmons, 1977) show that the peak in crack porosity as a function of closure pressure shifts to higher closure pressure and thus higher aspect ratio cracks as a result of thermal cycling. Wong and Brace (1978) have shown that the pressure required to produce reversible thermal expansion also increases after cycling. These effects have been observed qualitatively in Figures 3 through 6 showing linear strain as a function of pressure. Examples of crack widening due to slow thermal cycling have also been shown using scanning electron microscope photographs (Sprunt and Brace, 1974). The effect of thermal cycling to 400°C in

Chelmsford granite is to widen pre-existing cracks and to form new, fairly wide, cracks at the grain boundaries. Sprunt and Brace also show that upon thermal cycling there is a decrease in the number of low aspect ratio cracks (10^{-4}) while a substantial increase in the number of cracks with aspect ratios of 10^{-2} in Westerly granite.

Thus, wile the effect of cycling a rock to 400°C is to increase the overall crack porosity, these seem to be of high aspect ratio. This is most evident for the diabase and limestone, more or less crack free in their virgin states. Further heating produces a dramatic change in the crack porosity for the diabase and granite. It is possible that above 400°C, the rocks are unable to acomodate any more thermal expansion induced strain and low aspect ratio cracks are propagated. Thus we see a sharp increase in strain for low confining pressures. The change for the Solenhofen at 800°C (Figure 4) is not nearly as dramatic and this is reflected in the Q values which did not suffer a dramatic decrease for maximum temperatures above 400°C. The limestone probably deforms plastically at these temperatures and thus fine crack growth is inhibited.

For high heating rates, local thermal gradients in the rock may cause crack growth (Goodier and Florence, 1964; Todd, 1973; Wong and Brace, 1978). Calculated maximum gradients obrained in the high heating rate experiments exceed a critical value observed by Todd (1973) for gradient

induced cracking. Thermal stresses in this case exist over a volume larger than the grains and thus cracks may even propagate through grains, increasing contact area.

Strain amplitude effects may be incorporated into this model via several mechanisms. Mavko (1978) has hypothesized that observed amplitude dependent attenuation behavior is due to a combination of a linear mechanism, operative at low strains, and a sliding friction mechanism, producing nonlinear effects at high strains. Thus, friction is either masked by the linear mechanism or totally inoperative at low amplitudes. If the effect of low heating rate thermal cycling is to decrease the attenuation due to this linear mechanism and the effect of high heating rate cycling to increase attenuation, then the data may be explained if the contribution due to sliding friction is constant. This mechanism would be appealing except for the fact that the linear mechanism is undefined in Mavko's model and that cracks, or some grain contact phenomenon seems to be important even at low strains. This is borne out by measurements made at low amplitudes (Gardner et al., 1964; Winkler and Nur, 1978) where attenuation decreases with applied hydrostatic pressure just as observed in higher amplitude ultrasonic measurements (Toksöz et al., 1979; Johnston and Toksöz, 1979). All of these data are interpreted by the various investigators to be due to the closing of thin cracks, a process that affects the elastic

properties of rock as well (Walsh, 1965; Toksöz et al., 1976).

An alternative explanation may be found in variations of crack contact area and most easily thought of in terms of work done on the contact. Although the small displacement at low amplitudes suggest that macroscopic Coulomb friction may not be strictly applicable (Savage, 1969), it appears that the forces involved in attenuation are similar. Walsh and Grosenbaugh (1978) have proposed a crack model which holds great promise to quantitatively explain the data reported in this paper. The discussion here will be qualitative. Cracks are modeled as cavities formed by contact of two bumpy surfaces. The bumps, or asperities, are considered round and thus Hertzian contact theory is assumed. The distribution of asperity heights and therefore contact area or normal stress is taken to be nearly Gaussian in nature. While the exact form of this distribution is critical in terms of Walsh and Grosenbaugh's elastic model, it is sufficient for this discussion that there is merely a peak in the distribution. A Gaussian profile, however, is observed for slightly polished steel and bead blasted gold surfaces (Greenwood and Williamson, 1966).

Considering the effect of this model in terms of general amplitude dependence of attenuation, for low strains, work is done on the low contact area tail end of the distribution. Since the distribution here is relatively flat, Q would appear

independent of amplitude. As strain amplitude increases, work is done on contact areas near the peak of the distribution and Q decreases. At very high amplitudes, this theory would predict a leveling off of Q.

This same model predicts the behavior of amplitude effects for thermally cycled rocks. Thermal cracking that widens cracks will shift the peak in the distribution of contact area to lower values. This while the actual density of contacts may decrease and Q increases, the peak occurs at lower areas and the drop in Q due to amplitude effects happens at lower strains.

The essential feature of this model quite different from the Mavko model, is that contacts play a role at all strain amplitude investigated in this paper. This is more consistent with our notion that the increase in Q as a function of pressure measured at low amplitudes by resonance techniques is due to contact closing just as interpreted for the ultrasonic data. All of the amplitude dependent models, however, require further development.

In summary, the data presented on the variations of Q with strain amplitude and thermally induced crack porosity show that the attenuation is critically dependent not only on outgassing but also the number of cracks and their shapes or widths. Rocks thermally cycled at low heating and cooling rates up to 400°C show a marked increase in Q that cannot be

entirely explained by outgassing of volatiles. Such cycling widens thin cracks and grain boundaries thus reducing contact areas. In terms of a sliding friction-like mechanism, this would result in lower attenuation. Fast thermal cycling propagates thin cracks and Q decreases.

Q is dependent on strain amplitude. For low strains ($<10^{-7}$) Q appears independent of amplitude but decreases rapidly for strains greater than 10^{-6} to 10^{-5} for the rocks studied. There is no hysteresis in amplitude cycling suggesting that if friction is the dominant mechanism for attenuation, little or no damage to the sliding surface occurs at strains of 10^{-4} or smaller. Amplitude dependent behavior may explain discrepancies observed in Q values determined using different experimental techniques.

The behavior of amplitude dependent Q is also a function of the crack distribution in the rock. Slow thermally cycled samples experience the transition from high to low Q at lower amplitudes than virgin rocks. Again this is most easily explained by appealing to variations in contact area as a result of thermal cycling. All of the data imply that cracks and grain boundaries, and in particular, contact areas, primarily control the attenuation of seismic waves in dry rock.

References

Birch, F., The velocity of compressional waves in rocks to 10 kilobars, J. Geophys. Res., 65, 1083-1102, 1960.

Bozorth, R.M., W.P. Mason, and H.J. McSkimin, Frequency dependence of elastic constants and losses in nickel, Bell System Tech. J., 30, 970-989, 1951.

Brace, W.F., Some new measurements of linear compressibility of rocks, J. Geophys. Res., 70 (2), 391-398, 1965.

Cooper, H.W. and G. Simmons, Thermal cycling cracks in three igneous rocks, submitted to Int. J. Rock Mech. Min. Sci. and Geomech. Abstr., 1977.

Edwards, R.H., Stress concentrations around spheroidal inclusions and cavities, J. Applied Mech., 19-30, 1951.

Eshelby, J.D., The determination of the elastic field of an ellipsoidal inclusion, and related problems, Proc. Roy. Soc. (London), 241 (A), 376-396, 1957.

Gardner, G.H.F., M.R.J. Wyllie, and D.M. Droschak, Effects of pressure and fluid saturation on the attenuation of elastic waves in sands, J. Petroleum Tech., 189-198, 1964.

Goodier, J.N., and A.L. Florence, Localized thermal stress at holes, cavities, and inclusions disturbing uniform heat flow, Thermal crack propagation, Proc., 11th Int. Cong. of Applied Mech., Munich, 1964.

Gordon, R.B., and L.A. Davis, Velocity and attenuation of seismic waves in imperfectly elastic rock, J. Geophys. Res., 73, 3917-3935, 1968.

Gordon, R.B. and D. Rader, Imperfect elasticity of rock, its influence on the velocity of stress waves, "Geophysical Monograph Series, Vol. 14", J.G. Heacock, ed., Am. Geophys. Un., Washington, DC, 1971.

Greenwood, J.A. and J.B.P. Williamson, Contact of nominally flat surfaces, Proc. Roy. Soc. London, 295 (A), 300, 1966.

Johnson, B., A.F. Gangi, and J. Handin, Thermal cracking of rock subjected to slow, uniform temperature changes, in "19th U.S. Rock Mechanics Symposium", Univ. of Nevada, Reno, 259-267, 1978.

Johnston, D.H. and M.N. Toksöz, Ultrasonic P and S wave attenuation in dry and saturated rocks under pressure, submitted to J. Geophys. Res., 1979.

Marx, J.W., Use of the piezoelectric gauge for internal friction measurements, Rev. Sci. Instr., 22, 503-509, 1951.

Mavko, G., A more general description of frictional attenuation, Abstract, Trans. Am. Geophys. Un., (EOS), 59, 376.

Myklestad, N.O., Two problems of thermal stress in the infinite solid, J. Applied Mech., 136-143, 1942.

Peselnick, L. and W.F. Outerbridge, Internal friction and rigidity modulus of Solenhofen limestone over a wide frequency range, U.S. Geol. Survey, Prof. Paper No. 400B, 1961.

Quimby, S.L., On the experimental determination of the viscosity of vibrating solids, Phys. Rev., 25, 558-573, 1925.

Savage, J.C., Comments on a paper by R.B. Gordon and L.A. David. 'Velocity and attenuation of seismic waves in imperfectly elastic rock', J. Geophys. Res., 74, 726-728, 1969.

Sprunt, E.S. and W.F. Brace, Direct observation of microcavities in crystalline rocks, Rock Mech. Mining Sci. Geomech., 11, 139-150, 1974.

Tittmann, B.R., R.M. Housley, G.A. Alers, and E.H. Cirlin, Internal friction in rocks and its relationship to volatiles on the moon, in Lunar Science Conf., 5th Proc., Geochim. Cosmochim. Acta, Suppl. 5, v. 3, 2913-2918, 1974.

Tittmann, B.R., L. Ahlberg, and J. Curnow, Internal friction and velocity measurements, in Lunar Science Conf., 7th Proc., Geochim. Acta, Suppl. 4, v. 3, 3123-3132, 1976.

Todd, P.T., Effect of cracks on elastic properties of low porosity rocks, Ph.D. Thesis, M.I.T. Dept. of Earth and Planet. Sci., 1973.

Todd, T.P., H. Wang, W.S. Baldridge, and G. Simmons, Elastic properties of Apollo 14 and 15 rocks, in Proc. Third Lunar Sci. Conf., Geochim. Cosmochim. Acta, v. 3, M.I.T. Press, 2577-2586, 1972.

Toksöz, M.N., C.H. Cheng, and A. Timur, Velocities of seismic waves in porous rocks, Geophysics, 41, 621-645, 1976.

Toksöz, M.N., D.H. Johnston, and A. Timur, Attenuation of seismic waves in dry and saturated rocks, I. Laboratory measurements, Geophysics, in press, 1979.

Walsh, J.B., The effect of cracks on the compressibility of rock, J. Geophys. Res., 70, 381-389, 1965.

Walsh, J.B., Seismic wave attenuation in rock due to friction, J. Geophys. Res., 71, 2591-2599, 1966.

Walsh, J.B. and M.A. Grosenbaugh, A new model for analyzing the effect of fractures on compressibility, submitted to J. Geophys. Res., 1978.

Winkler, K. and A. Nur, Attenuation and velocity in dry and water-saturated Massilon sandstone (Abstract), Abstracts and Biographics, 48th Annual Mtg., Soc. Expl. Geophys., p. 40, 1978.

Wong, T.F. and W.F. Brace, Thermal expansion of rocks, some measurements at high pressure, submitted to Tectonophysics, 1978.

Table 1

Comparison of Resonance and Ultrasonic Q Data

	Berea	Navajo
Resonance, low amplitude	75	60
Resonance, high amplitude	30	28
Ultrasonic P wave	20	30

Table 2

Crack Porosity (%) From Thermal Cycling

	Virgin	400°C	800°C
Frederick Diabase	--	0.05	0.28
Solenhofen Limestone	--	0.09	0.18
Westerly Granite			
perpendicular	0.30	0.54	2.70
parallel	0.12	0.34	2.07

FIGURE CAPTIONS

Fig. 1. Q and bar velocity as a function of strain amplitude for longitudinal waves in the dry Berea sandstone. Also shown is Q as a function of strain amplitude for plexiglass. In this and later figures, representative error bars are shown.

Fig. 2. Q as a function of strain amplitude for longitudinal waves in the dry Navajo sandstone.

Fig. 3. Linear strain as a function of confining pressure in Frederick diabase for a virgin sample and samples thermally cycled to 400 and 800°C.

Fig. 4. Linear strain as a function of confining pressure in Solenhofen limestone for virgin and thermally cycled samples.

Fig. 5. Linear strain as a function of confining pressure in Westerly granite for the "soft" direction. Curves for the virgin and 400°C cycled samples are shown.

Fig. 6. Linear strain as a function of confining pressure in Westerly granite for the "stiff" direction.

Fig. 7. Linear strain as a function of confining pressure in Westerly granite for both directions for samples thermally cycled to 800°C.

Fig. 8. Q (solid symbols) and bar velocity (open symbols) as a function of maximum temperature achieved in slow thermal cycling in the Frederick diabase. Two separate experiments were run and the results are denoted by the different symbols. Representative error bars are also shown.

Fig. 9. Q and bar velocity as a function of maximum temperature in Solenhofen limestone. See Figure 8 for explanations.

Fig. 10. Q and bar velocity as a function of maximum temperature in Westerly granite for both directions. See Figure 8 for explanations.

Fig. 11. Q (solid symbols) and bar velocity (open symbols) as a function of maximum temperature achieved in fast thermal cycling in Solenhofen limestone.

Fig. 12. Q and bar velocity as a function of maximum temperature (fast cycling) in Frederick diabase.

Fig. 13. Q as a function of strain amplitude in Frederick diabase for virgin and several slow thermally cycled samples.

Fig. 14. Q as a function of strain amplitude in Solenhofen limestone for virgin and several slow thermally cycled samples.

Fig. 15. Q as a function of strain amplitude in Westerly granite (soft direction) for virgin and several slow thermally cycled samples.

Fig. 16. Comparison of amplitude dependent Q behavior for slow and fast cycled samples of Frederick diabase.

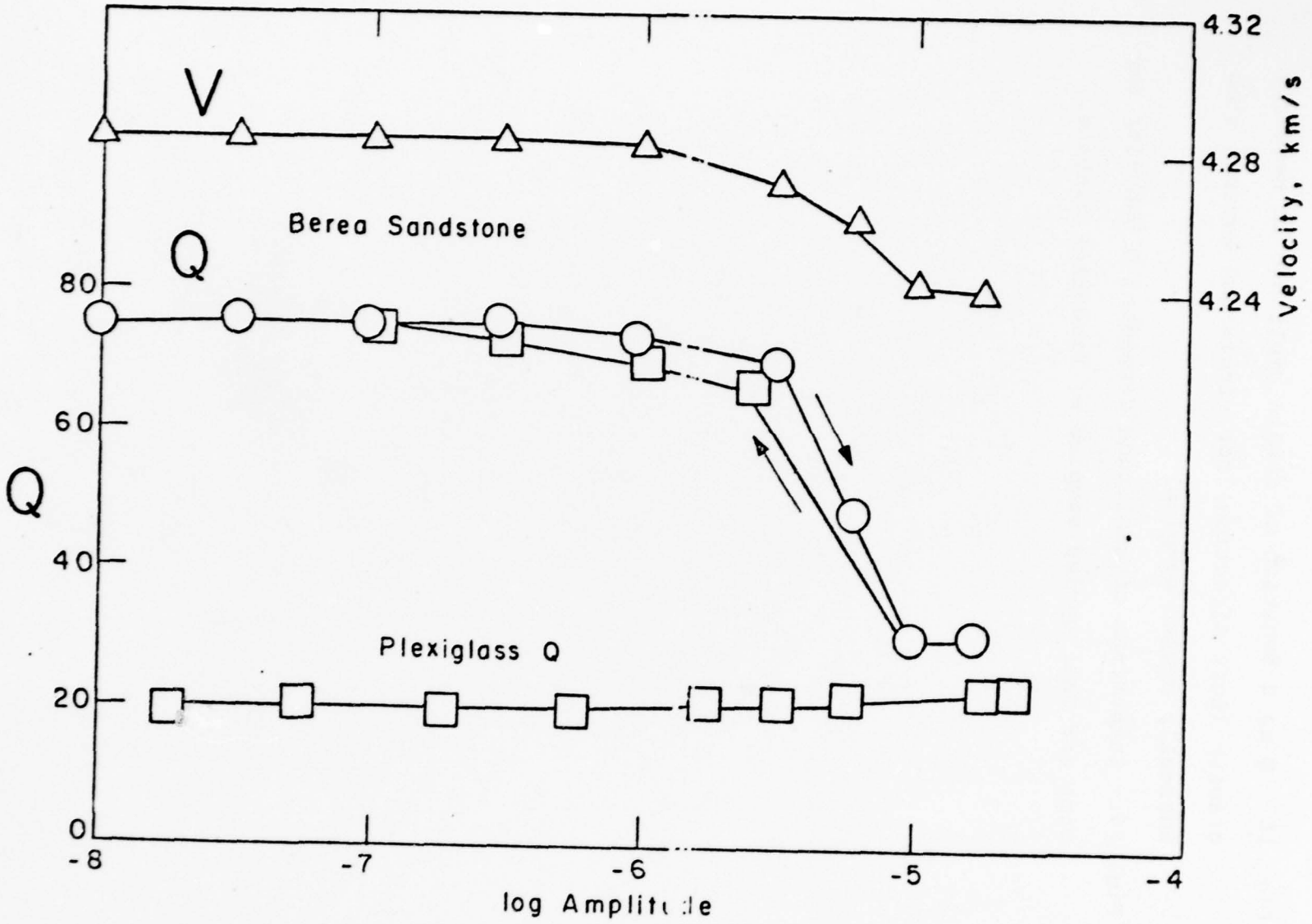
V
Berea Sandstone
Q
Plexiglass Q
Q
80
60
40
20
0
4.32
4.28
4.24
Velocity, km/s
-8
-7
-6
-5
-4
log Amplitude

Figure 1

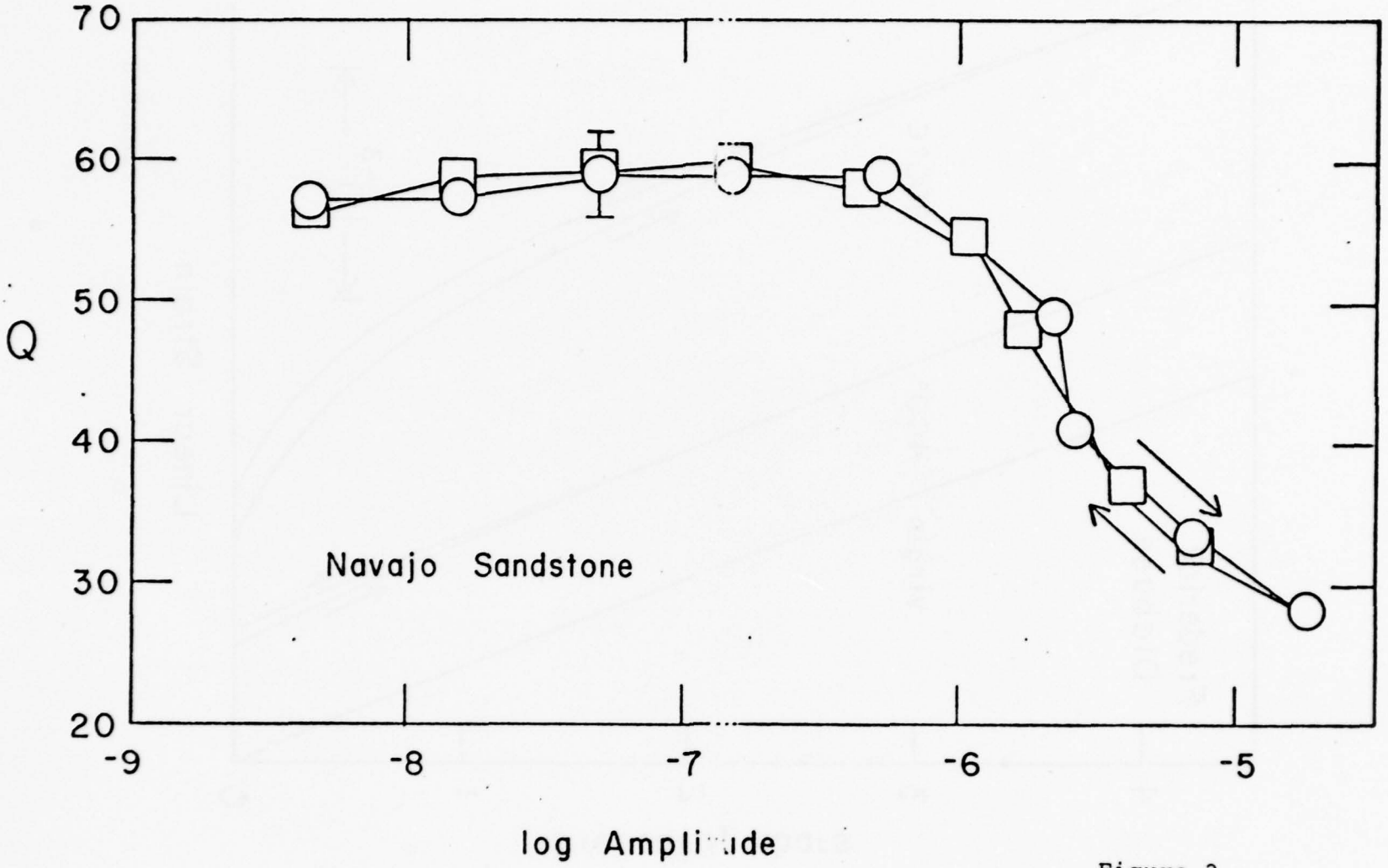

Figure 2

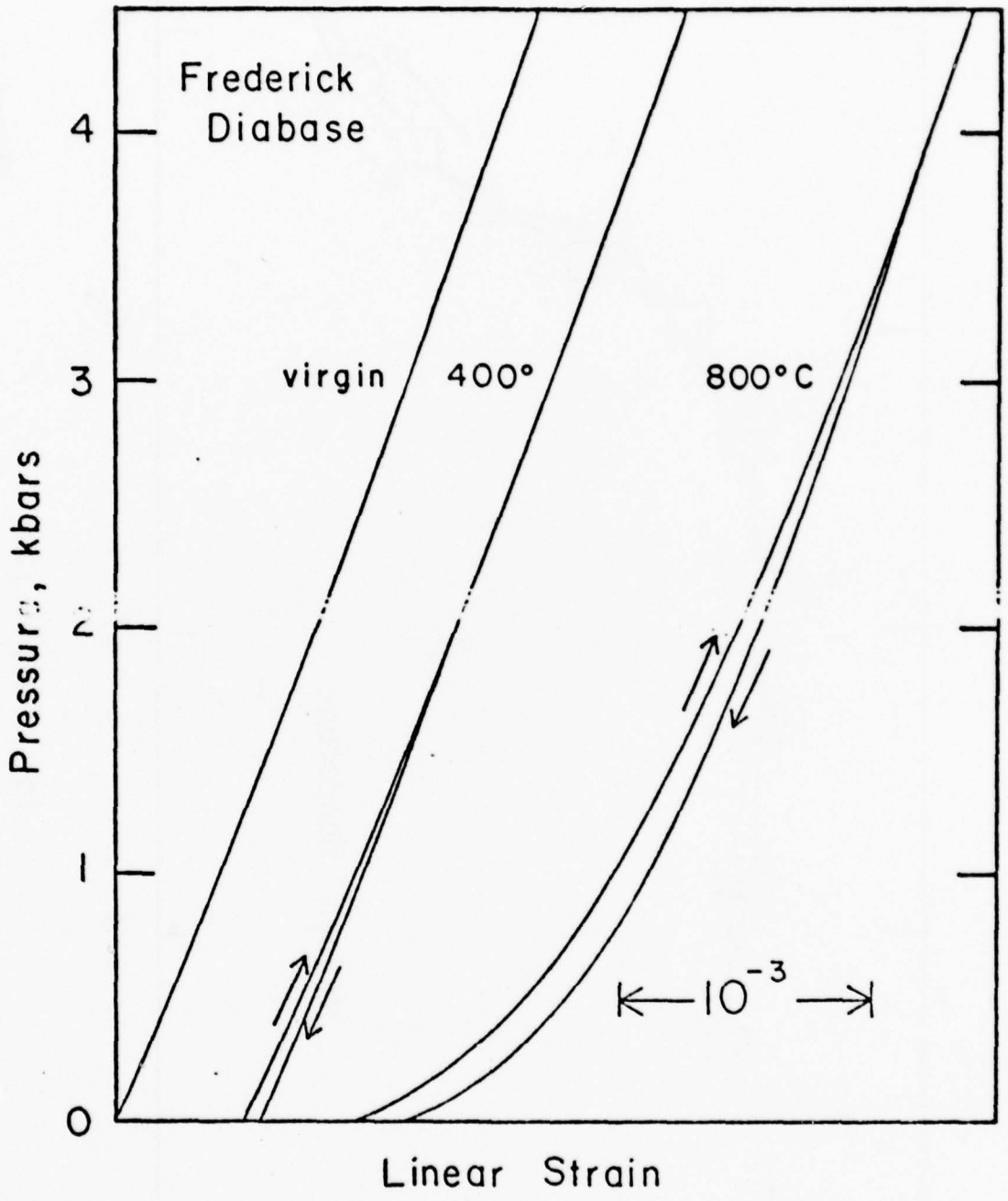
Frederick
Diabase
virgin
400°
800°C
4
3
1
0
Pressure, kbars
$\leftarrow 10^{-3} \rightarrow$
Linear Strain

Figure 3

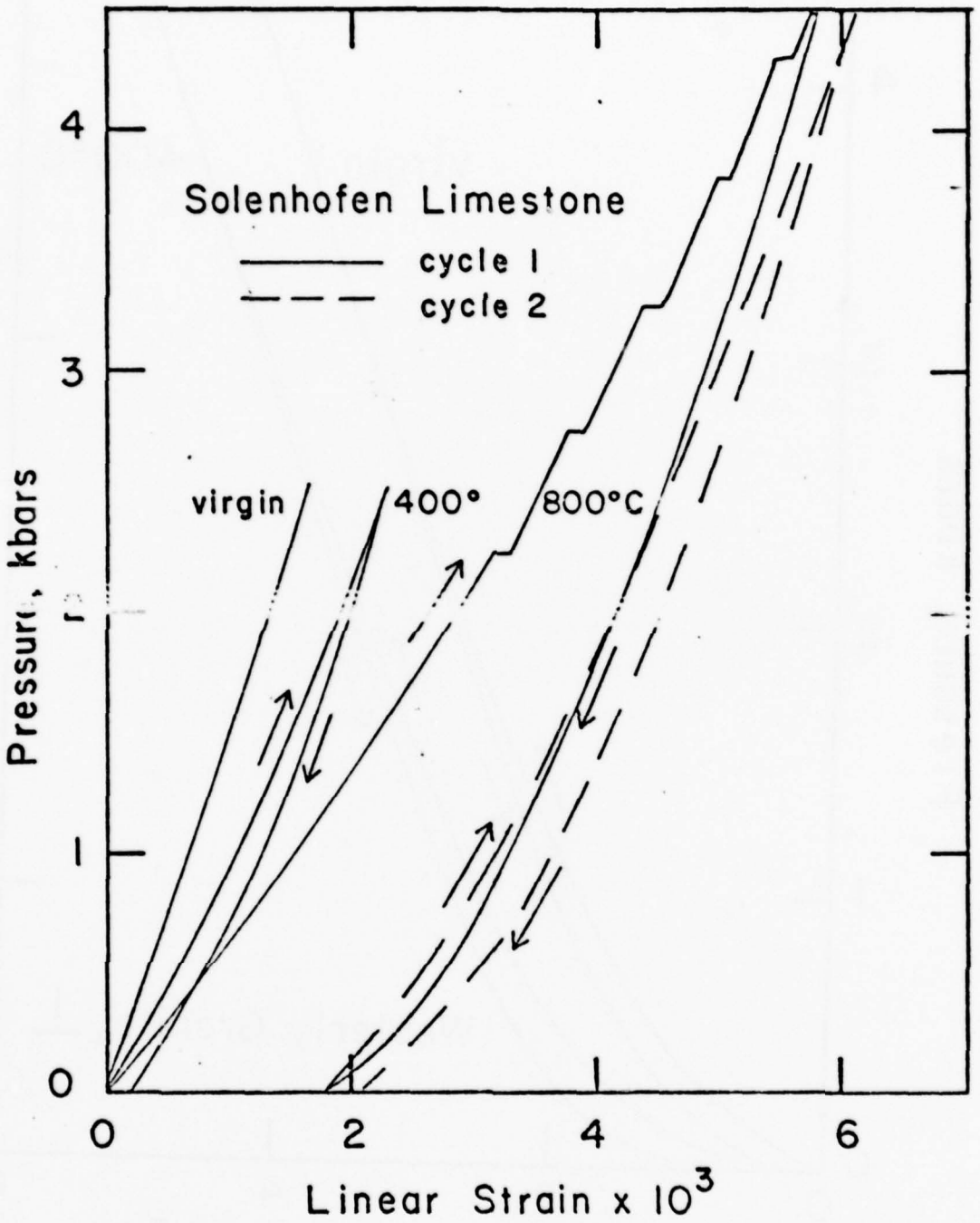
Solenhofen Limestone
cycle 1
cycle 2
virgin
400°
800°C
Pressure, kbars
0
1
3
4
0
2
4
6
Linear Strain x 10^3

Figure 4

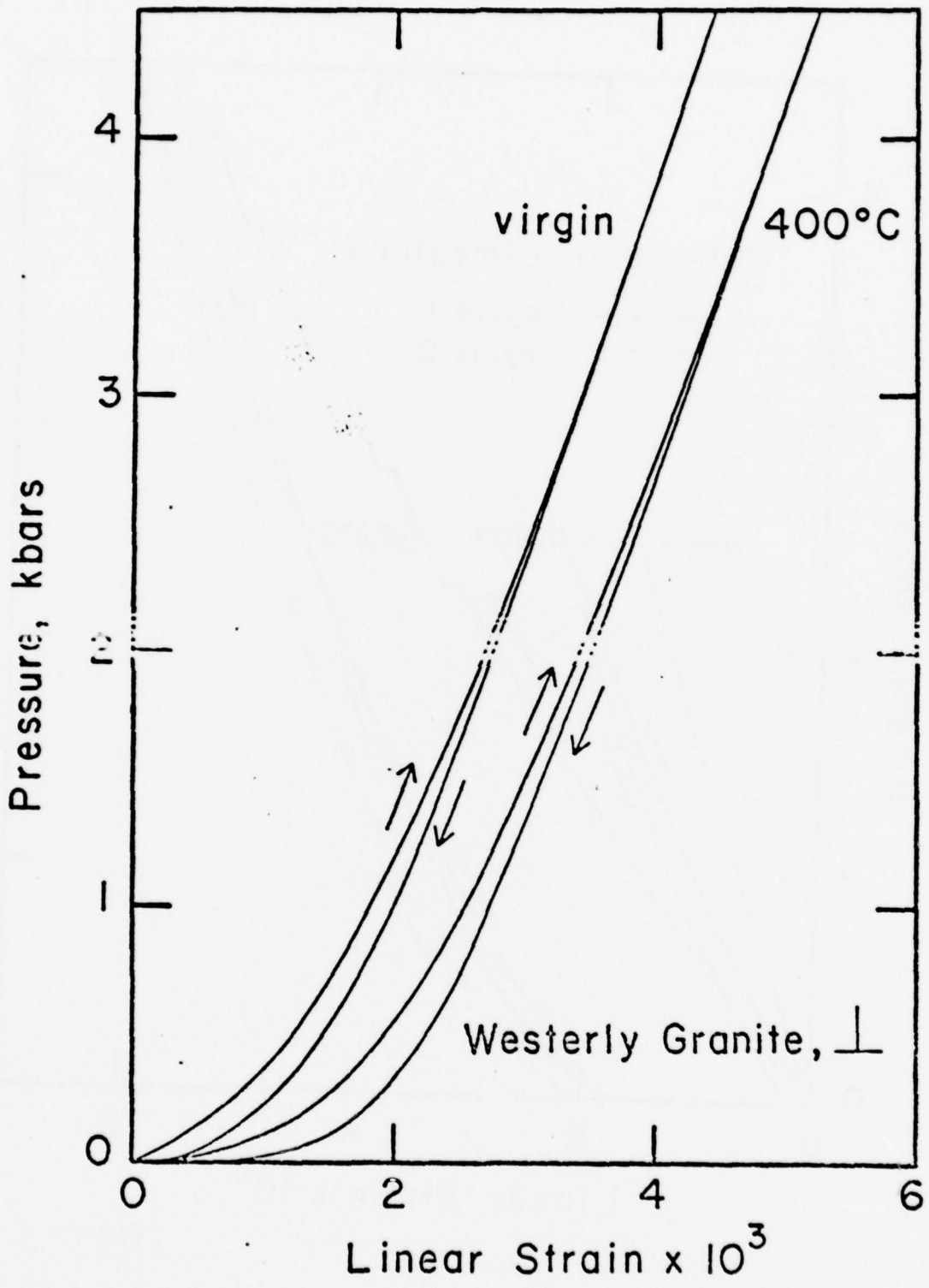
virgin
400°C
Westerly Granite, ⊥
Pressure, kbars
0
1
3
4
0
2
4
6
Linear Strain x 10³

Figure 5

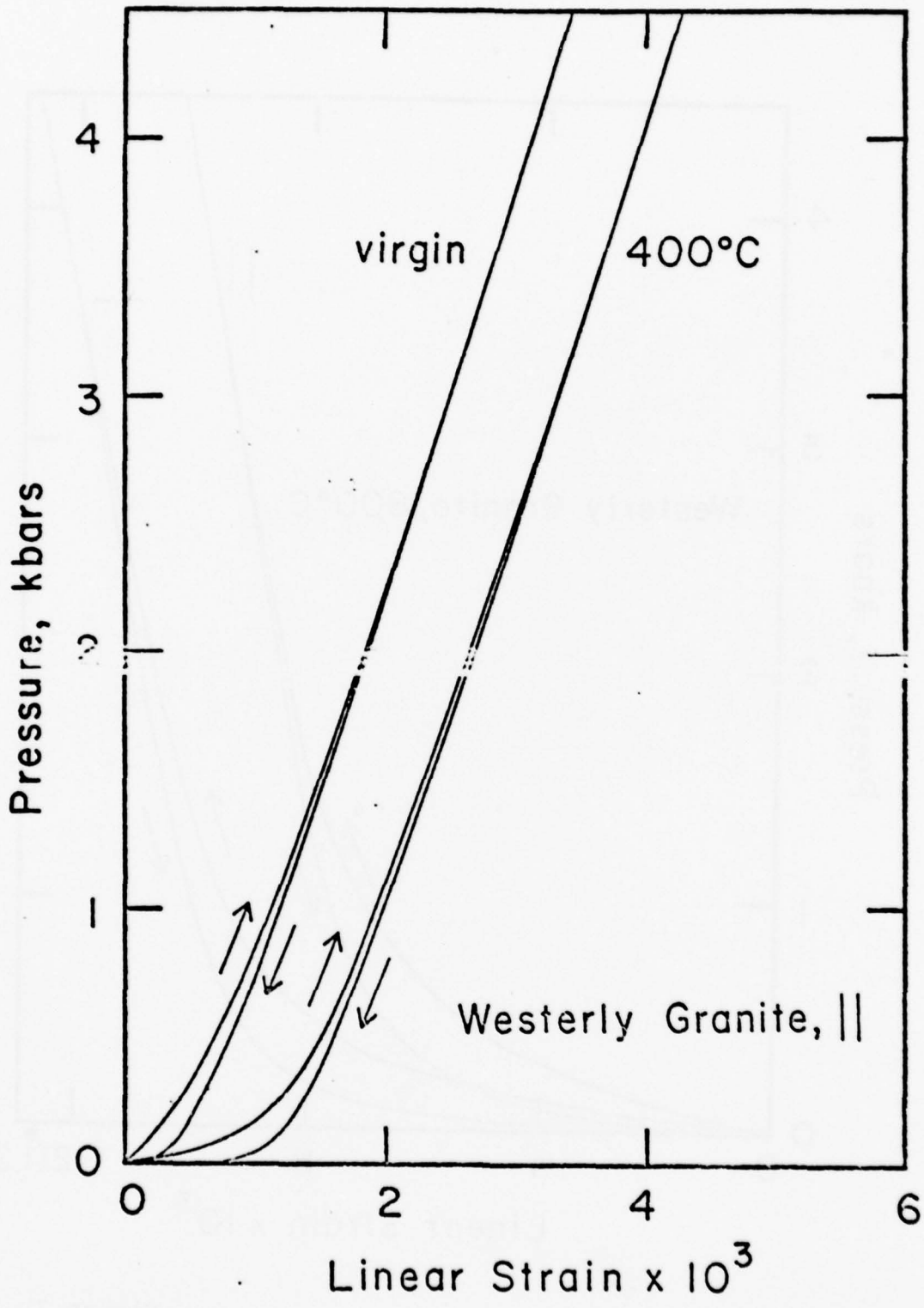
virgin
400°C
Westerly Granite, ||
Pressure, kbars
Linear Strain x 10^3
0
1
3
4
0
2
4
6

Figure 6

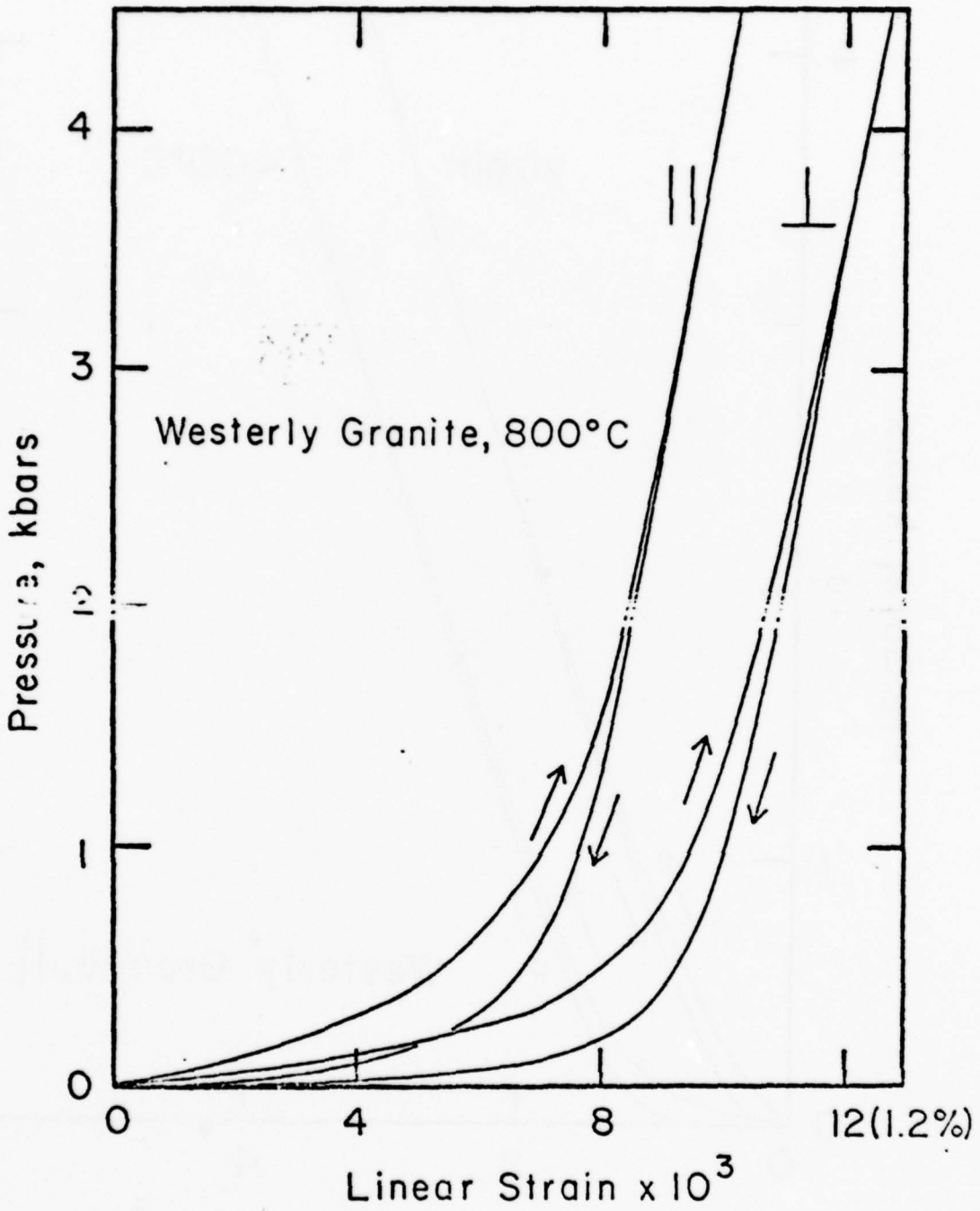
Westerly Granite, 800°C
Pressure, kbars
0
1
3
4
0
4
8
12(1.2%)
Linear Strain x 10^3
||
⊥

Figure 7

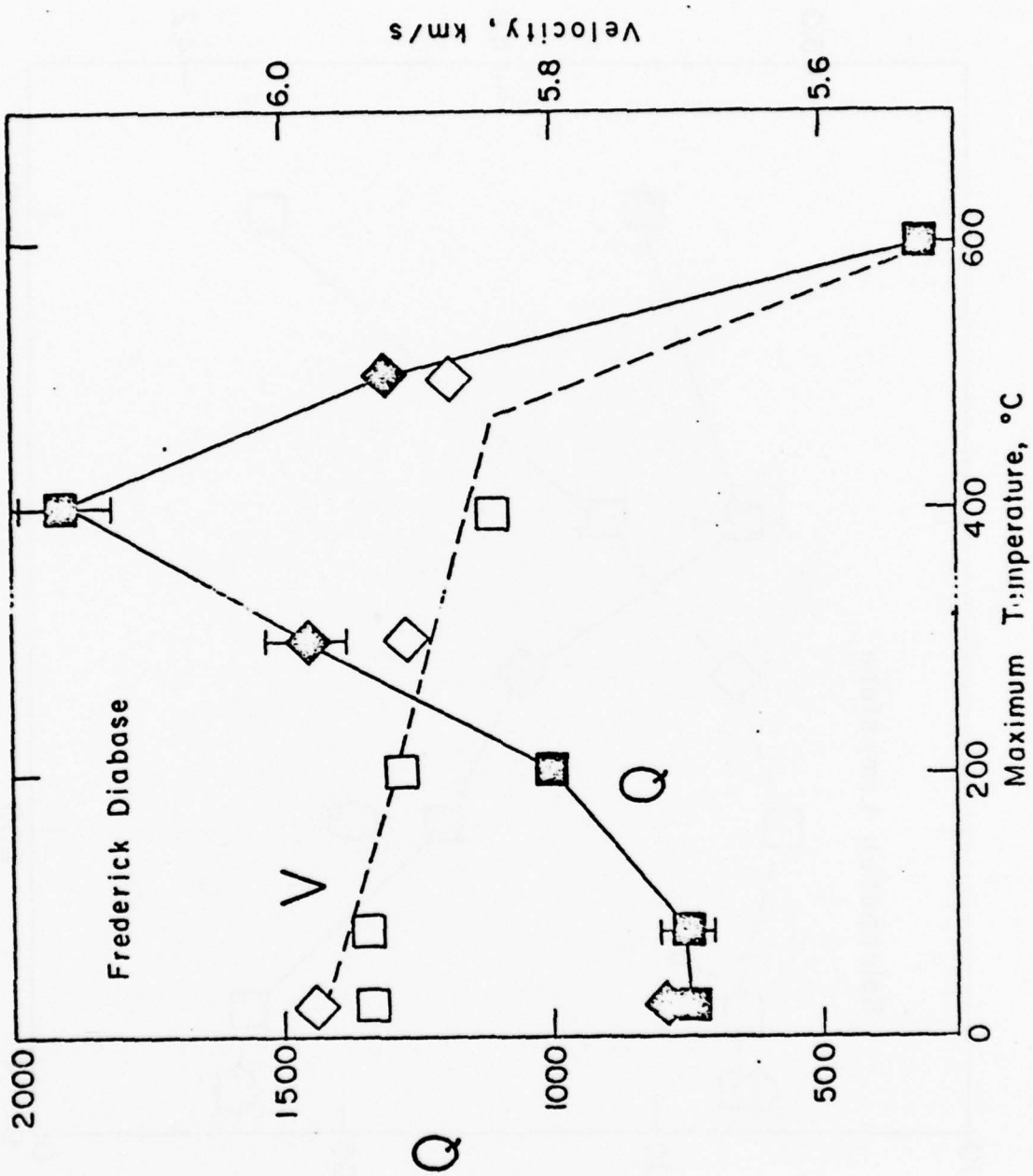
Velocity, km/s
6.0
5.8
5.6
Frederick Diabase
V
Q
Q
2000
1500
1000
500
0
200
400
600
Maximum Temperature, °C

Figure 8

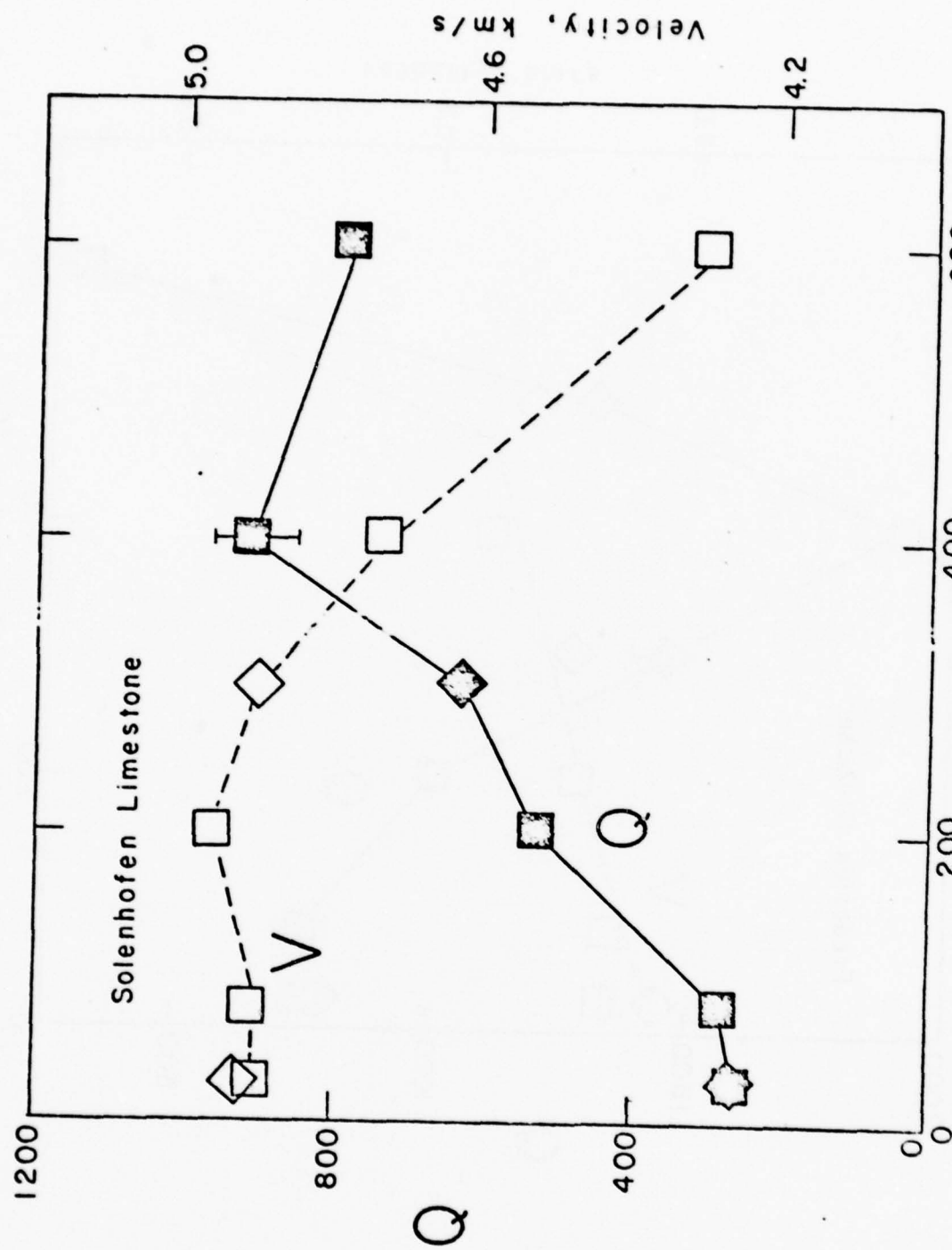
Solenhofen Limestone
Q
V
Q
1200
800
400
0
0
200
400
600
Maximum Temperature, °C
5.0
4.6
4.2
Velocity, km/s

Figure 9

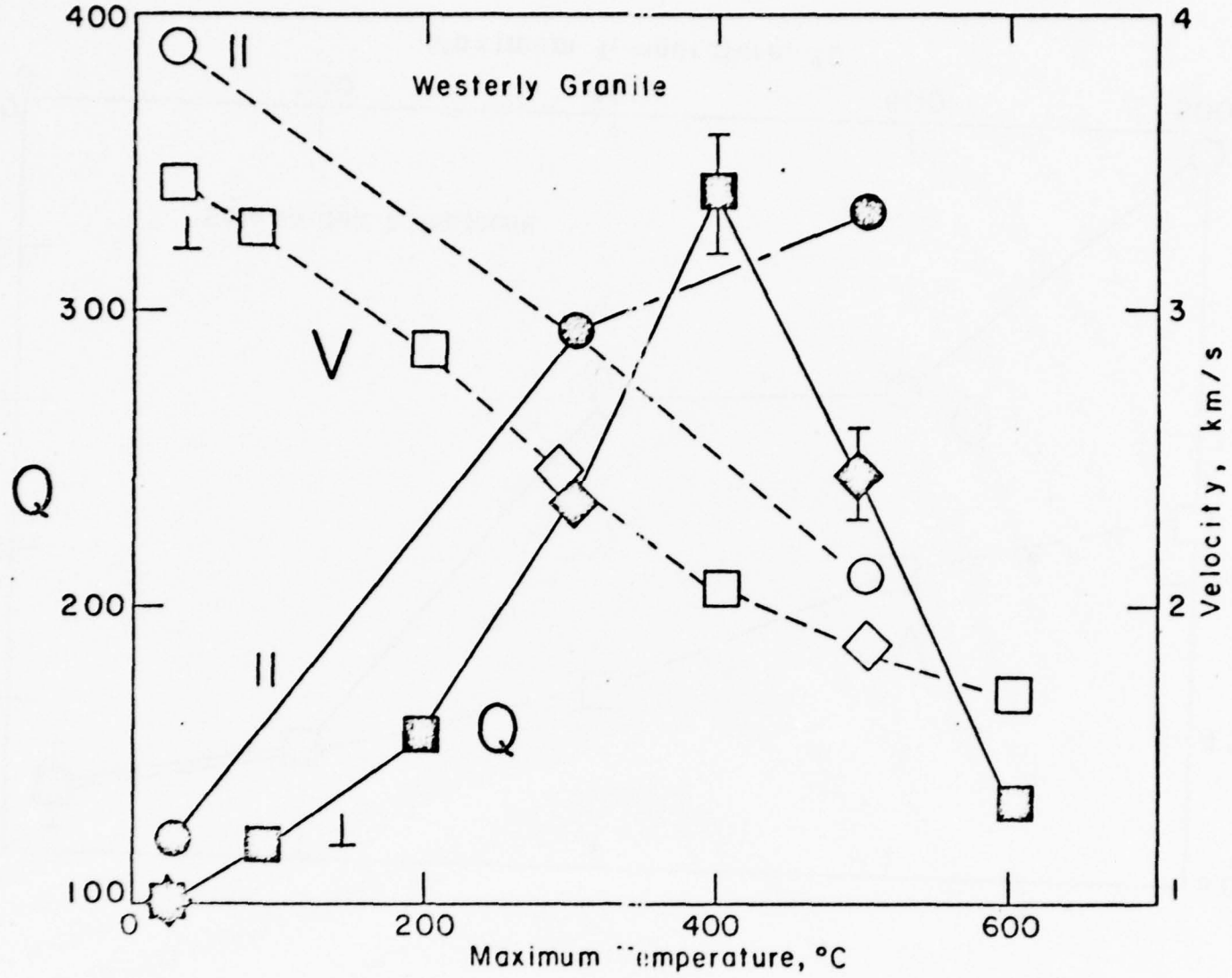
Westerly Granite
400
300
200
100
0
200
400
600
4
3
2
1
Q
V
Velocity, km/s
Maximum Temperature, °C
II
⊥
II
⊥
Q

Figure 10

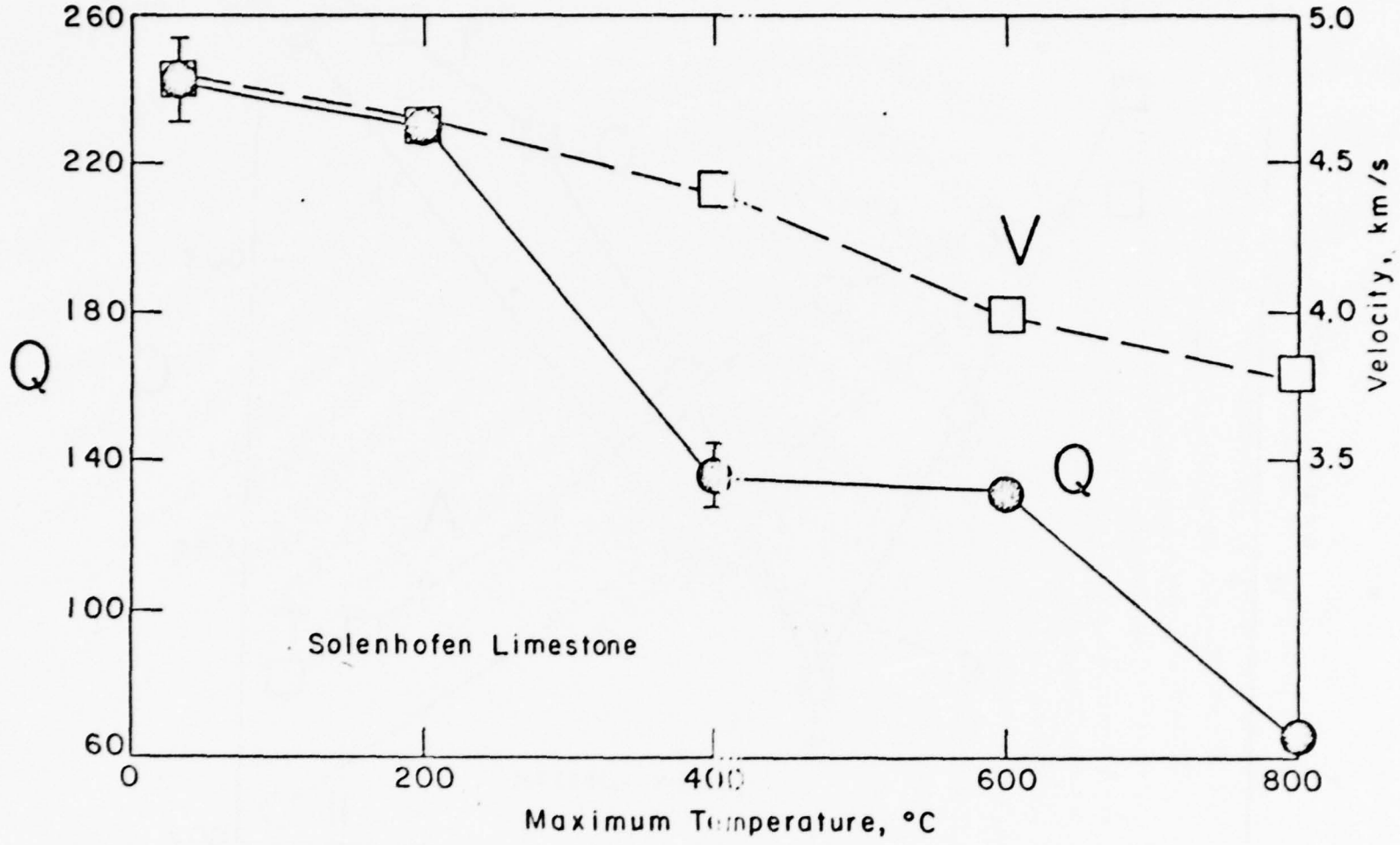
260
220
180
140
100
60
Q
5.0
4.5
4.0
3.5
Velocity, km/s
V
Q
Solenhofen Limestone
0
200
400
600
800
Maximum Temperature, °C

Figure 11

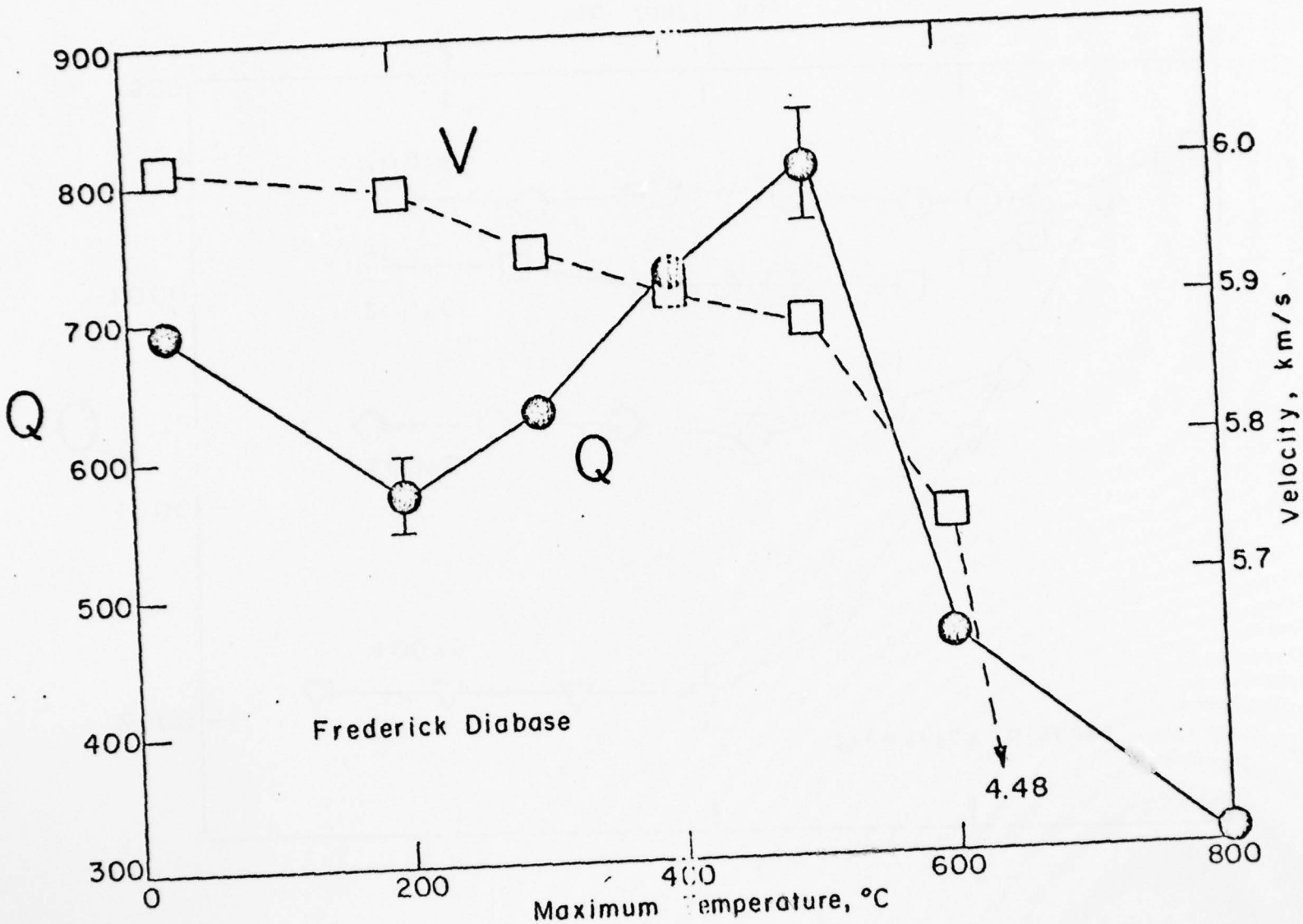
900
800
700
600
500
400
300
Q
V
Q
6.0
5.9
5.8
5.7
Velocity, km/s
Frederick Diabase
4.48
0
200
400
600
800
Maximum Temperature, °C

Figure 12

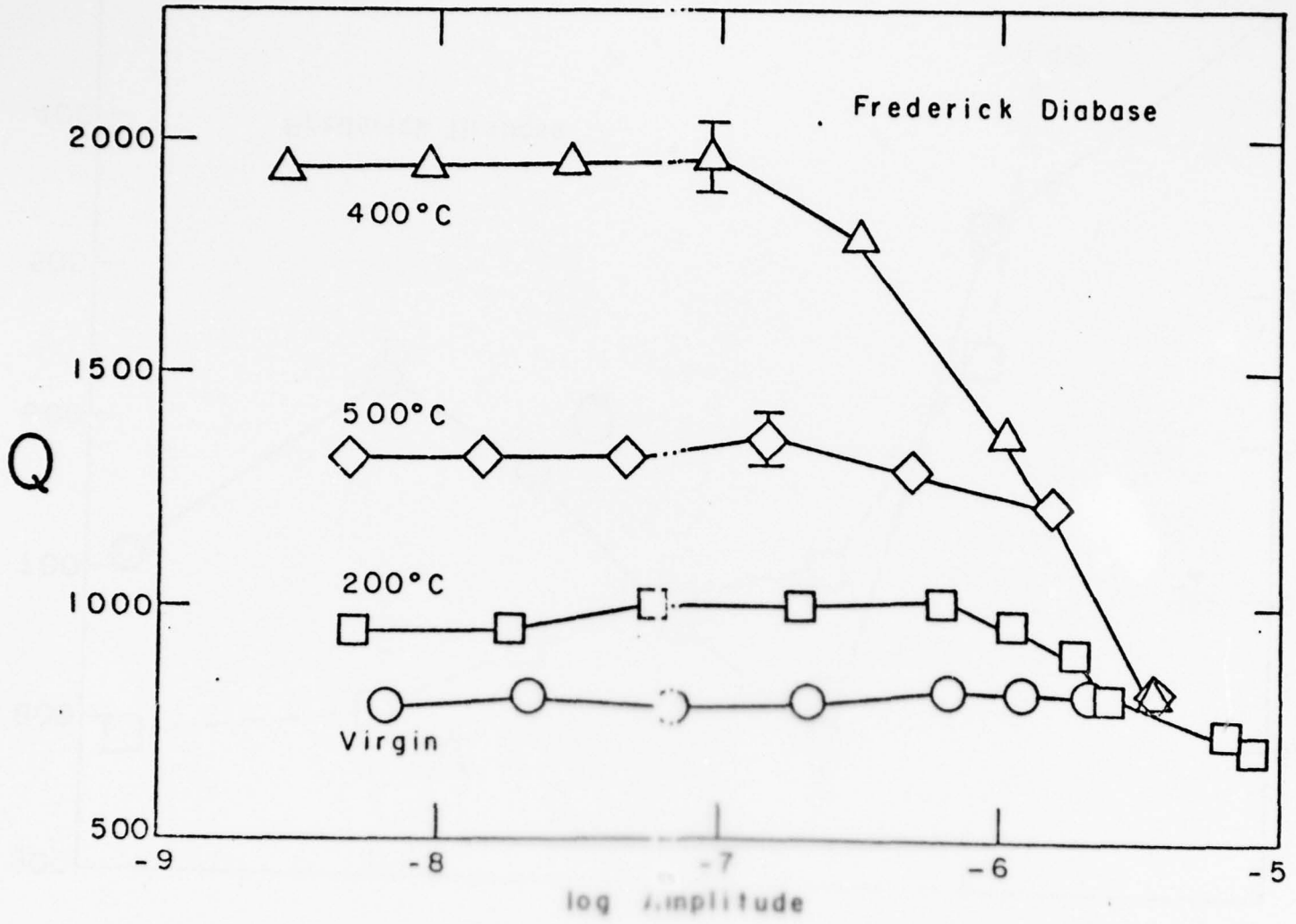
Frederick Diabase
400°C
500°C
200°C
Virgin
Q
2000
1500
1000
500
-9
-8
-7
-6
-5
log Amplitude

Figure 13

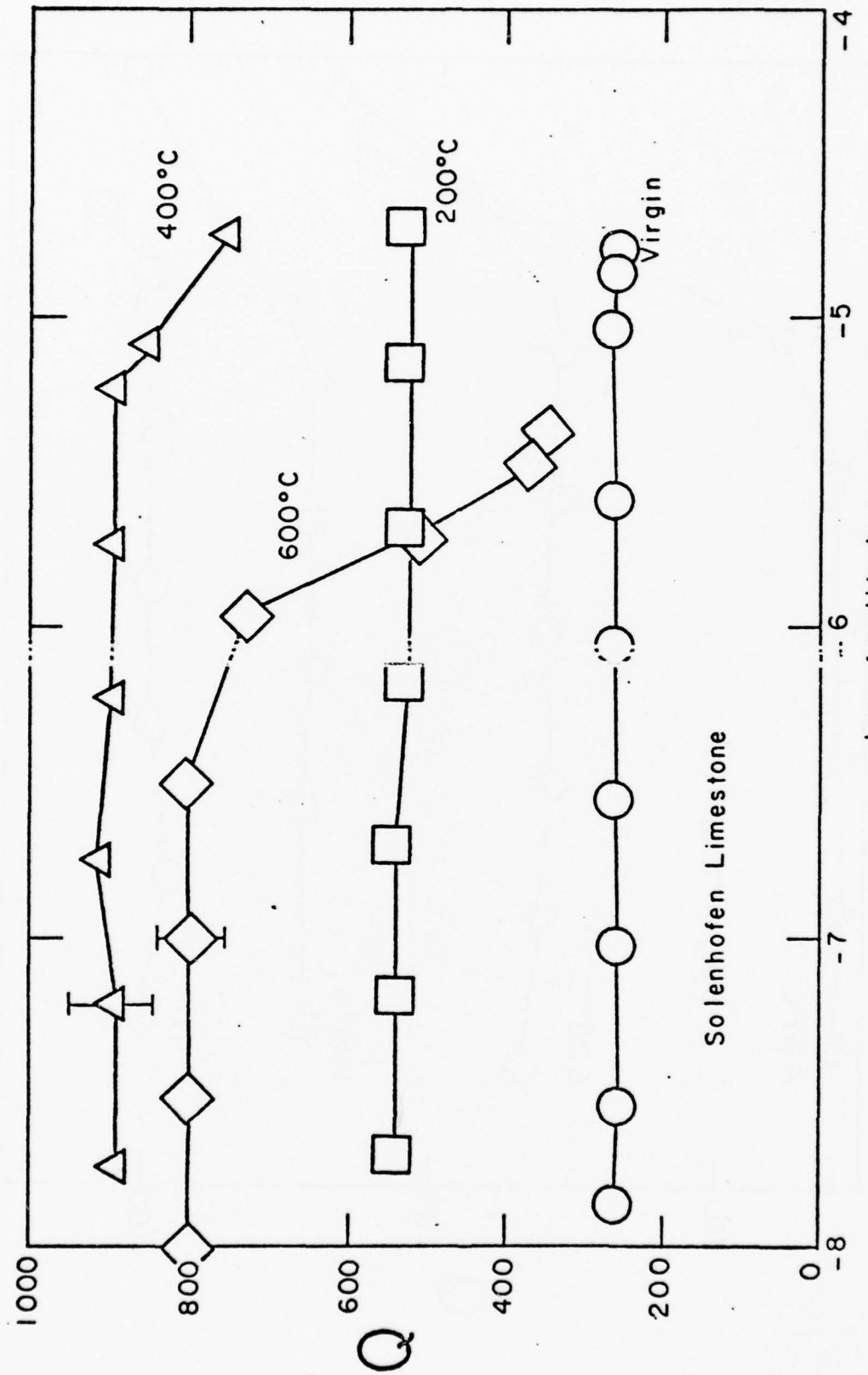
400°C
200°C
600°C
Virgin
Solenhofen Limestone
Q
1000
800
600
400
200
0
-4
-5
-6
-7
-8
log Amplitude

Figure 14

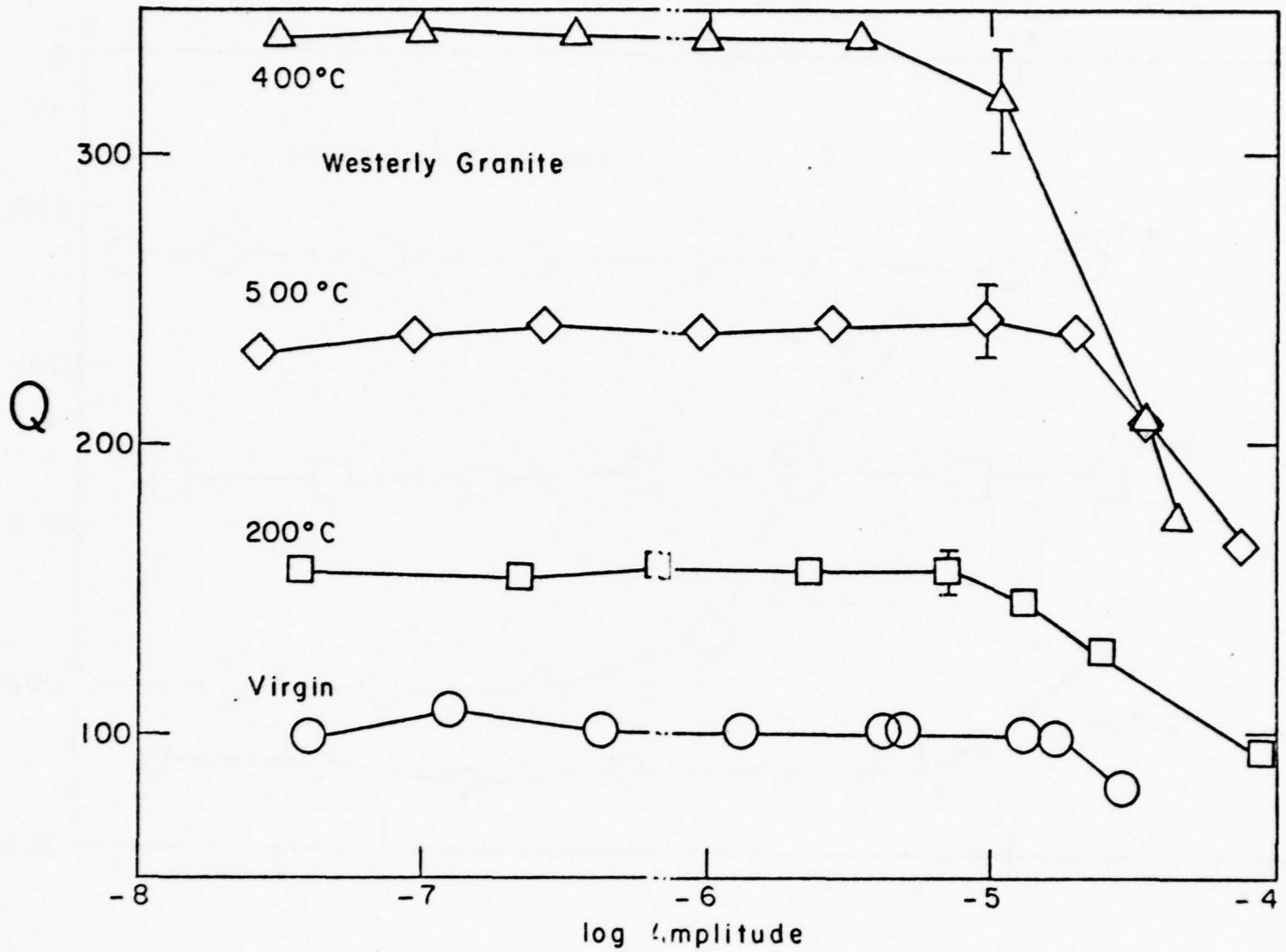
400°C
Westerly Granite
500°C
200°C
Virgin
Q
300
200
100
-8
-7
-6
-5
-4
log Amplitude

Figure 15

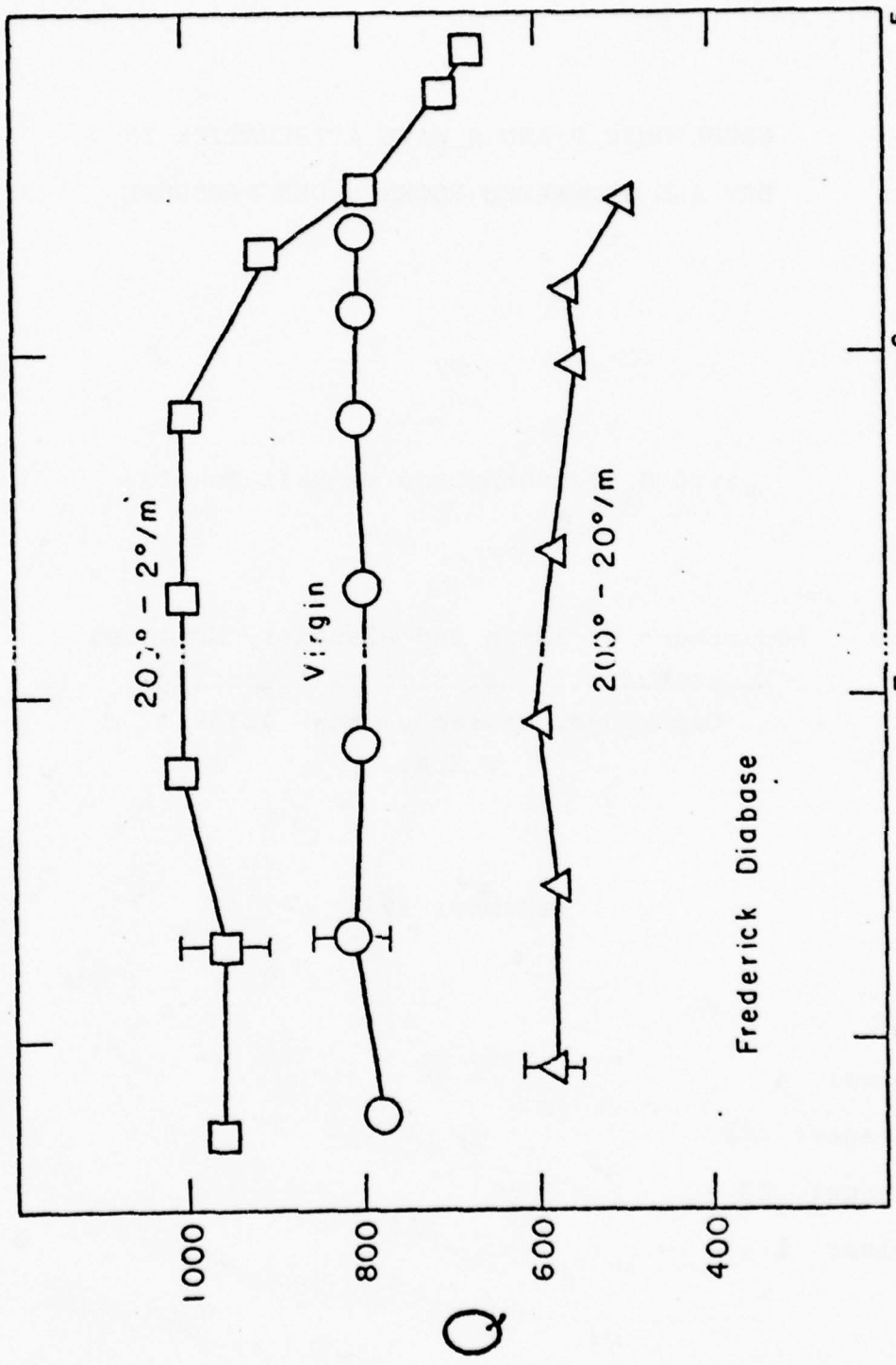
Q
1000
800
600
400
-5
-6
-7
-8
log Amplitude
Frederick Diabase
Virgin
200° - 2°/m
200° - 20°/m

Figure 16

ULTRASONIC P AND S WAVE ATTENUATION IN DRY AND SATURATED ROCKS UNDER PRESSURE

by

David H. Johnston and M. Nafi Toksöz

Department of Earth and Planetary Sciences
Massachusetts Institute of Technology
Cambridge, Massachusetts 02139
U.S.A.

December 1978

Copies: 4

MS Pages: 63

Figures: 23

Tables: 1

Address correspondence to: M.N. Toksöz, M.I.T. 54-518,
Cambridge, MA 02139

ABSTRACT

Ultrasonic P and S wave Q values as functions of hydrostatic pressure are presented for the Berea and Navajo sandstones, Bedford limestone, two shales and two tuffs. In most cases, the attenuation was obtained for both dry and water saturated samples. Q is determined by measuring the attenuation of the rock sample relative to a high Q standard of identical geometry using Fourier spectral ratios. The data show that Q increases with pressure, the rate of increase being dependent on rock type and crack density and distribution. Q_S is about equal to or larger than Q_P for dry rocks and less than Q_P for saturated rocks. In all cases, Q's for saturated rocks are lower than for dry samples. The variations of attenuation in shales are not crack controlled and an oil shale studied shows extreme and unusual anisotropy in velocity and Q. At ultrasonic frequencies, the attenuation in the tuffs studied is dominated by scattering losses.

INTRODUCTION

The attenuation of seismic waves has great potential as a tool to understand the physical conditions of rocks in the upper crust. Unfortunately, the systematics of the behavior of attenuation with pressure and saturation conditions are not well studied. In this paper we present ultrasonic Q data as functions of pressure for several dry and saturated crustal rocks.

Attenuation measurements have been carried out on samples in the laboratory using a variety of techniques (Attewell and Ramana, 1966; Birch and Bancroft, 1938; Born, 1941; Bradley and Fort, 1966; Gardner et al., 1964; Hamilton, 1972; Jackson, 1969; Knopoff, 1964; Nur and Simmons, 1969; Peselnick and Zietz, 1959; Peselnick and Outerbridge, 1961; Spetzler and Anderson, 1968; Tittmann et al., 1974; Toksöz, et al., 1979; Warren et al., 1974; Watson and Wuenschel, 1973; Wyllie et al., 1962). In a most general way, these measurements show that Q is independent of frequency, fluid saturation increases attenuation (Gardner et al., 1964; Obert et al., 1946; Watson and Wuenschel, 1973; Wyllie et al., 1962), and increasing pressure decreases attenuation (Gardner et al., 1964; Gordon and Davis, 1968; Klima et al., 1964; Levykin, 1965; Toksöz et al., 1979). However, more laboratory data are needed under controlled conditions to determine the effects of fluids and pressure on the attenuation in porous rocks.

EXPERIMENTAL METHOD

Q values for P and S body waves are determined with an ultrasonic pulse transmission technique described in Toksöz et al. (1979). The attenuation is measured relative to a reference sample of low attenuation using spectral ratios, Pulse transmission methods are superior to resonant bars for measurements taken on jacketed samples under pressure if geometric factors such as beam spreading and reflections can be corrected for. Only one-way transmission effects are measured. The sample to be studied and reference sample have exactly the same shape and geometry. Essentially, two measurements are made using identical procedures, one with the rock of interest and again with the reference sample.

The amplitudes of plane seismic waves for the reference and the sample can be expressed as

$$A_1(f) = G_1(x)\, e^{-\alpha_1(f)}\, e^{i(2\pi f t - k_1 x)}$$

$$A_2(f) = G_2(x)\, e^{-\alpha_2(f)}\, e^{i(2\pi f t - k_2 x)} \qquad (1)$$

where A = amplitude, f = frequency, x = distance, $k = 2\pi f/v$ = wavenumber, v = velocity, and G(x) is a geometrical factor which includes spreading, reflections, etc. $\alpha(f)$ is the frequency dependent attenuation coefficient. Subscripts 1 and 2 refer to the reference and sample respectively. From

available data it is reasonable to assume that over the frequency range of measurements, 0.1-1.0 MHz, α is a linear function of frequency, although the method itself tests this assumption (Knopoff, 1964; Jackson and Anderson, 1970; McDonal, et al., 1958). Then one can write:

$$\alpha(f) = \gamma f \tag{2}$$

where γ is constant and related to the quality factor Q by

$$Q = \frac{\pi}{\gamma V} \tag{3}$$

When the same geometry is used for both the sample and standard (i.e., same sample dimensions, transducers, arrangements) then G_1 and G_2 are frequency independent scale factors. The ratio of the Fourier amplitudes are:

$$\frac{A_1}{A_2} = \frac{G_1}{G_2} e^{-(\gamma_1 - \gamma_2) f x} \tag{4}$$

or

$$\ln \frac{A_1}{A_2} = (\gamma_2 - \gamma_1) f x + \ln \frac{G_1}{G_2} \tag{5}$$

Since G_1/G_2 is independent of frequency and x is the sample

length, $(\gamma_2 - \gamma_1)$ can be found from the slope of the line fitted to $\ln(A_1/A_2)$ versus frequency. If the Q of the standard reference is known, γ_2 of the sample can be determined. When the Q of the standard is very high (i.e. $Q_1 = \infty$) then $\gamma_1 = 0$ and γ_2 of the rock sample can be determined directly from the slope.

The samples used in this study are cylindrical, 2.54 cm long and 3.175 cm in diameter. Transmitter and receiver transducers (each 2.5 cm in diameter) are mounted in a stacked P and S wave arrangement at opposite ends of jacketed samples. The pore or fluid pressure, P_f, system, capable of 2 kb, is controlled independently of the confining pressure, P_c (rated to 10 kb). Generally, the experiments are run to a maximum differential pressure, $P_d = P_c - P_f$, of 2.25 kb in discrete steps. At each pressure step, velocity for the ultrasonic pulse is determined by matching an electronically delayed timing pulse with the first arrival, transit time being measured to a 10 ns accuracy using a time interval counter. Full P and S waveforms are recorded at each step and then manually digitized. These waveforms are then windowed and cosine tapered at the end to remove reflections. A standard FFT routine is used to obtain the amplitude spectra.

In this study we used aluminum as a standard reference. Q for aluminum is about 150,000 (Zamanek and Rudnick, 1961), as opposed to $Q \leq 1000$ for rocks. Thus taking $\gamma_1 = 0$ never

introduces more than 1% error. For typical rocks where $Q = 10\text{-}100$, the error is less than 0.1% and is negligible. A more serious concern is the validity of assumption that the geometric factors G_1 and G_2 have the same frequency dependence, and G_1/G_2 is independent of frequency. With polished rock surfaces and good coupling between the transducer holder and sample, one would not expect frequency dependent reflection coefficients at the interface.

Formal errors of the Q measurements, however, are difficult to assign. Strict interpretation of the errors on fitting a straight line to the amplitude ratios only determines the modulation character of the ratios and not the accuracy of the method. It is clear, however, that a reliable estimate of Q may be obtained only if the slope of $\ln(A_1/A_2)$ versus frequency is large. Thus the method is not satisfactory for samples with high Q (>100).

The resolution and accuracy of the method can be based only on reproducibility and comparison with other techniques. Repeated measurements showed that pulse amplitudes, shapes and spectra were duplicates and Q values determined to within about 15%. Digitizing errors were found to be no larger than the repeatability. Furthermore, results described in this paper for the Berea sandstone may be compared to data (Toksöz et al., 1979) for the same rock at the same pressure and saturation conditions using the same technique but obtained at a different laboratory with different sample dimensions.

There is excellent agreement. Thus the reproducibility of the Q measurements may be conservatively estimated at 15-20%. To check for bias in the method, Q was obtained for plexiglas using the ultrasonic pulse and resonant bar techiques. The Q values determined, 20 and 22 respectively, agreed to within the resolution of the spectral ratio method and thus we may assume are not overly biased. Error bars for several reprentative data points are shown on each graph in this paper.

As examples of the Q measurement technique, waveforms, normalized spectra and spectral ratios are shown for P and S waves in the dry Navajo sandstone in Figures 1a.b for two confining pressures. In these figures, the dashed line in the spectrum plots corresponds to the aluminum standard (Al). Only waveforms for the rock sample are shown. A rather large DC shift is noted for the S waves. This feature, common to many of the experiments, is due to low frequency noise. This could be filtered out prior to time windowing but was not necessary since the low frequency portion of the spectrum is not used in determining Q. One can see from the figures, though, that the slopes of the spectral ratio plots clearly decrease with increasing pressure indicating an increase in Q. Q values are calculated from these slopes and the measured P and S wave velocities.

DESCRIPTION OF SAMPLES

The rock samples chosen for this study include two sandstones, a limestone, two shales and two tuffs. Relatively low Q's were expected in these rocks making them amenable to the pulse technique. Furthermore, most of the samples are quite commonly used in the laboratory and thus much subsidiary information on their properties may be obtained. In fact, the Berea sandstone and Bedford limestone are accepted "standard" rocks by the U.S. Bureau of Mines (Krech et al., 1974).

Each sample was characterized in terms of mineral content, grain size and contacts, density, porosity, permeability and static stress-strain properties. Detailed sample descriptions may be found in Johnston (1978). Several important physical parameters for each rock are listed in Table 1. Specifically the following rocks were studied:

1. Berea Sandstone. The Berea is a relatively clean, medium to fine-grained protoquartzite with silica and clay cement. The porosity of the sample used was 18% with a permeability of about 75 md. Its static response, typical of many rocks, is shown in Figure 2 where linear strain is plotted as a function of hydrostatic confining pressure. The non-linear portion of the curve is due to crack closure (Walsh, 1965) and permanent hysteresis upon unloading indicates that not all the cracks have closed elastically.

2. Navajo Sandstone. The Navajo is classified as an orthoquartzite cemented primarily by silica with only minor

amounts of clay. The sample studied had a porosity of 16% and an estimated permeability of 100 md. The static response is very similar to that observed for the Berea sandstone.

3. Bedford Limestone. Also known as the Salem, Spergen and Indiana limestone, the Bedford is coarse grained, made of poorly sorted fossil debris cemented by crystalline calcite. The porosity of the sample used was 12% and the permeability is about 1 md (Krech et al., 1974). Pore collapse under hydrostatic pressure occurs at about 1 kb as shown in Figure 3. Upon unloading the sample, a large increase in crack porosity due to the pore collapse is noted. It will be seen that this has a large effect on the acoustic properties.

4. Esopus Shale. The Esopus is a dark gray, calcareous silty shale found in eastern New York state. The porosity and permeability were both too small to be measured. Furthermore, when dry, the rock is extremely friable and thus only a saturated experiment was run.

5. Colorado Oil Shale. The sample used in this study was obtained from the Anvil Points Mine and represents a typical, medium grade oil shale with about 20% kerogen by weight. Again there is no measureable porosity or permeability. The rock is visually aniostropic and cores were taken both normal and perpendicular to the bedding planes. Static measurements show a 30% anisotropy in linear strain. Little or no crack porosity is evident and there is little permanent hysteresis.

6. Ammonia Tanks Tuff. The Ammonia Tanks is classified as a moderately welded quartz latite and is compositionally complex (Byers et al., 1976). The porosity of the sample used was measured as 5.8% but this probably does not include substantial unconnected porosity. Grain sizes can be as large as 5 mm. The static response of this and the following tuff at low stresses (<60 bars) suggest that compared to the sandstones, far fewer fine cracks exist (Morrow et al., 1977). The total crack porosity, however, is larger (Johnston, 1978) implying that the bulk of the cracks in the tuffs are fairly wide.

7. Tunnel Beds Tuff. The Tunnel Beds is an ash fall tuff, poorly sorted with very coarse grains 2-4 mm in diameter. The measured porosity was 29.6%. As with the Bedford limestone, pore collapse occurs under hydrostatic compression but at a pressure of about 500 bars.

EXPERIMENTAL DATA

In this section, ultrasonic Q data as functions of saturation and pressure are presented. For each experiment an aluminum sample with the same shape of the rock sample was used as a standard reference. Q values were calculated from spectral ratios of rock - aluminum pairs at each pressure.

1. Berea Sandstone

The Berea sandstone is a particularly well-studied rock and Q values as functions of pressure and saturation have been published in Toksöz et al. (1979). Here, those

experiments are repeated and several new ones run. In all, four experiments were run on the Berea: one with a dry sample, the second fully water saturated, the third partially saturated and the fourth an experiment where gas is released from solution in water by the reduction of pore pressure.

Unless otherwise noted, for the saturated runs of the Berea and other rocks presented in this paper, Q values are plotted as a function of differential pressure, P_d, defined as $P_c - P_f$ where P_c is the confining or overburden pressure and P_f is the fluid or pore pressure.

In the first experiment, Q values and velocities were determined for a vacuum dried sample at confining pressures up to 1 kbar. The velocity determinations are shown in Figure 4. The increase for P and S waves at low pressures is due to the closing of cracks (Toksöz et al., 1976) and corresponds to non-linear region of the static stress strain curve in Figure 2.

Q values, calculated from the slopes of the spectral ratios and velocities are shown in Figure 5. Q for the dry Berea sandstone increases rapidly with pressure, approaching a value over 100. As stated earlier, at high pressures, where Q values become high, the relative error

increases. However, the trend in Q versus pressure is clear. Q_s is about equal to Q_p.

A Berea sample was then saturated with distilled water and the experiment repeated. The fluid pressure was maintained at 0.465 the confining pressure for differential pressures ranging from 45 to 2000 bars. This ratio of pore-fluid and confining pressures is a nominal value for saturated sedimentary rocks where the fluid pressure is equal to the hydrostatic pressure of a water column.

The presence of water increases the velocity of P waves while decreasing the velocity of S waves as illustrated in Figure 4. The increase in velocity with pressure is not as great as for the dry sample. Q values are shown in Figure 6 as functions of differential pressure. Both Q_p and Q_s are substantially lower than their dry counterparts and in the saturated case Q_s is much lower than Q_p, approaching a value of only about 30 even at high pressure. Q_p increases to a value of about 60 by a pressure of about 750 to 1000 bars. While it appears that the effect of fluid saturation is to dramatically increase the attenuation, especially for S waves, the dependency of the Q values on pressure is still observed.

A similar set of Q determinations for the Berea sandstone were obtained by Toksöz et al. (1979). While the physical conditions (pressure and saturation) of the experiments were similar to those presented here, the geometry was somewhat different. The results of the two sets of experiments agree very well, enhancing our confidence in the experimental technique.

Finally, two experiments were run to investigate the effects of partial water saturation on Q. The primary influence of water saturation in known from data like those presented by Gardner et al. (1964) for the Berea. Q for both longitudinal and torsional vibrations of bars was observed to decrease rapidly relative to a dry sample for small amounts of water saturation. In these experiments we start from fully saturated samples and then reduce the water saturation.

In the first run, partial saturation was obtained by partially drying out a completely saturated sample. The sample was stored in an airtight plastic bag for over a week to allow the pore water to equilibrate throughout the rock. Prior to jacketing, the sample was reweighed and the saturation was determined to be 37%. Q values for this experiment are shown in Figure 7. Comparing these data with those of the completely water saturated Berea sandstone (Figure 6), one finds that Q_p is slightly lower relative to the fully saturated sample at intermediate pressures while Q_s is essentially unchanged. There is no evidence, however, that P wave attenuation changes more than a factor of two relative to full saturation at this degree of partial saturation.

In order to examine this in greater detail, an experiment was designed so that partial saturation could be achieved by the release of helium gas from saturated pore water by reducing the fluid pressure in a closed system. The pore pressure apparatus and the procedure used for this experiment

is described in Johnston (1978). At a fluid pressure of 200 bars and a confining pressure of 400 bars, the completely water saturated sample and pore pressure system was injected with the volume of gas required to completely saturate the water at a fluid pressure of 1000 bars. Fluid pressure was then increased to 1200 bars maintaining a differential pressure of 200 bars by simultaneously raising the confining pressure to 1400 bars. Then, fluid and confining pressure were both lowered, allowing the gas to come out of solution. Starting from zero gas saturation at 1000 bars fluid pressure, a total gas saturation of 5% was obtained at a fluid pressure of 150 bars. Velocities were determined and waveforms recorded at discrete pressures.

The presence of free gas in the rock was confirmed two ways. First, the compressibility of the pore fluid could be roughly determined by the volume change required to affect a given pressure drop. This clearly indicated an increase in compressibility at fluid pressures below 1000 bars but assumed that the gas phase was homogeneously distributed throughout the system. More concrete evidence was found in the velocities shown in Figure 8. Here, V_p and V_s are plotted as functions of pore fluid pressure and calculated gas saturation. Clearly, V_p decreases with increasing gas saturation while V_s remains constant. This behavior is exactly as would be expected from theory but as a check, V_p was determined theoretically

(Kuster and Toksöz, 1974; Toksöz et al., 1976) for a change was the compressibility of the water as a function of fluid pressure. This calculation is shown as the dashed line in Figure 8 and obviously does not explain the data except for the two high pressure points which are supposed to be completely water saturated anyway. It appears then, that the experiment was indeed successful in releasing helium gas from solution in the rock.

Q_p and Q_s are shown as functions of gas saturation and fluid pressure in Figure 9. The average values of both are comparable to those obtained at 200 bars differential pressure in the previous experiments. Clearly, there is no change in Q_s as a function of gas saturation in 0 to 5% range. There are variations in Q_p and even though they are within the resolution of the experimental technique, they might be significant. In particular, there is a reduction in Q_p up to a gas saturation of 3 or 4% at which Q_p increases to its full water saturation value.

While the significance of these results are questionable, it should be pointed out that the maximum effects of partial gas saturation are to be expected at low pore pressures. Thus, the changes in Q observed here might possibly be amplified somewhat.

2. Navajo Sandstone

As with the Berea sandstone, Q values were obtained for the Navajo in a vacuum dried sample and a water saturated sample. Velocity as a function of pressure is shown in Figure 10 for P and S waves. Consistent with static stress-strain measurements, velocity increases more rapidly at lower pressures than for the Berea. Furthermore, the values for velocity are higher - 3.56 km/s versus 3.22 km/s for P waves in dry rock at 45 bars and 4.37 km/s versus 4.23 km/s at 1000 bars as examples. Similar comparisons may be made for the saturated samples and for S waves.

Q values for the dry rock obtained from the spectral ratios are shown in Figure 11. Again, it must be mentioned that the high Q values at the higher pressures are unreliable - a restriction of the experimental technique. However, for pressures less than 500 bars, one may say that the Q's calculated for both P and S waves behave in much the same manner as for the dry Berea sandstone. The absolute values of Q are higher than for the Berea - 30 compared to 24 for P waves at 45 bars confining pressure. Q also seems to increase at a slightly faster rate with pressure.

In the second experiment the sample was saturated with distilled water and as with one of the Berea runs, P_f was maintained at 0.465 P_c. Q values are shown in Figure 12. In this case, the differences between the Navajo and Berea sandstones are more clearly observed. While the Q's obtained

for the Navajo are substantially the same as those for the Berea at pressures greater than 600-700 bars, the increase in Q at low pressures is much faster for the Navajo. Also, as with the dry case, the absolute Q values, particularly for P waves, are higher for the Navajo. This is in good agreement with the differences observed in the velocity measurements. Clearly, this is a good example of how the same parameters that determine elastic properties also affect attenuation.

3. Bedford Limestone

The Bedford limestone presents an interesting comparison to the sandstone. Although the total porosity is rather high (12%), the crack porosity is somewhat lower than the sandstone. Also, pore collapse, initiated at 1000 bars, alters the typical behavior of both velocity and Q observed in the sandstones. Again, two experiments were run, one dry and the other saturated. For the water saturated case P_f was maintained at .465 P_c throughout the experiment.

P and S wave velocities for the Bedford limestone are shown in Figure 13. We note the general features of an increase in velocity due to crack closure up to about 500 bars and higher P wave and lower S wave velocities for the saturated sample. At 1000 bars the effect of pore collpase becomes evident. During the loading cycle (increasing differential pressure), velocity increases as the large pores collapse. As the rock is unloaded (decreasing pressure), it behaves

elastically until about 800 bars at which point, cracks induced by pore collapse open, reducing the velocities to a point well below those obtained during the loading cycle. This type of behavior was identified by Nur (1969) and, of course, confirmation lies in the static stress-strain measurements shown in Figure 3. The effect is observed for both P and S waves in both dry and saturated samples.

There was some question as to the quality of the shear waves in the dry rock and thus the results should be used with caution. As we will see, the dry Q_s values are not consistent with the other data. There is no explanation at the present time as to why this is so. The resulting Q values for the dry sample are plotted as functions of confining pressure (P_f = 0) in Figure 14. Concentrating on the P wave values, we see that Q_p is much higher than for sandstones at low pressures - around 70 at 105 bars. The rate of increase with pressure is lower than the sandstones however, and at pressures of 700-800 bars, Q_p is only slightly higher than the values attained by the sandstones. While the data is shown only to a pressure of 1000 bars (subjected to the constraints of the experimental method), the sample was run to a maximum pressure of 2250 bars. During the unloading cycle, the effect of pore collapse is evident at the lower pressures. Q_p is sharply reduced at pressures less than 1000 bars due to the large increase in crack porosity. For example, at 100 bars

the Q is lowered by 52% (118% increase in attenuation). This may be compared to the 344% increase in crack porosity obtained from the static measurements. Clearly, not all of these cracks are of sufficiently low aspect ratio (crack width to length ratio) at 100 bars to contribute to the attenuation. Indeed, Q appears to level off from 250 to 100 bars on the unloading cycle implying a lower limit to the induced crack aspect ratio spectrum at surface pressure.

Q values calculated for the saturated Bedford limestone are shown in Figure 15. Again the Q is lower than for the dry case - by a factor of two for P waves at 500 bars for example, and Q_s is lower than Q_p. However, we see little difference between the supposed dry Q_s values (Figure 14) and the wet ones. Nor do the dry S results increase with pressure as the wet data. We would expect from what we have seen in the velocities, that the changes in Q for the dry rock at pressures less than 500 bars would be more rapid than the wet rock.

In any event, the rapid increase in Q at low pressure is followed by a levelling off up to about 900 bars. An increase in Q, particularly for S waves, occurs at that point due to pore collapse. The final value of Q_s obtained at 2000 bars is nearly twice that obtained by the sandstones. The increase in Q_p is not as dramatic. However, upon unloading the sample, the effect of induced cracks is much greater for P waves than S waves although both obtain lower values than during the loading cycle.

4. Shales

The first experiment run was on the Esopus Shale. Because the porosity and permeability of this sample is so low, a full series of pressures was not used. Furthermore, since the rock becomes very friable when dry, only a water saturated test was run. Rather than applying pore pressure, the sample remained with atmospheric pore pressure during the course of the experiment.

Data were obtained at 105, 500, 1000, and 2000 bars confining pressure. The sample was held at each pressure for two hours to allow the pore pressure to equilibrate. Velocities were continuously monitored during this time and the experiment continued once the velocity leveled off to a constant value. However, the sample was kept at 1000 bars overnight (16 hours) resulting in a further increase in velocity. This implied that 2 hours were not enough to equilibrate pore pressure. Velocities obtained unloading the sample show that the data from 1000 bars (after the 16 hours wait) and 2000 bars probably most closely represent the completely equilibrated values.

V_p and V_s for the 2 hour equilibrated points and the 16 hour equilibrated run at 1000 bars are shown as functions of confining pressure in Figure 16. The changes in velocity are not nearly as great as for the sandstones or limestones

due to the absence of fine cracks implied by the lack of effective porosity or permeability. The unloading portions of the velocity curves, while offset from the low pressure loading curves due to pore pressure equilibration, have essentially the same curvature, further corroborating the absence of fine cracks.

Very little obvious change in the nature of the waveforms and spectra was observed implying that Q does not change very drastically. This is, in fact, clear in Figure 17 where the Q values obtained from the spectral ratios are plotted as functions of confining pressure. The effect of pore pressure equilibrium and unloading is the same for attenuation as velocity. The Q values for the Esopus shale are consistently higher than for the saturated sandstones at all pressures although the difference is minimized at higher pressures where the fine cracks in the sandstones have closed. The large difference between Q_p and Q_s may be due to slippage in clay lubricated grain contacts oriented parallel to the bedding and perpendicular to the direction of S wave propagation. Both Q_p and Q_s are also higher than in situ values (32 and 10 respectively) obtained for the Pierre shale by McDonal et al. (1958) but lie well within the range of Q values for various shales listed by Bradley and Fort (1966).

Two experiments were run for the Colorado Oil Shale - one perpendicular to the bedding and the other parallel.

As with the Esopus shale the samples were completely saturated but $P_f = 0$ throughout the experiment. The velocities, plotted in Figure 18 are consistent with the static measurements mentioned earlier. For both P and S waves, velocity is higher in the direction parallel to the bedding. There is little evidence of microcracks since the velocities show no rapid changes at low pressures and increase less than 20% by 2000 bars compared to an increase of over 30% for sandstones.

Because the slopes of velocity versus pressure are virtually identical for both orientations, we may assume that the variations in velocity observed are not controlled by cracks. Furthermore, the presence of kerogen in the shale seems to play an important role in determining both the elastic and anelastic properties. First, the Poisson's ratio calculated from the velocities is 0.40 - implying that the shale is behaving more like some polymers than rock. For comparison, the Poisson's ratio of the Esopus shale is 0.27. Secondly, it was very difficult to propagate S waves, particularly those in the direction normal to the bedding (plane of polarization parallel to bedding.) Furthermore, a frequency dependent component of the spectral ratios was observed. This was not true for the Esopus shale.

Q versus confining pressure ($P_f = 0$) for both P and S waves in both directions are shown in Figure 19. The results are peculiar - not all expected. First note that Q in all

cases remain unchanged with pressure - confirming the lack of cracks. Q_s is very low, as would be expected, and Q_s for the perpendicular direction is lower than the parallel one, mimicking the anisotropic velocity behavior. However, the anisotropy of Q in P waves is reversed from that of velocity. Furthermore, there is a large discrepancy in the differences between Q_p and Q_s for the two orientations. In the parallel case Q_s is nearly equal to Q_p. Finally, this is the only case we have seen in which the changes in Q with pressure are less than the changes in velocity.

5. Tuffs

The study of attenuation in tuffs was prompted by interesting differences in pore, grain size and crack distributions compared to the sandstones implied by static measurements. It was found that the tuffs contain fewer small aspect ratio cracks than either the Berea or Navajo sandstones even though the total porosities are roughly equivalent. Also, the observed attenuation in both Ammonia Tanks and Tunnel Beds tuffs appear to be dominated by scattering even though the effect of cracks is evident.

In Tunnel Beds, the Q measurements are further complicated by the presence of pore collapse under pressure. For both tuffs, only dry samples were examined.

P and S wave velocities for the Ammonia Tanks tuff are shown as functions of confining pressure ($P_f = 0$) in Figure 20. Velocity increases more gradually with pressure than for the sandstones and does not begin to level off until about 1500 bars. P wave velocities are similar in magnitude to the Navajo and about 5% higher than the Berea even though the measured porosity is much less, 5% compared to 16-18%. S wave velocities are uniformly lower than the sandstones by about 5%. This implies that isolated pores and cracks may exist in the rock and that the actual porosity is higher than that measured.

The Q analysis was complicated by the presence of scattering which introduces a frequency dependent component to the apparent attenuation. Thus the spectral ratios are not linear over a broad frequency range. The Q values calculated are strictly applicable only to a frequency bandwidth limited to the peak power of the spectrum. For the Ammonia Tanks, this occurs at about 0.4 MHz for P waves and 0.5 MHz for S waves. The resulting Q values are shown in Figure 21. The most outstanding features of the data are the low Q values at all pressures and that Q_s is nearly 1.5 times Q_p. Since one would intuitively expect that the attenuation due to scattering would be relatively constant

with pressure, the increase in Q_p and Q_s with pressure may be due to crack closure just as with the sandstones. However, as with velocity, the rate of increase is slow compared to the sandstones.

The large difference between Q_s and Q_p (also observed in the Tunnel Beds as will be seen) is obtainable from the Walsh (1966) friction mechanism but requires a lower coefficient of friction than for the dry sandstone since the Poisson's ratio is 0.24 compared to 0.17. Another explanation may be that the attenuation due to scattering of incident S waves is less than for incident P waves.

The Tunnel Beds tuff was more difficult to work with compared to the Ammonia Tanks. With its very high porosity (30%), vugular pore spaces, and large grain sizes, scattering completely dominates the anelastic behavior at ultrasonic frequencies. Pore collapse, initiated at about 800 bars and observed in the velocities shown in Figure 22, further complicates the picture. P and S wave velocities, about 25-30% lower than the Ammonia Tanks do, however, behave predictably and in a manner similar to the Bedford limestone. Under loading, velocity increases slightly at low pressures due to crack closure and then levels off. At 800 bars, velocity increases again as pores collapse. During unloading of the sample, velocities are higher than the loading cycle for pressures greater than 800 bars but are lower at lower pressures due to cracks generated during pore collapse.

Q values were again determined for a limited bandwidth centered on roughly 0.4 MHz for both P and S waves and are plotted in Figure 23. Q is essentially constant with pressure, consistent with the domination of scattering. There is, however, evidence of the effect of pore collapse barely observable in the loading cycle but more evident in the unloading cycle. A clear decrease in Q relative to the loading path that can be attributed to crack production during pore collapse. As with the Bedford limestone, the difference seems to be greater for P waves. Also, as seen for the Ammonia Tanks, Q_p is less than Q_s by about the same amount. Here, however, the Poisson's ratios are comparable with the sandstones.

CONCLUSIONS

Ultrasonic P and S wave Q values have been presented for a suite of dry and saturated rocks including sandstones, a limestone, shales and tuffs as functions of pressure. These measurements showed the effects of different rock properties on the attenuation of seismic waves. Several general aspects concerning the behavior of attenuation under the experimental conditions studied in this paper are:

1. Q increases (attenuation decreases) as a function of confining pressure (or differential pressure for saturated rocks). The rate of increase varies depending on rock type and crack density and distribution.

2. For the sandstones and limestone measured under dry and water saturated conditions, both Q_p and Q_s are higher

for the dry case as compared to the saturated values.

3. For the dry sandstones, Q_s is about equal to or slightly higher than Q_p. Q_s is larger than Q_p by nearly a factor of two in the dry tuffs.

4. For all the saturated rocks (including the shales), Q_s is lower than Q_p.

5. The pressure effects are dramatically enhanced during pore collapse as evident from both the velocity and attenuation data for the Bedford limestone and Tunnel Beds tuff.

6. The attenuation in tuffs appears to be controlled by factors other than those affecting the attenuation in other rocks such as sandstones and limestones. The behavior of Q in the tuffs, associated with scattering of the ultrasonic wave points out the fact that two different rock types with similar porosities may exhibit large differences in attenuation.

7. The behavior of attenuation in shales also seems to indicate a different mechanism than might be proposed for the sandstones or limestone. In particular, the lack of change in Q with pressure for the oil shale suggests that cracks are not involved.

8. Anisotropy in velocity is probably accompanied by anisotropy in attenuation. As illustrated by the oil shale data though, the anisotropic behavior of attenuation may not correspond directly to that of velocity.

The comparison of the data presented in this paper to in situ or other laboratory measurements of attenuation must be approached with caution. Ultrasonic attenuation data for the Berea sandstone (Toksöz et al., 1979) similar to the results shown here, have been modelled in terms of several attenuation mechanisms (Johnston et al., 1979) including sliding friction at cracks and grain boundaries, (Walsh, 1966), Biot (1956a,b; 1962a,b) type fluid flow, squirting flow from thin cracks to larger pores (Mavko and Nur, 1975; O'Connell and Budiansky, 1977), viscous shear relaxation in fluid saturated cracks and pores (Walsh, 1968 and 1969) and scattering from pores in the rock (Yamakawa, 1962). These theoretical models may be used to extrapolate the ultrasonic data to other frequencies.

While the frequency dependence of attenuation may possibly be determined, one aspect of the problem not considered in this paper is the variation of Q with strain amplitude. Numerous experimental studies have shown that although Q is relatively independent of amplitude for strains less than about 10^{-6} it decreases rapidly at higher strains (Gordon and Davis, 1968; Gordon and Radu, 1971; Peselnick, and Outerbridge, 1961; Winkler and Nur, 1978). Johnston (1978) has shown that apparent discrepancies in Q measurements obtained using low amplitude resonant bar techniques and ultrasonic methods may in part be explained by amplitude

dependence. Thus, if amplitudes at seismic frequencies are different from those used in laboratory measurements, absolute estimates of Q are invalidated.

Further work is required to characterize the differences in Q within specific rock types, to investigate the nature of crack lubrication due to fluid saturation and to study the effects of anisotropy such as observed in the oil shale. These could eventually lead to predictive models of attenuation in rocks providing information on both microstructure and fluid content.

REFERENCES

Attewell, P.B., Y.V. Ramana, Wave attenuation and internal friction as functions of frequency in rocks, Geophysics, 31, 1049-1056, 1966.

Biot, M.A., Theory of propagation of elastic waves in a fluid-saturated porous solid. I. Low frequency range, J. Acoust. Soc. Am., 28, 168-178, 1956a.

Biot, M.A., Theory of propagation of elastic waves in a fluid-saturated porous solid, II. High frequency range, J. Acoust. Soc. Am., 28, 179-191, 1956b.

Biot, M.A., Mechanics of deformation and acoustic propagation in porous media, J. Appl. Phys., 33, 1482-1498, 1962a.

Biot, M.A., Generalized theory of acoustic propagation in porous dissipative media, J. Acoust. Soc. Am., 34, 1254-1264, 1962b.

Birch, F. and D. Bancroft, Elasticity and internal friction in a long column of granite, Bull. Seism. Soc. Am., 28, 243-254, 1938.

Born, W.T., Attenuation constant of earth materials, Geophysics, 6, 132-148, 1941.

Bradley, J.J. and A.N. Ford, Jr., Internal friction in rocks, in "Handbook of Physical Constants", S.P. Clark, Jr., ed., Geol. Soc. Am. Publication, 175-193, 1966.

Byers, F.M., W.J. Carr, P.T. Orkild, W.D. Quinlivan, and K.A. Sargent, Volcanic suites and related cauldrons of Timber Mountain - Oasis Valley Caldera complex, southern Nevada, U.S.G.S. Prof. Paper, 919, 1976.

Gardner, G.H.F., M.R.J. Wyllie, and D.M. Droschak, Effects of pressure and fluid saturation on the attenuation of elastic waves in sands, J. Petr. Tech., 189-198, 1964.

Gordon, R.B., and L.A. Davis, Velocity and attenuation of seismic waves in imperfectly elastic rock, J. Geophys. Res., 73, 3917-3935, 1968.

Gordon, R.B. and D. Rader, Imperfect elasticity of rock, its influence on the velocity of stress waves, "Geophysical Monograph Series, Vol. 14", D.G. Heacock, ed., Am. Geophys. Un., Washington, DC, 1971.

Hamilton, E.L., Compressional wave attenuation in marine sediments, Geophysics, 37, 620-646, 1972.

Jackson, D.D., Grain boundary relaxations and the attenuation of seismic waves, Ph.D. Thesis, M.I.T., Dept. of Earth and Planet. Sci., 1969.

Jackson, D.D. and D.L. Anderson, Physical mechanisms of seismic wave attenuation, Rev. Geophys. Space Phys., 8, 1-63, 1970.

Johnston, D.H., The attenuation of seismic waves in dry and saturated rocks, Ph.D. Thesis, M.I.T., Dept. of Earth and Planet. Sci., 1978.

Johnston, D.H., Toksöz, M.N. and Timur, A., Attenuation of seismic waves in dry and saturated rocks, II, Mechanisms, Geophysics, in press, 1979.

Klima, K., J. Vanek, and Z. Pros., The attenuation of longitudinal waves in diabase and greywacke under pressures up to 4 kilobars, Studia Geoph. et Geod., 8, 247-254, 1964.

Knopoff, L., Q: Rev. Geophys., 2, 625-660, 1964.

Krech, W.W., F.A. Henderson, and E. Hjelmstad, A standard rock suite for rapid excavation research, U.S. Bureau of Mines, RI 7865, 1974.

Kuster, G.T., and M.N. Toksöz, Velocity and attenuation of seismic waves in two-phase media, Part I - Theoretical formulations, Geophysics, 39, 587-606, 1974.

Levykin, A.I., Longitudinal and transverse wave absorption and velocity in rock specimens at multilateral pressures up to 4000 kg/cm^2, Physics of the Solid Earth, 1, 94-98, 1965.

Mavko, G. and A. Nur, Melt squirt in the aesthenosphere, J. Geophys. Res., 80, 1444-1448, 1975.

McDonal, F.J., F.A. Angona, R.L. Mills, R.L. Sengbush, R.G. Van Nostrand, and J.E. White, Attenuation of shear and compressional waves in Pierre Shale, Geophysics, 23, 421-439, 1958.

Morrow, C., W.F. Brace, and E. Carter, Dramatic electrical changes in porous rocks at low stress, abstract, Trans. Am. Geophys. Un (EOS), 58, 1235, 1977.

Nur, A., Effect of stress and fluid inclusions on wave propagation in rock, Ph.D. Thesis, M.I.T., Dept. Earth and Planet. Sci., 1969.

Nur, A., and G. Simmons, The effect of viscosity of a fluid phase on velocity in low porosity rocks, Earth Planet. Sci. Lett., 7, 99-108, 1969.

Obert, L., S.L. Windes, and W.I. Duvall, Standardized tests for determining the physical properties of mine rocks, U.S. Bur. Mines R.I. 3891, 1946.

O'Connell, R.J., and B. Budiansky, Viscoelastic properties of fluid saturated cracked solids, J. Geophys. Res., 82, 5719-5736, 1977.

Peselnick, L. and I. Zietz, Internal friction of fine-grained limestones at ultrasonic frequencies, Geophysics, 24, 285-296, 1959.

Peselnick, L. and W.F. Outerbridge, Internal friction and rigidity modulus of Solenhofen limestone over a wide frequency range, U.S. Geol. Survey, Prof. Paper No. 400B, 1961.

Spetzler, H. and D.L. Anderson, The effect of temperature and partial melting on velocity and attenuation in a simple binary system, J. Geophys. Res., 73, 6051-6060, 1968.

Tittmann, B.R., R.M. Housely, G.A. Alers, and E.H. Cirlin, Internal friction in rocks and its relationship to volatiles on the moon, in Lunar Science Conf., 5th Proc. Geochem. Cosmochim. Acta, Suppl. 5, 3, 2913-2918, 1974.

Toksöz, M.N., C.H. Cheng, and A. Timur, Velocities of seismic waves in porous rocks, Geophysics, 41, 621-645, 1976.

Toksöz, M.N., D.H. Johnston, and A. Timur, Attenuation of seismic waves in dry and saturated rocks, I. Laboratory measurements, Geophysics, in press, 1979.

Walsh, J.B., The effect of cracks on the compressibility of rock, J. Geophys. Res., 70, 381-389, 1965.

Walsh, J.B., Seismic wave attenuation in rock due to friction, J. Geophys. Res., 71, 2591-2599, 1966.

Walsh, J.B., Attenuation in partially melted material, J. Geophys. Res., 73, 2209-2216, 1968.

Walsh, J.B., New analysis of attenuation in partially melted rock, J. Geophys. Res., 74, 4333-4337, 1969.

Warren, N., R. Trice, and J. Stephens, Ultrasonic attenuation, Q measurements on 70215, 29, Geochim. Cosmochim. Acta, Suppl. 5, 2927-2938, 1974.

Watson, T.H. and P.C. Wuenschel, An experimental study of attenuation in fluid saturated porous media, compressional waves and interfacial waves, presented at the 43rd Annual Meeting of the Society of Exploration Geophysicists, 1973.

Winkler, K. and A. Nur, Attenuation and velocity in dry and water-saturated Massilon sandstone (abst.), Abstracts and Biographies, 48th Annual Meeting, Soc. Expl. Geophys., p. 40, 1978.

Wyllie, M.R.J., G.H.F. Gardner, and A.R. Gregory, Studies of elastic wave attenuation in porous media, Geophysics, 27, 569-589, 1962.

Yamakawa, N., Scattering and attenuation of elastic waves, Geophysical Magazine (Tokyo), 31, 63-103, 1962.

Zamanek, J., Jr., and I. Rudnick, Attenuation and dispersion of elastic waves in a cylindrical bar, J. Acoust. Soc. Am.,33 1283-1288, 1961.

Table 1. Sample Parameters

	Total Porosity %	Permeability md	Grain Diameter	ρbulk g/cm^3	ρgrain g/cm^3
Berea Sandstone	18.4	75	0.10	2.137	2.620
Navajo Sandstone	16.4	100	0.15	2.189	2.620
Bedford Limestone	11.9	1	0.75	2.335	2.652
Esopus Shale	-	-	-	2.606	-
Colorado Oil Shale	-	-	-	2.004	-
Ammonia Tanks Tuff	5.8	-	1-2	2.314	2.457
Tunnel Beds Tuff	29.6	-	2-5	1.607	2.283

FIGURE CAPTIONS

Fig. 1a. Attenuation characteristics of P waves in the dry Navajo sandstone at two confining pressures, P_c = 45 and 300 bars (P_f = 0). Left: Pulse shapes in the sandstone. Middle: Normalized Fourier amplitude as a function of frequency for the rock (solid line) and aluminum standard (dashed line). Right: Natural logarithm of the aluminum (A1) to rock (A2) amplitude ratios as a function of frequency. Points are actual ratios and the dashed line is the linear fit to the data. The slope of this line is proportional to 1/Q.

Fig. 1b. Attenuation characteristics of S waves in the dry Navajo sandstone. See Fig. 1a for explanations.

Fig. 2. Linear strain as a function of hydrostatic confining pressure in the Berea sandstone. Loading and unloading paths are denoted by the arrows.

Fig. 3. Linear strain as a function of hydrostatic confining pressure in the Bedford limestone for two successive pressure cycles.

Fig. 4. Compressional (P) and shear (S) wave velocities for the dry (open symbols) and water saturated (solid symbols) Berea sandstone as a function of differential pressure. As with the following plots of velocity, the errors are within the size of the symbols and thus no error bars are drawn. These velocities are used for the Q calculations.

Fig. 5. Q values of P and S waves as a function of confining pressure in the dry Berea sandstone ($P_f = 0$). In this and later plots of Q, representative error bars are shown.

Fig. 6. Q values of P and S waves as a function of differential pressure in the saturated Berea sandstone ($P_f = 0.465$ Pc).

Fig. 7. Q values of P and S waves of a function of confining pressure in the partially saturated Berea sandstone ($P_f = 0$).

Fig. 8. P and S wave velocities as a function of fluid pressure and calculated gas saturation for the gas release experiment in the Berea sandstone. The dashed line represents the theoretically calculated P wave velocity for a fully saturated rock. The differential pressure is 200 bars.

Fig. 9. Q values of P and S waves as a function of fluid pressure and calculated gas saturation in the Berea sandstone ($P_d = 200$ bars).

Fig. 10. P and S wave velocities as a function of differential pressure in the dry and saturated Navajo sandstone.

Fig. 11. Q values of P and S waves as a function of confining pressure in the dry Navajo sandstone ($P_f = 0$).

Fig. 12. Q values of P and S waves as a function of differential pressure in the saturated Navajo sandstone ($P_f = 0.465\ P_c$).

Fig. 13. P and S wave velocities as a function of differential pressure in the dry and saturated Bedford limestone. The unloading path is denoted by the dashed lines.

Fig. 14. Q values of P and S waves as a function of confining pressure in the dry Bedford limestone ($P_f = 0$). The unloading path for the P wave is denoted by the dashed line.

Fig. 15. Q values of P and S waves as a function of differential pressure in the saturated Bedford limestone ($P_f = 0.465\ P_c$). Unloading paths are denoted by dashed lines.

Fig. 16. P and S wave velocities as a function of confining pressure in the saturated Esopus shale ($P_f = 0$). The sample was held at 1000 bars for 16 hours resulting in the velocity increase due to pore pressure equilibration. Dashed lines denote unloading paths.

Fig. 17. Q values of P and S waves as a function of confining pressure in the saturated Esopus shale ($P_f = 0$). Dashed lines denote unloading paths.

Fig. 18. P and S wave velocities as a function of confining pressure in the Colorado Oil Shale ($P_f = 0$) for the directions perpendicular and parallel to the bedding planes.

Fig. 19. Q values of P and S waves as a function of confining pressure in the Colorado Oil Shale ($P_f = 0$) for directions perpendicular and parallel to the bedding planes.

Fig. 20. P and S wave velocities as a function of confining pressure for the dry Ammonia Tanks tuff ($P_f = 0$).

Fig. 21. Q values of P and S waves as a function of confining pressure in the dry Ammonia Tanks tuff ($P_f = 0$).

Fig. 22. P and S wave velocities as a function of confining pressure in the dry Tunnel Beds tuff ($P_f = 0$). Dashed lines denote unloading paths.

Fig. 23. Q values of P and S waves is a function of confining pressure in the dry Tunnel Beds tuff ($P_f = 0$). Dashed lines denote unloading paths.

Dry Navajo Sandstone - P wave

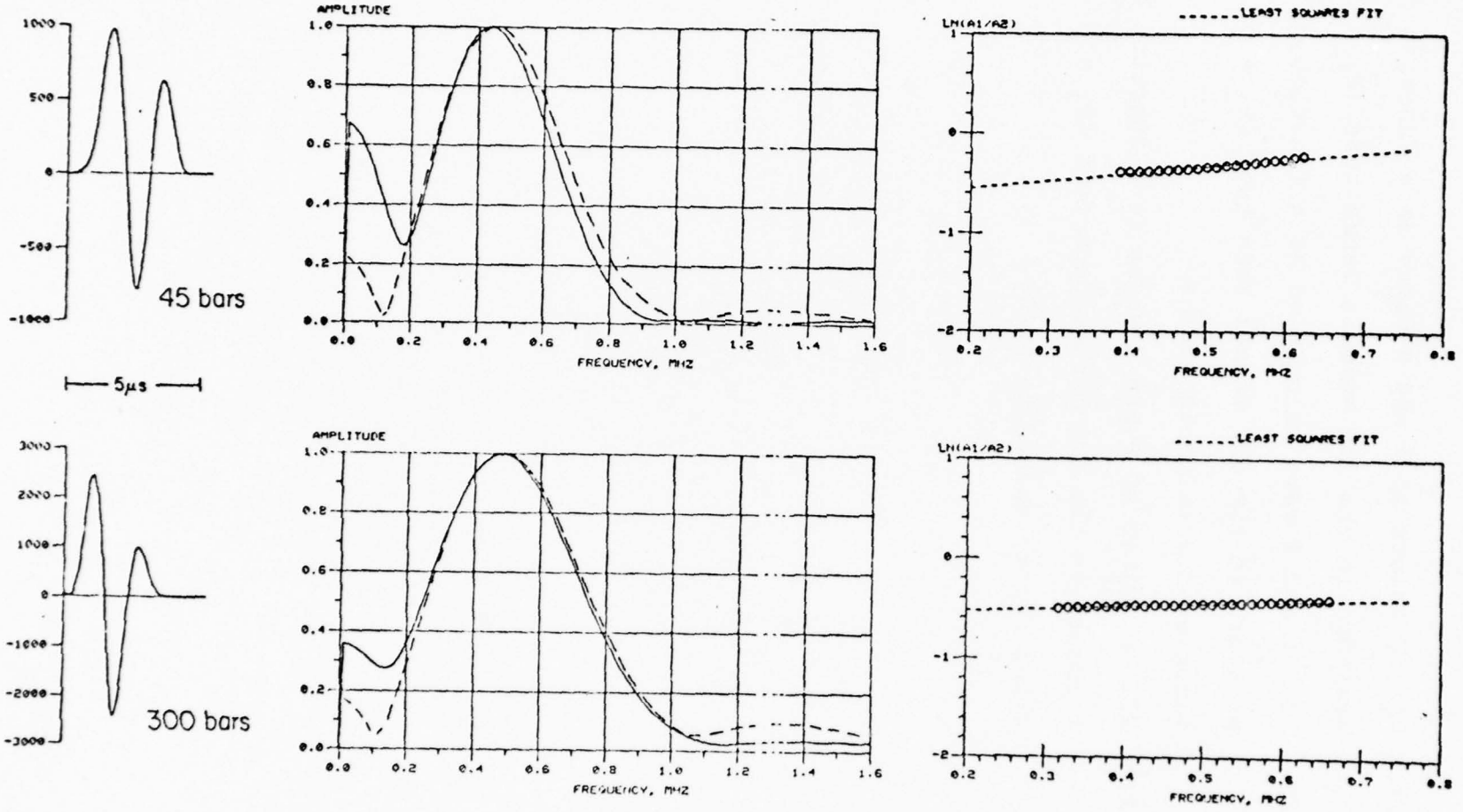

Figure 1a

Dry Navajo Sandstone - S wave

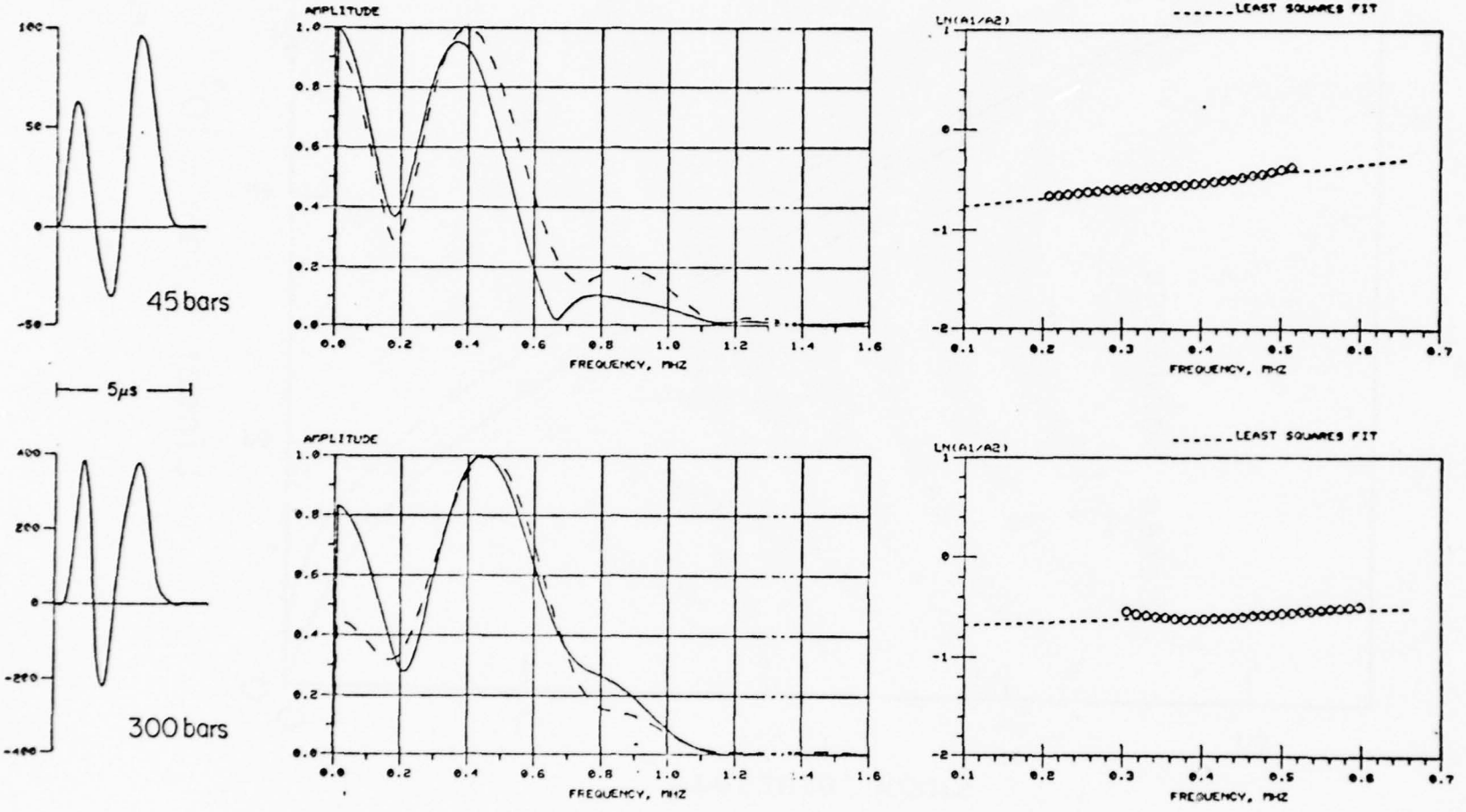

Figure 1b

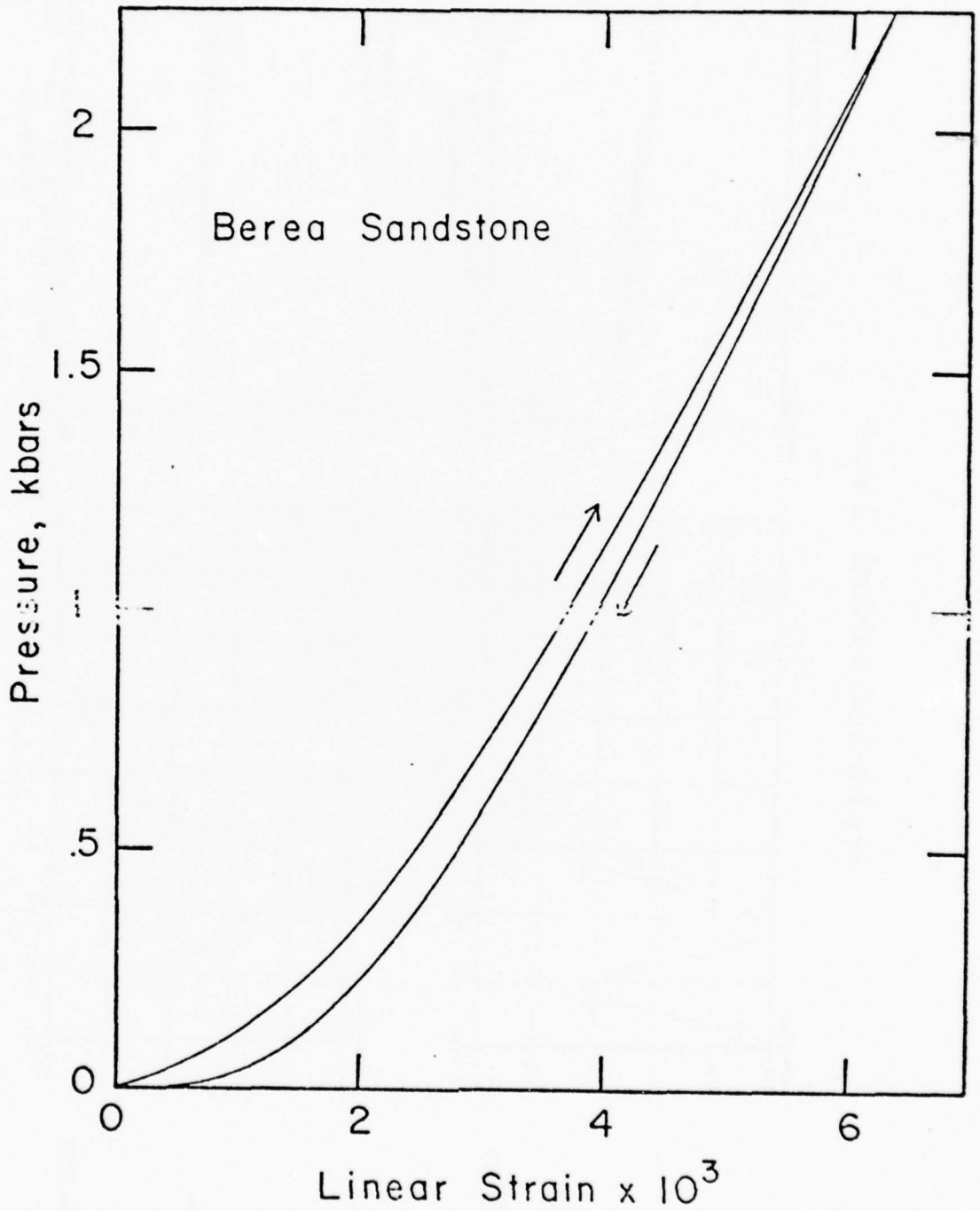
Berea Sandstone
Pressure, kbars
2
1.5
.5
0
0
2
4
6
Linear Strain x 10^3

Figure 2

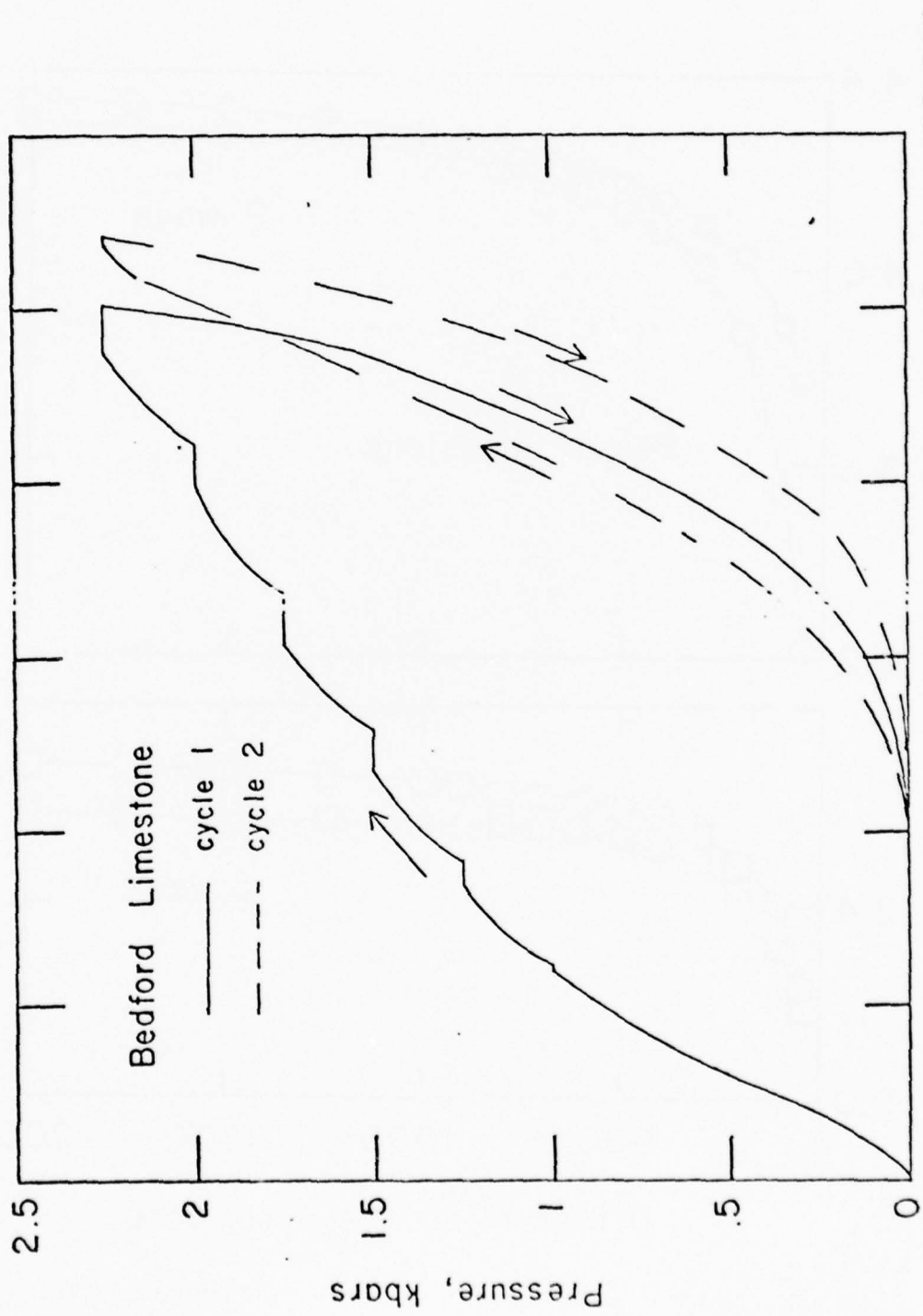
Bedford Limestone
cycle 1
cycle 2
Pressure, kbars
2.5
2
1.5
1
.5
0
0
2
4
6
8
10
12(1.2%)
Linear Strain x 10^3

Figure 3

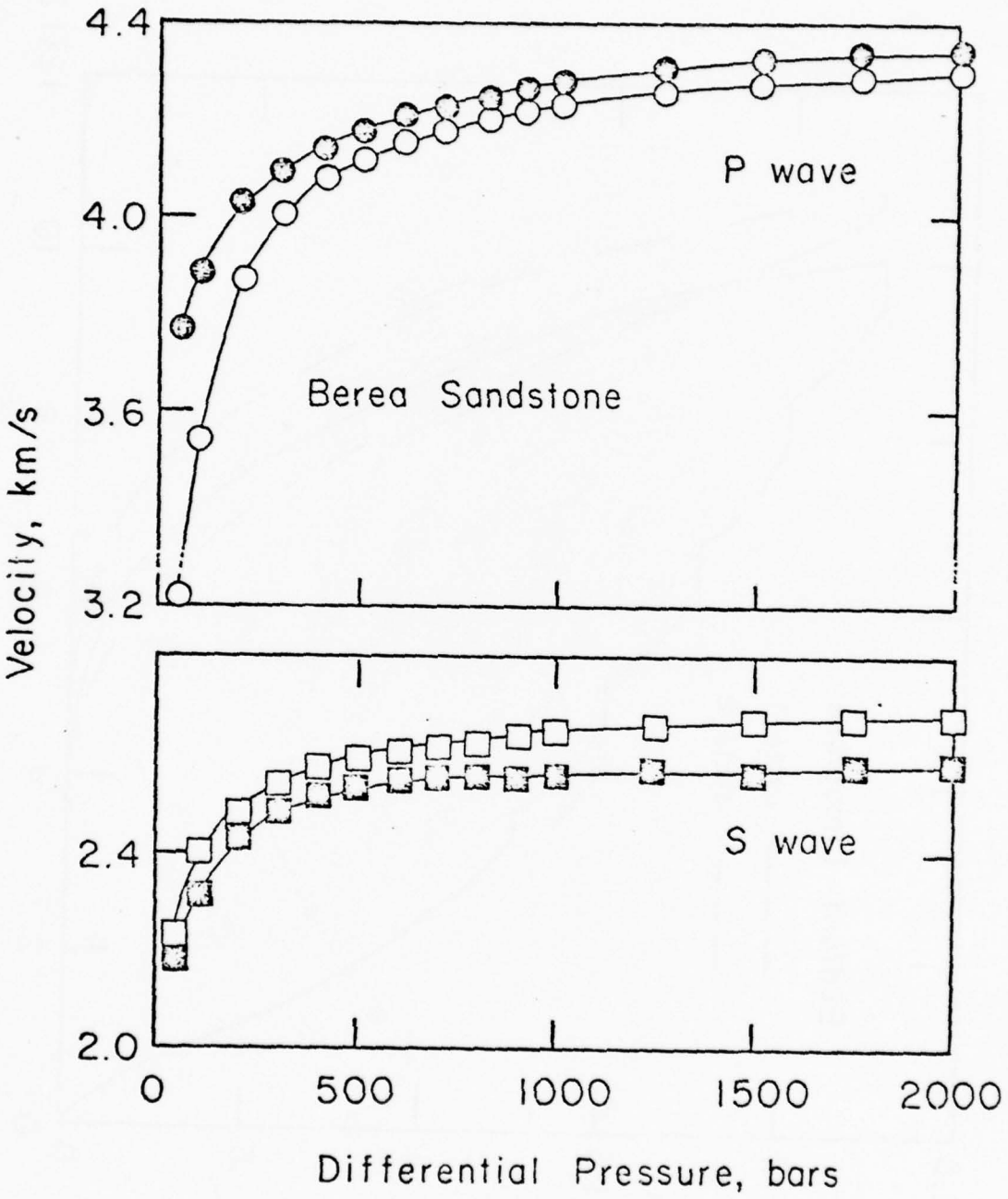
4.4
4.0
3.6
3.2
P wave
Berea Sandstone
Velocity, km/s
2.4
2.0
S wave
0
500
1000
1500
2000
Differential Pressure, bars

Figure 4

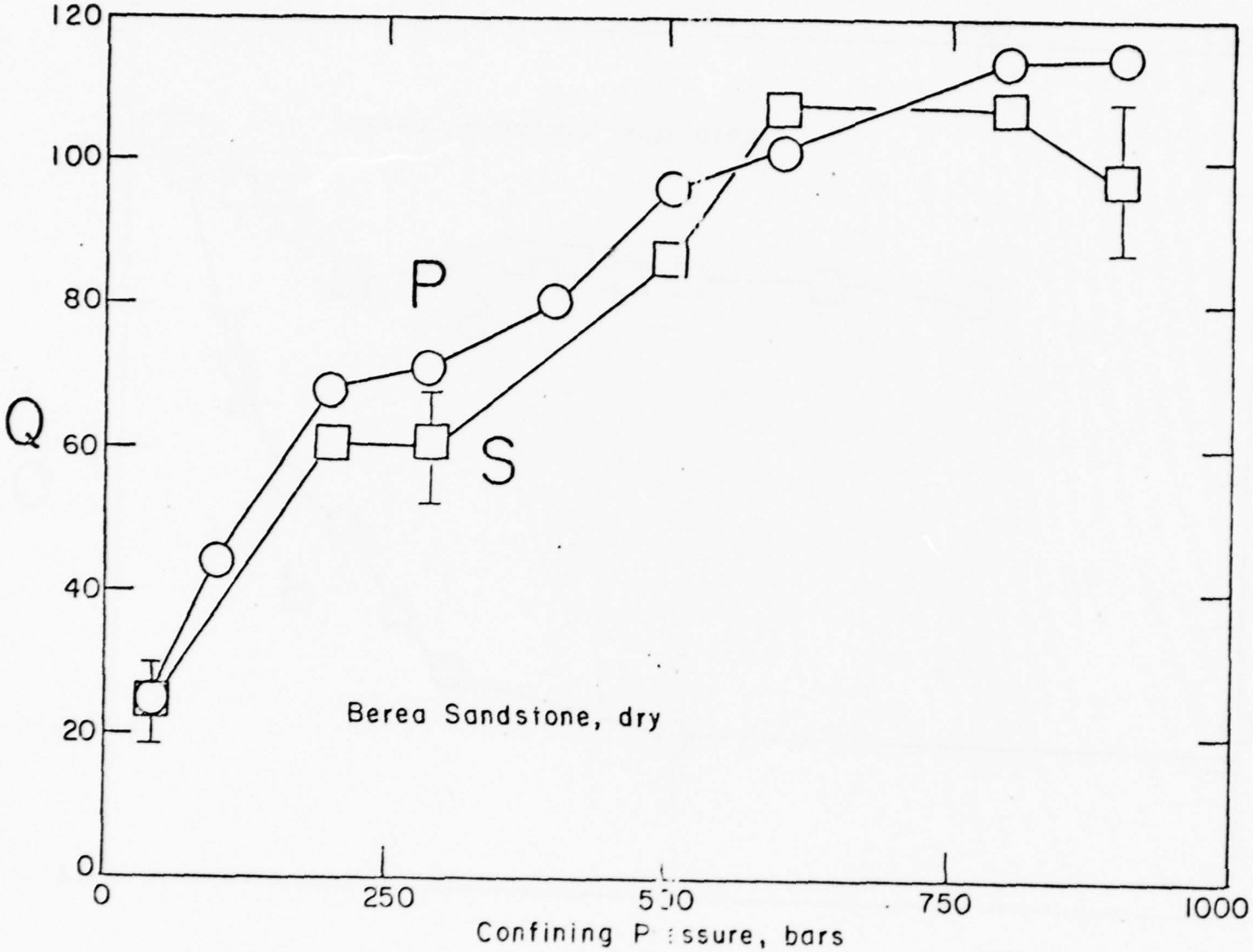
120
100
80
60
40
20
0
Q
P
S
Berea Sandstone, dry
0
250
500
750
1000
Confining P ssure, bars

Figure 5

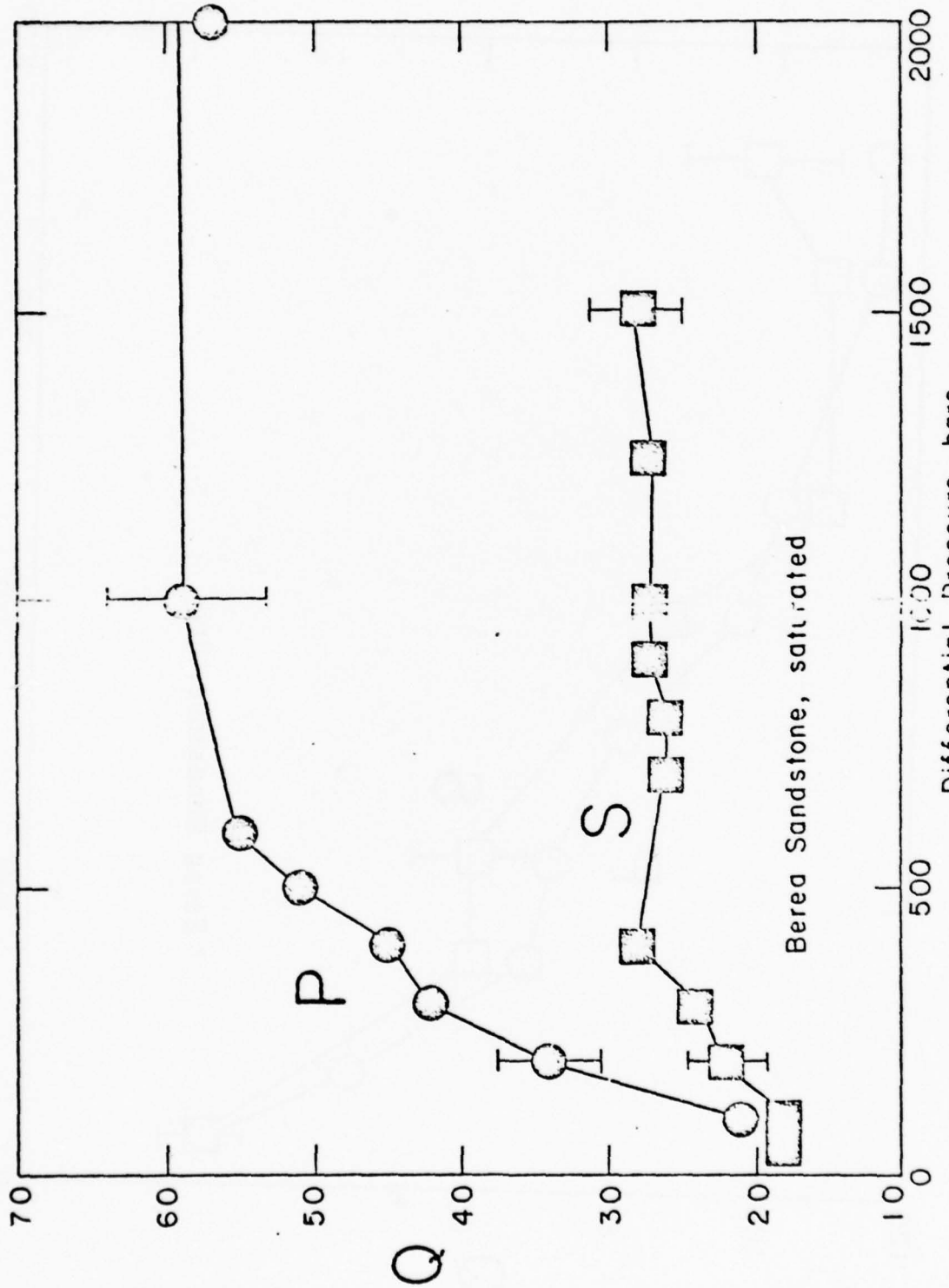
Q
70
60
50
40
30
20
10
0
500
1500
2000
P
S
Berea Sandstone, saturated
Differential Pressure, bars

Figure 6

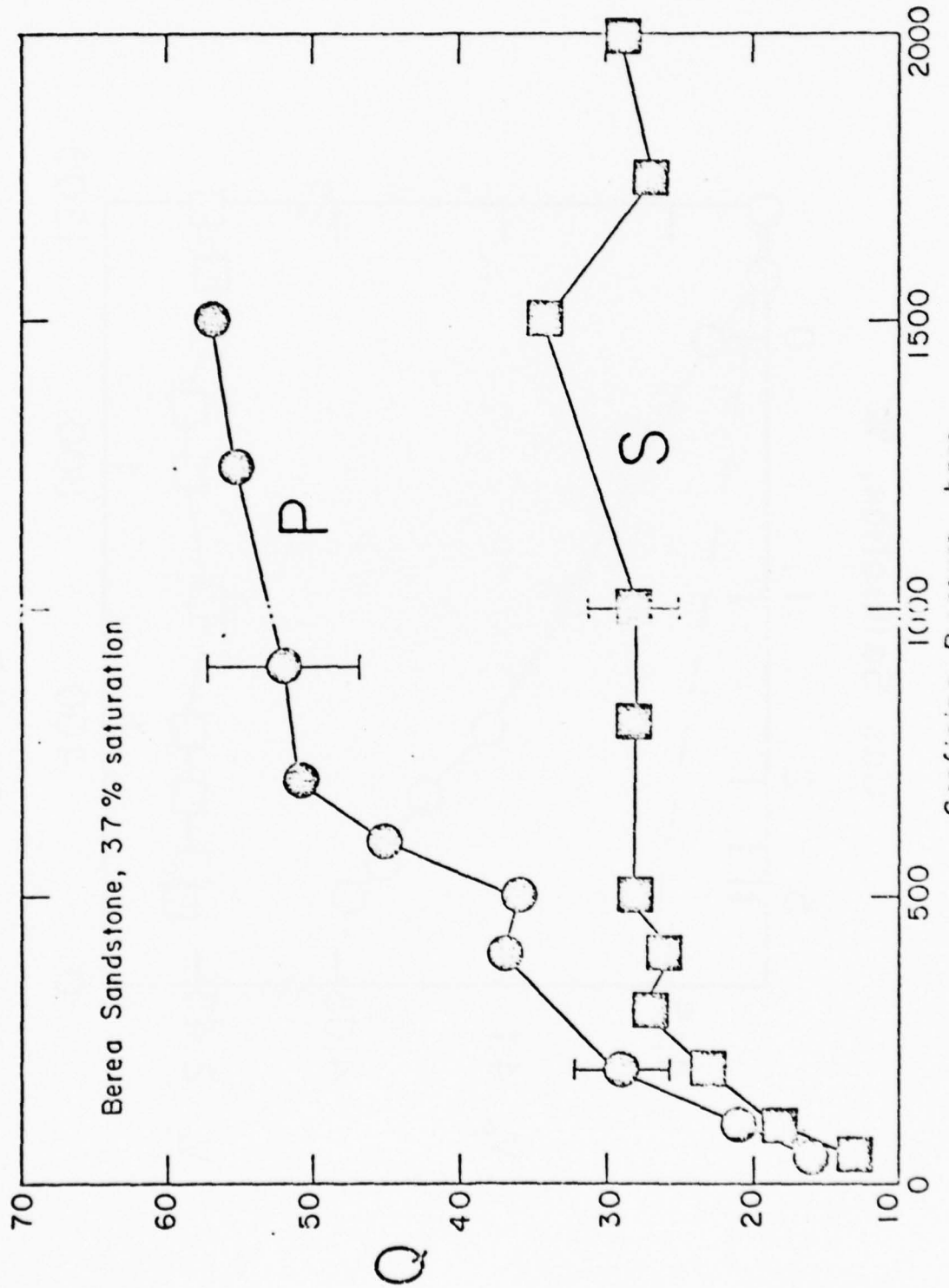
Berea Sandstone, 37% saturation
P
S
Q
70
60
50
40
30
20
10
0
500
1000
1500
2000
Confining Pressure, bars

Figure 7

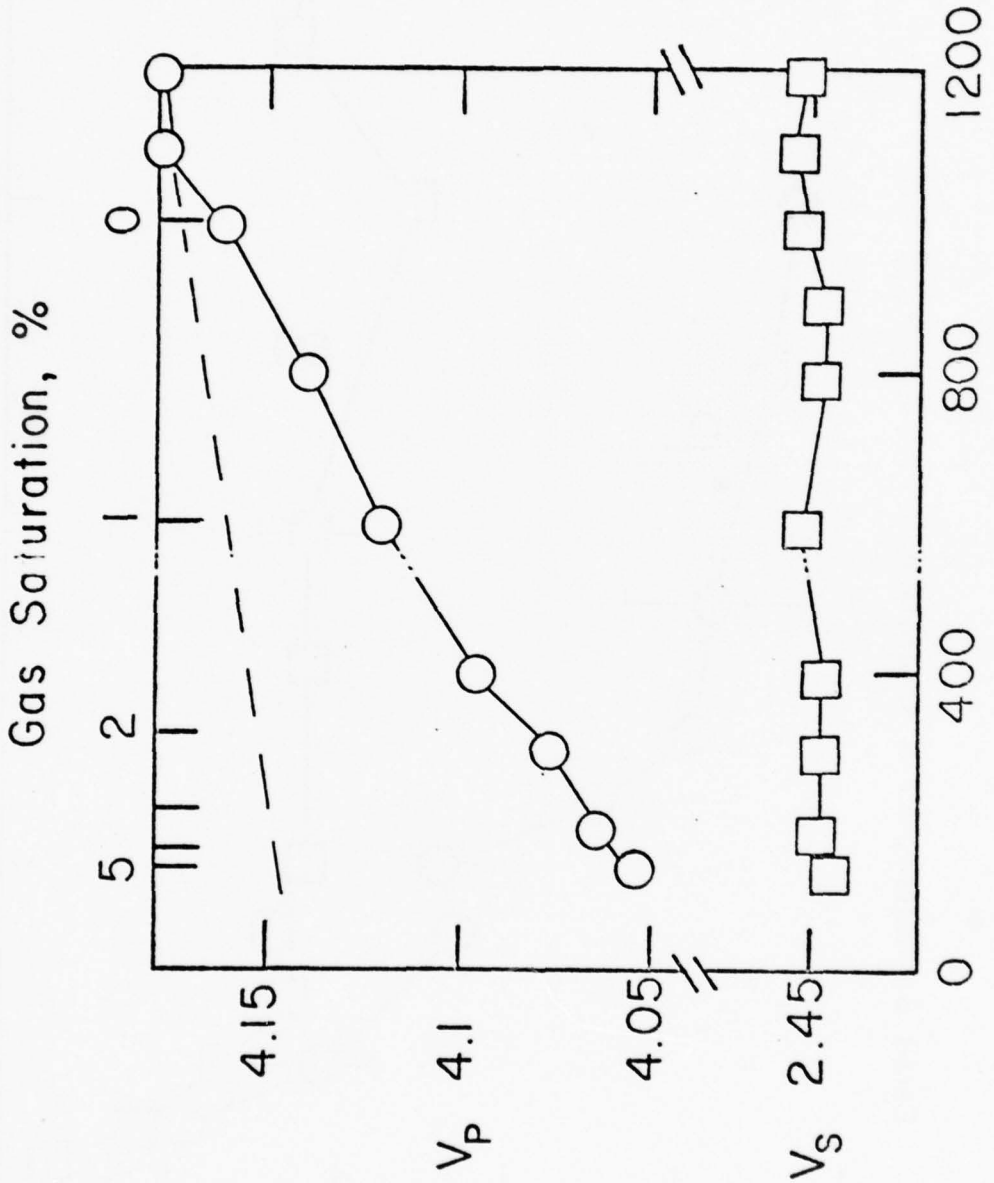
Gas Saturation, %
0
1
2
5
4.15
4.1
4.05
V_P
2.45
V_S
0
400
800
1200
Fluid Pressure, bars

Figure 8

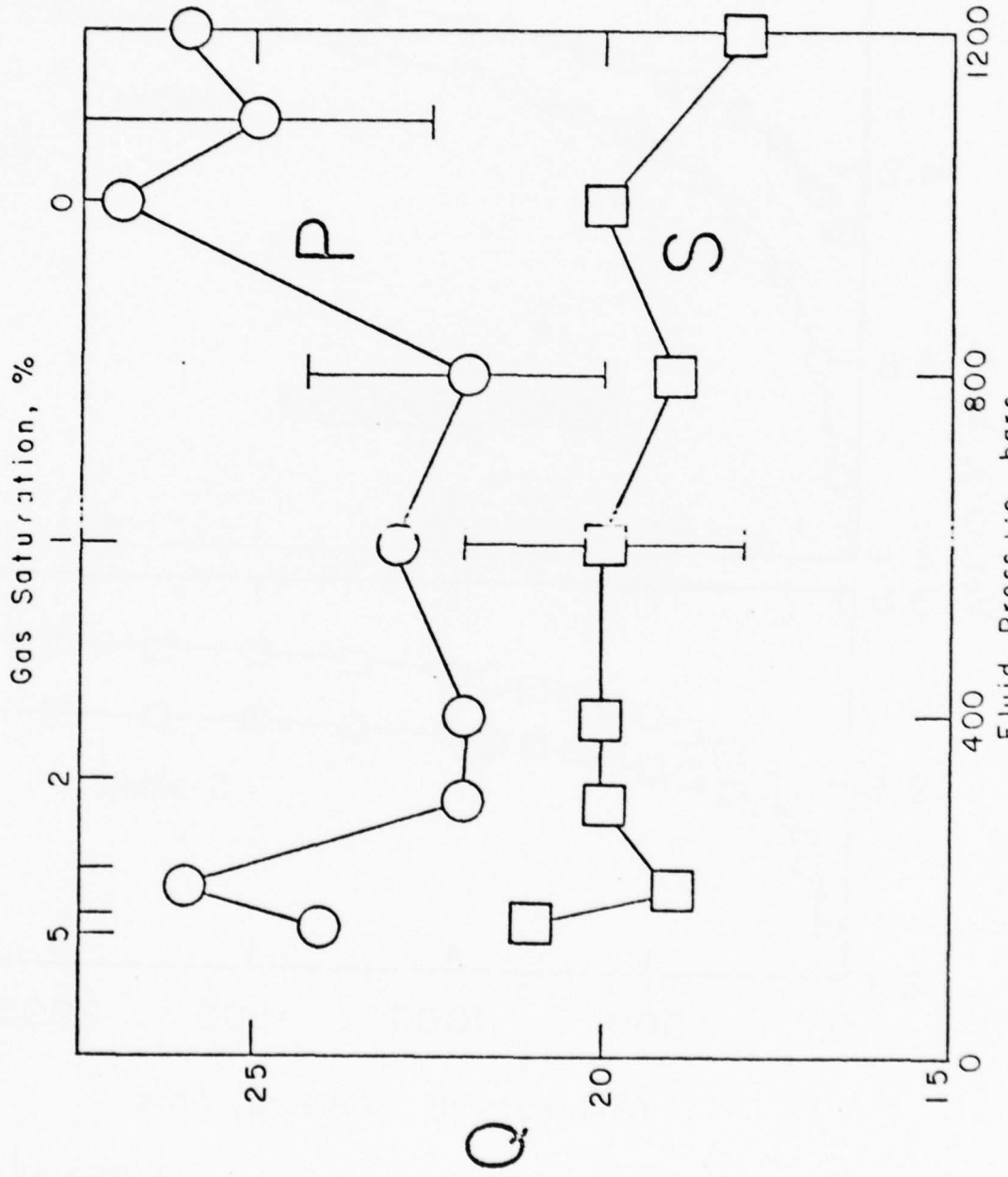
Gas Saturation, %
0
1
2
5
P
S
Q
25
20
15
0
400
800
1200
Fluid Pressure, bars

Figure 9

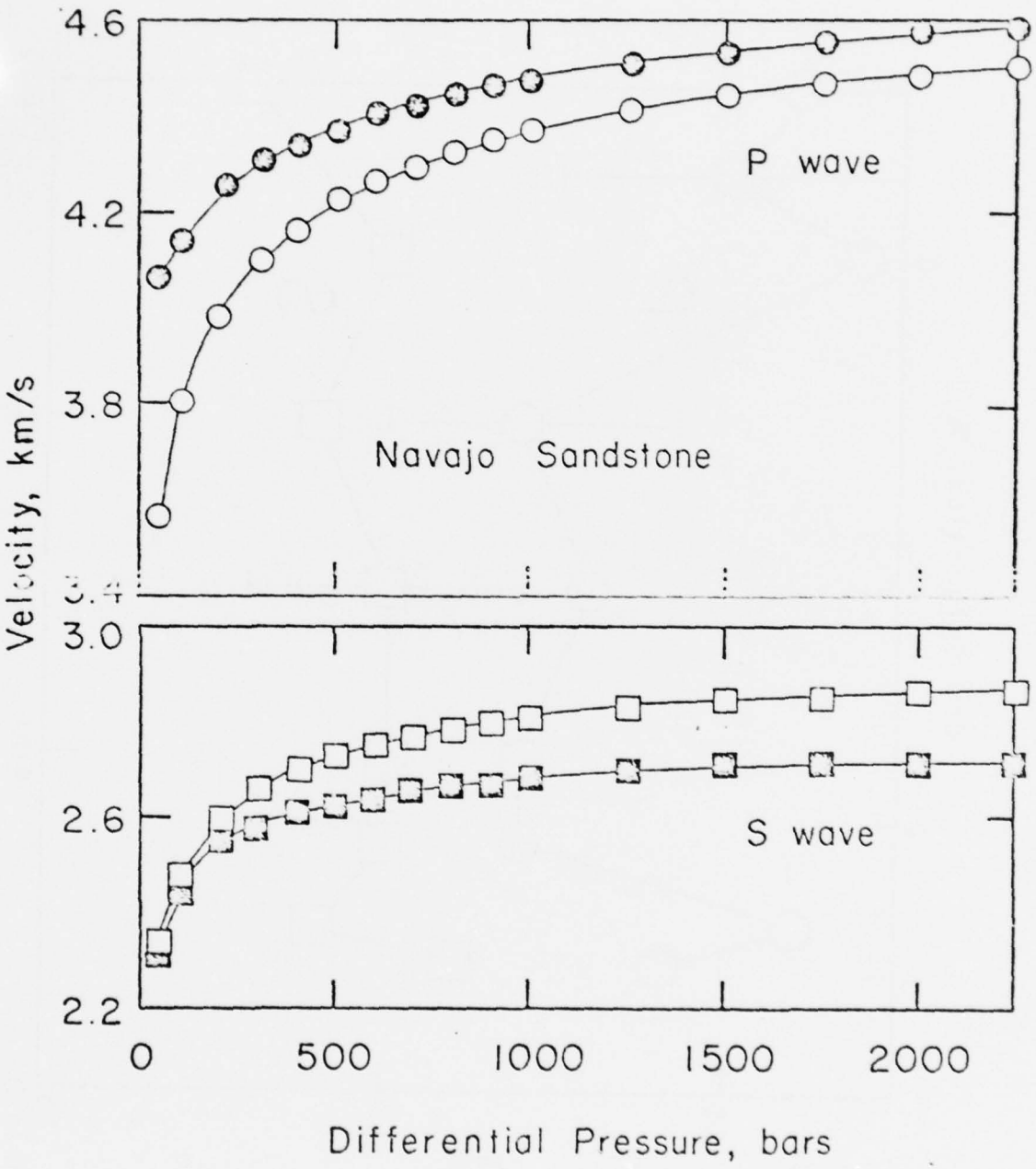
4.6
4.2
3.8
3.4
P wave
Navajo Sandstone
Velocity, km/s
3.0
2.6
2.2
S wave
0
500
1000
1500
2000
Differential Pressure, bars

Figure 10

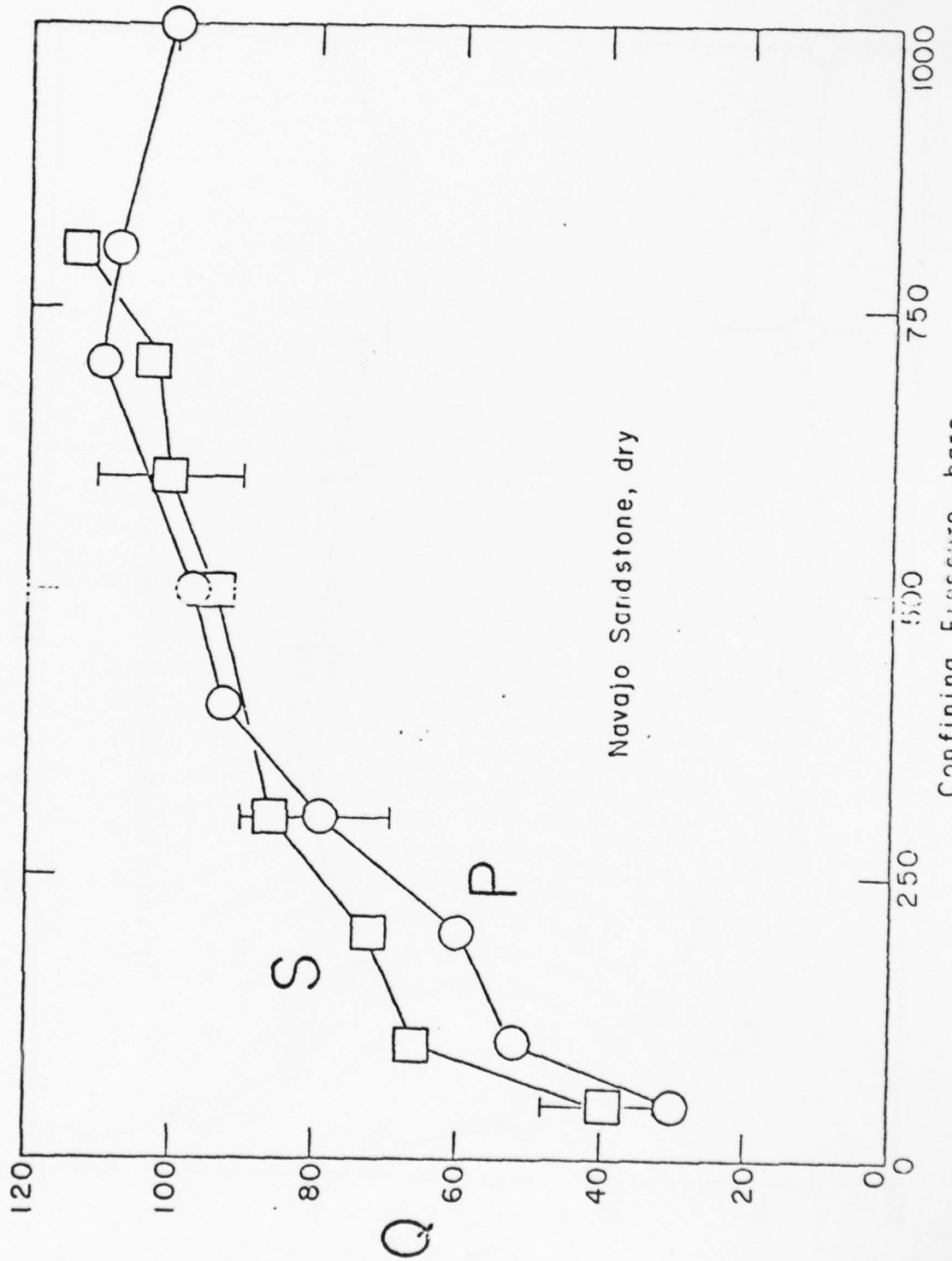
Q
120
100
80
60
40
20
0
0
250
500
750
1000
Confining Pressure, bars
Navajo Sandstone, dry
S
P

Figure 11

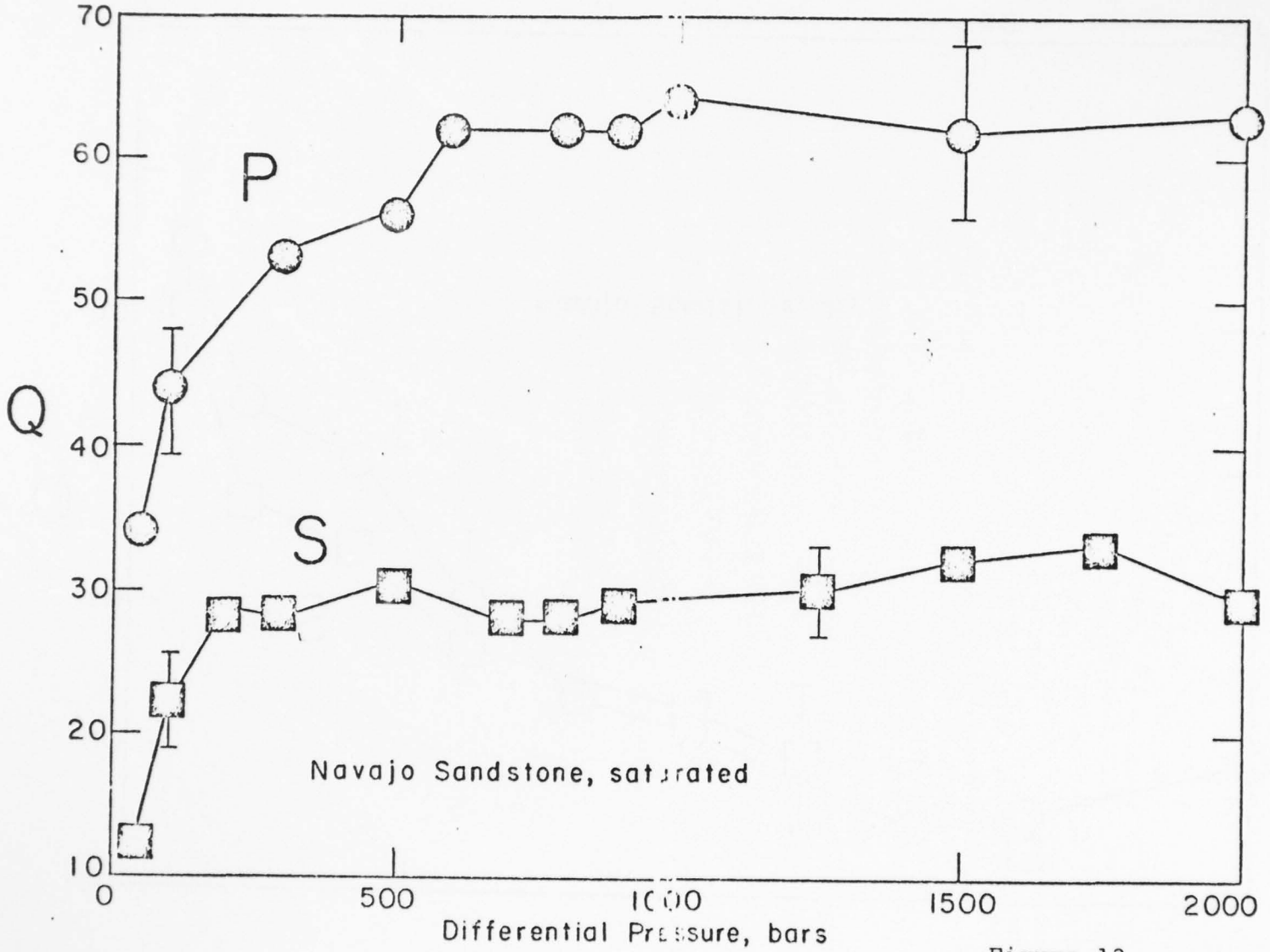
70
60
50
40
30
20
10
Q
P
S
Navajo Sandstone, saturated
0
500
1000
1500
2000
Differential Pressure, bars

Figure 12

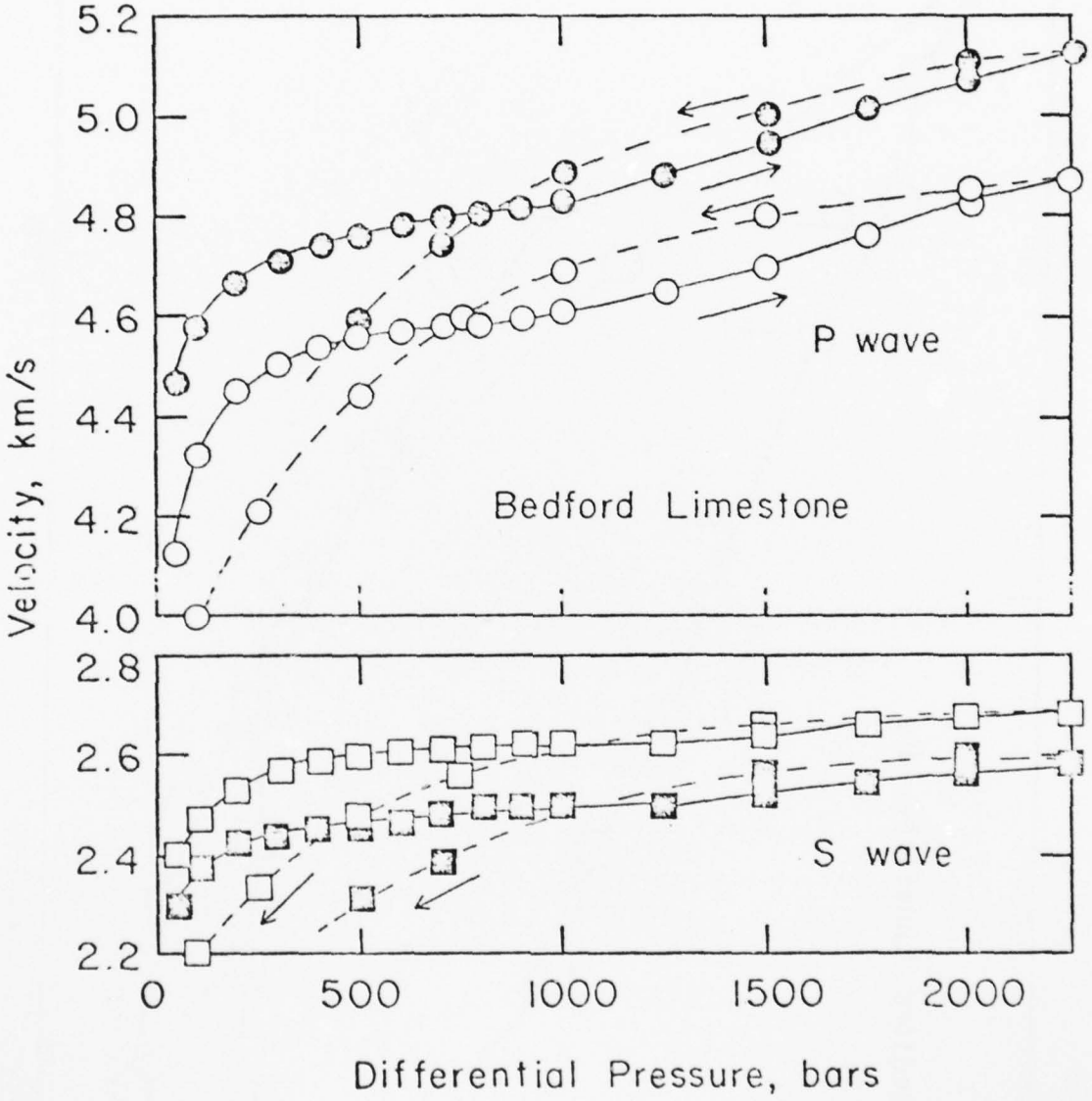
5.2
5.0
4.8
4.6
4.4
4.2
4.0
Velocity, km/s
P wave
Bedford Limestone
2.8
2.6
2.4
2.2
S wave
0
500
1000
1500
2000
Differential Pressure, bars

Figure 13

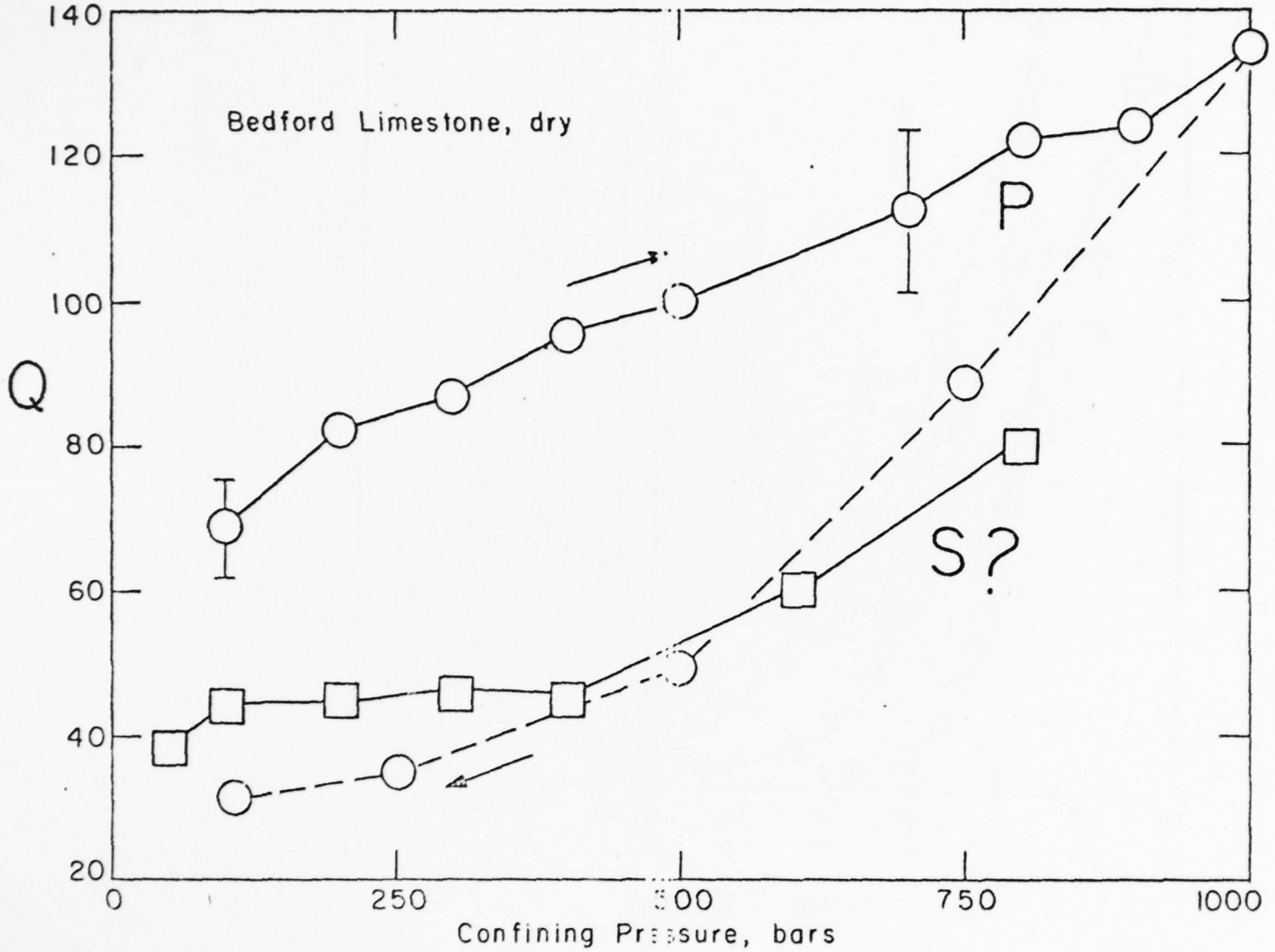
Bedford Limestone, dry
P
S?
Q
140
120
100
80
60
40
20
0
250
500
750
1000
Confining Pressure, bars

Figure 14

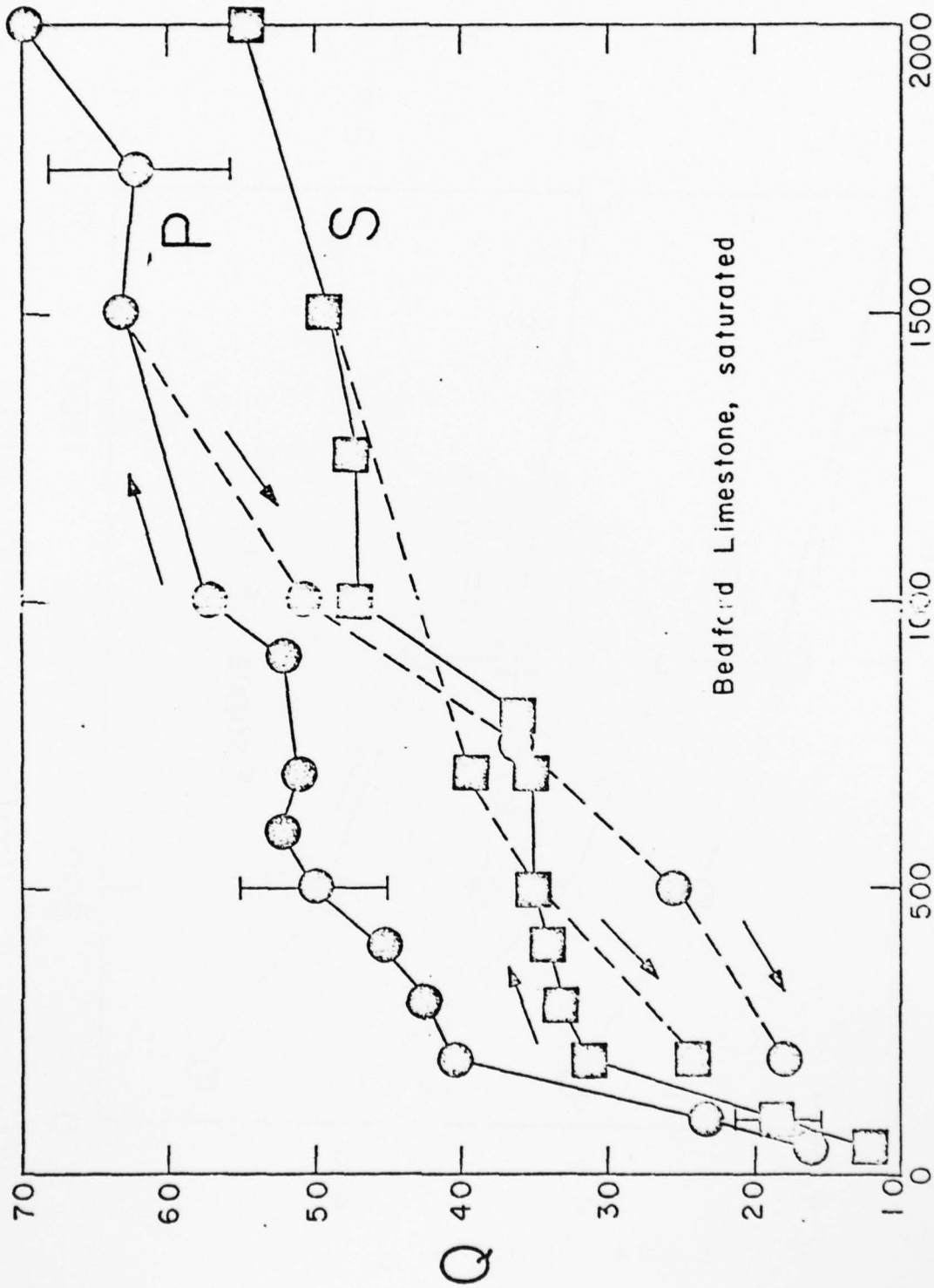
Q
70
60
50
40
30
20
10
0
500
1000
1500
2000
Differential Pressure, bars
Bedford Limestone, saturated
P
S

Figure 15

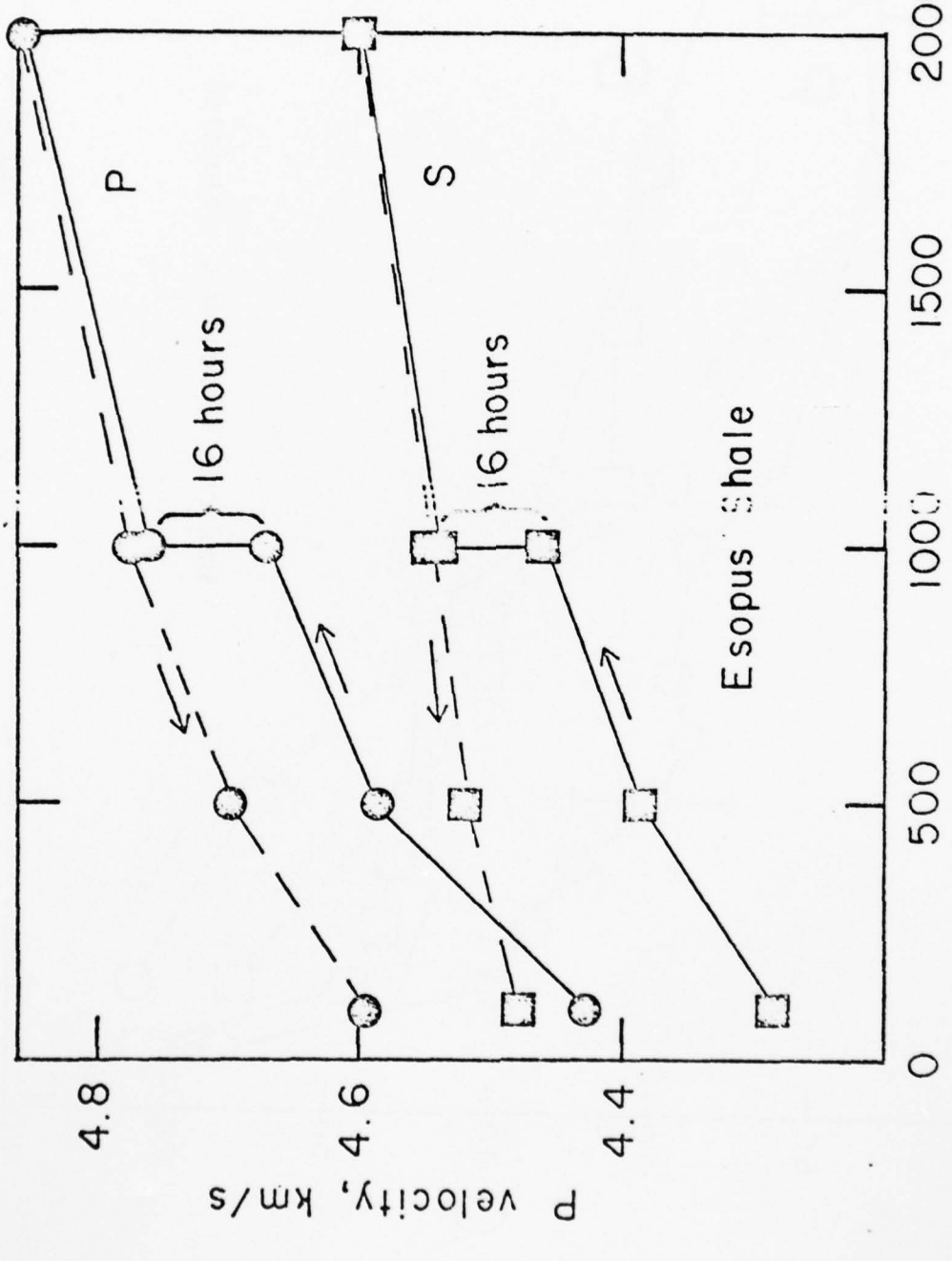
P velocity, km/s
4.8
4.6
4.4
S velocity, km/s
2.8
2.6
2.4
0
500
1000
1500
2000
Confining Pressure, bars
P
S
16 hours
16 hours
Esopus Shale

Figure 16

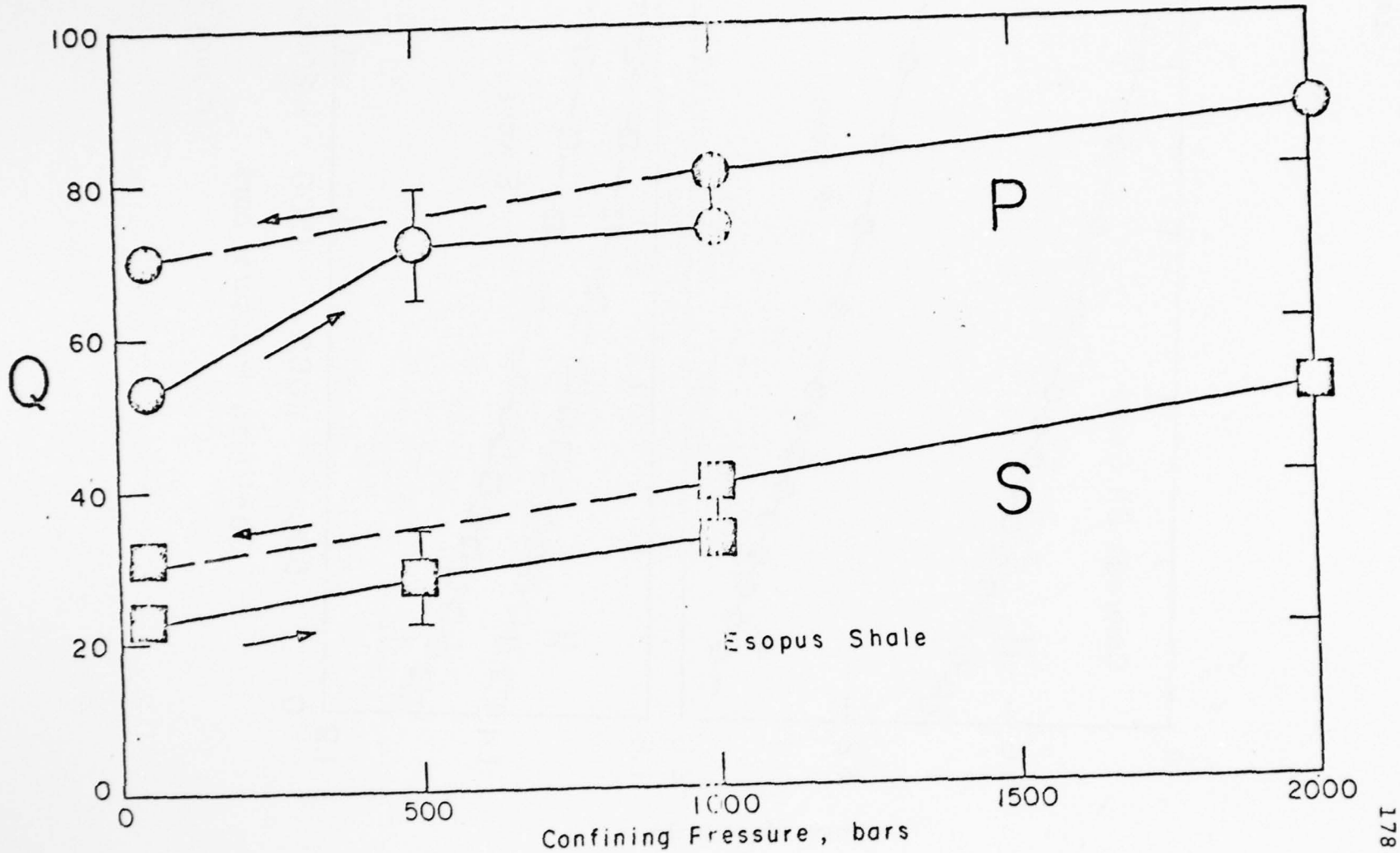
100
80
60
40
20
0
Q
P
S
Esopus Shale
0
500
1000
1500
2000
Confining Fressure, bars

Figure 17

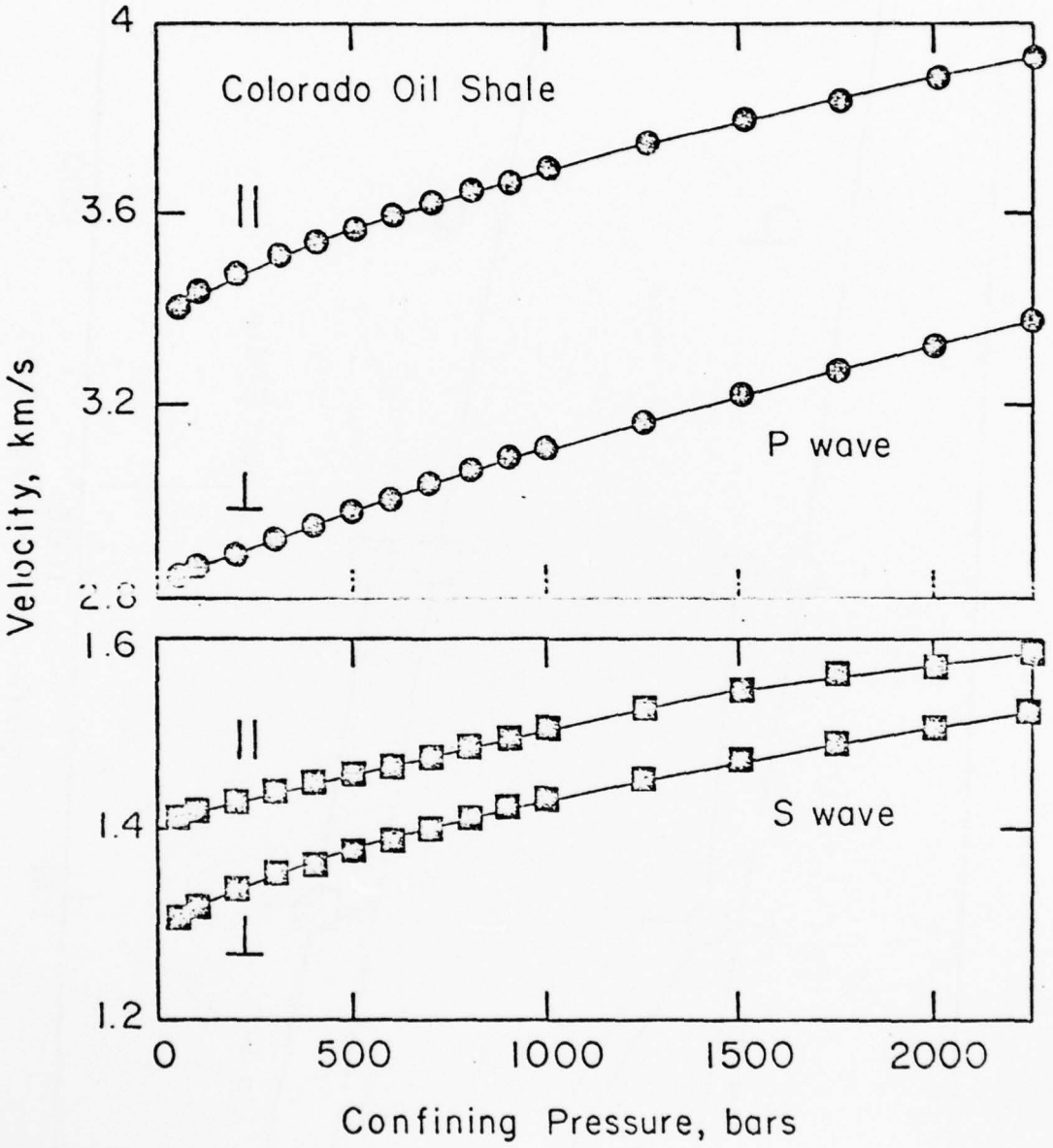
Colorado Oil Shale
P wave
S wave
Velocity, km/s
Confining Pressure, bars
4
3.6
3.2
1.6
1.4
1.2
0
500
1000
1500
2000

Figure 18

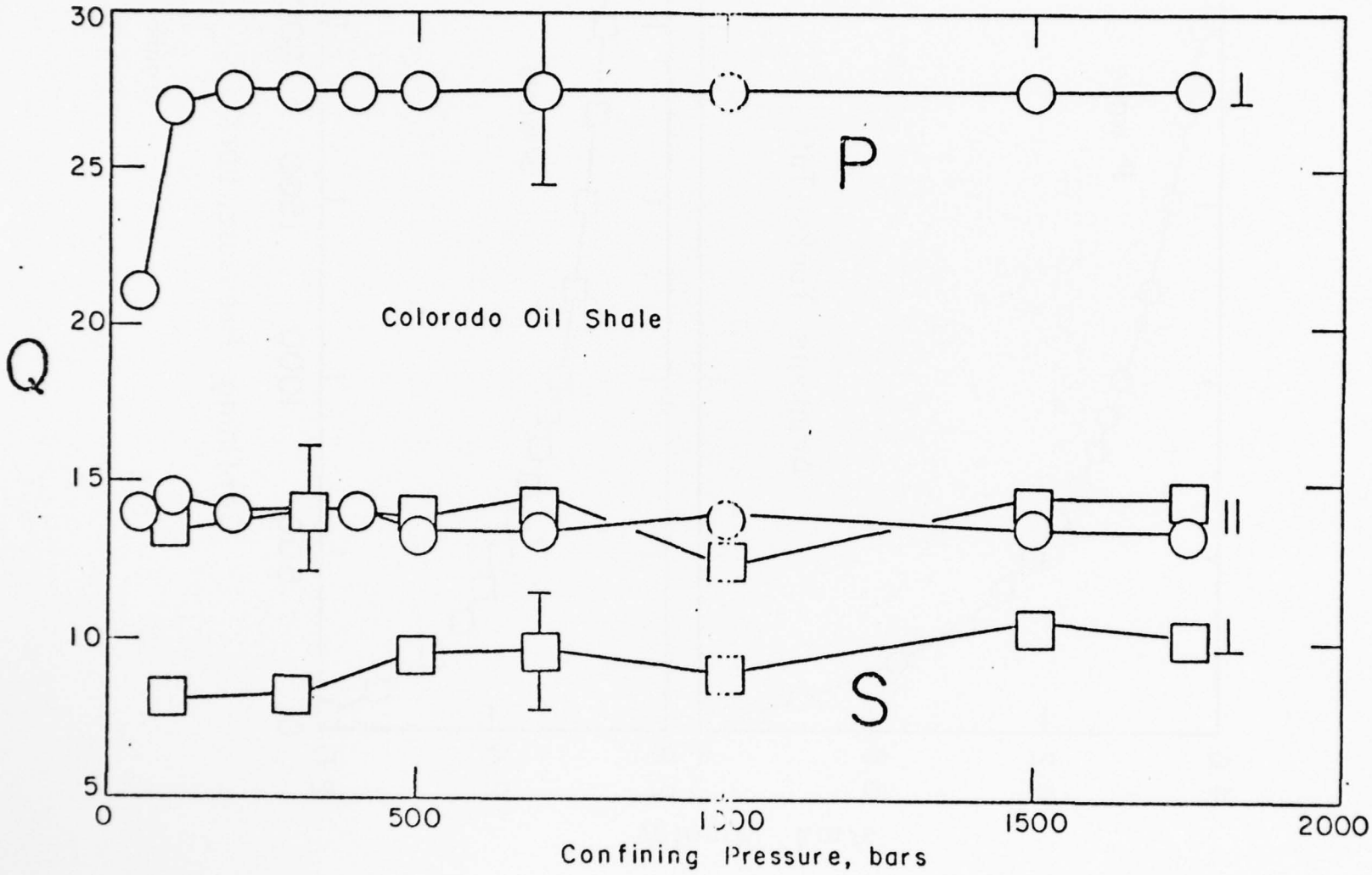
30
25
20
15
10
5
Q
P
⊥
Colorado Oil Shale
∥
S
⊥
0
500
1000
1500
2000
Confining Pressure, bars

Figure 19

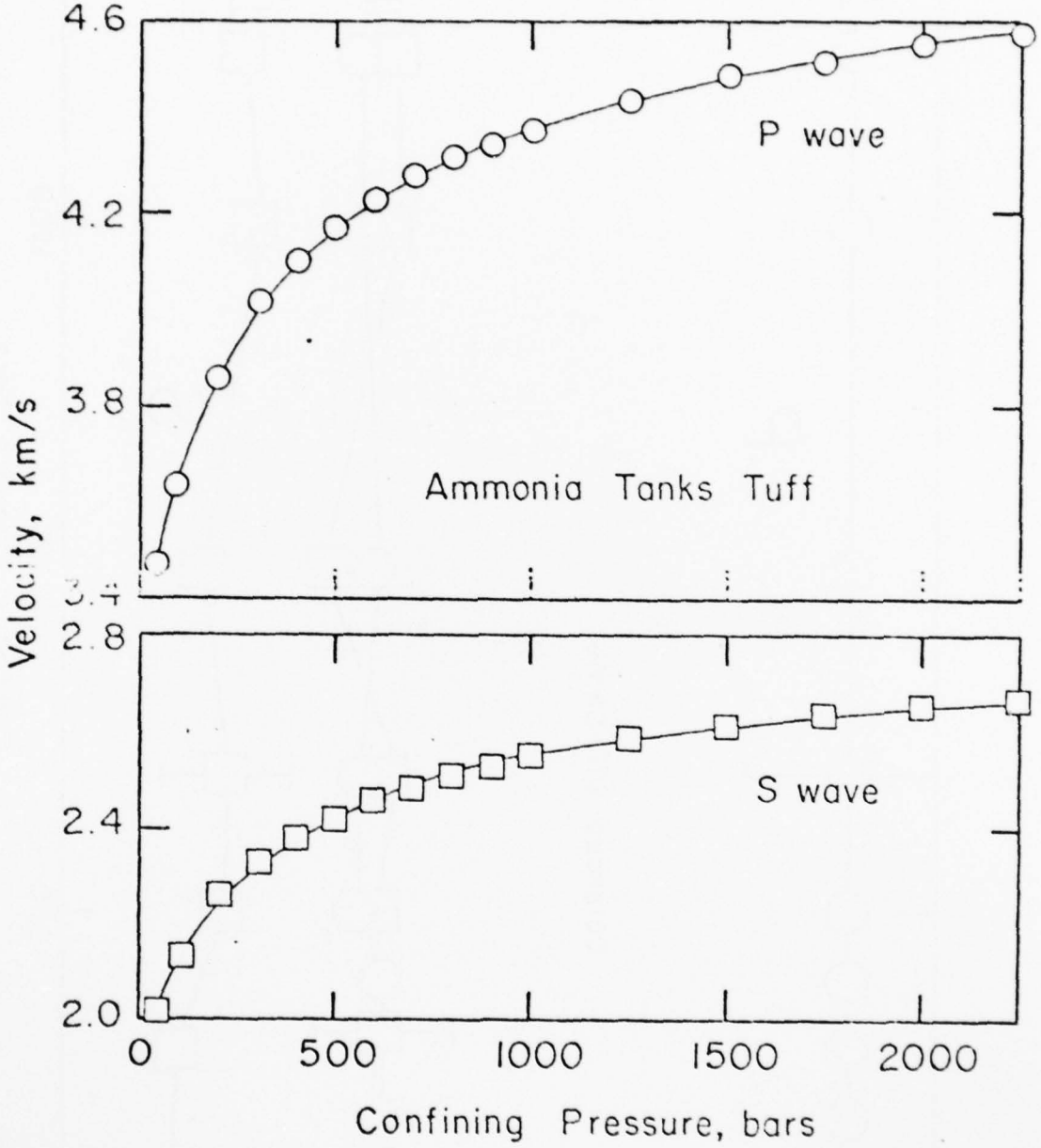
4.6
4.2
3.8
P wave
Ammonia Tanks Tuff
Velocity, km/s
2.8
2.4
2.0
S wave
0
500
1000
1500
2000
Confining Pressure, bars

Figure 20

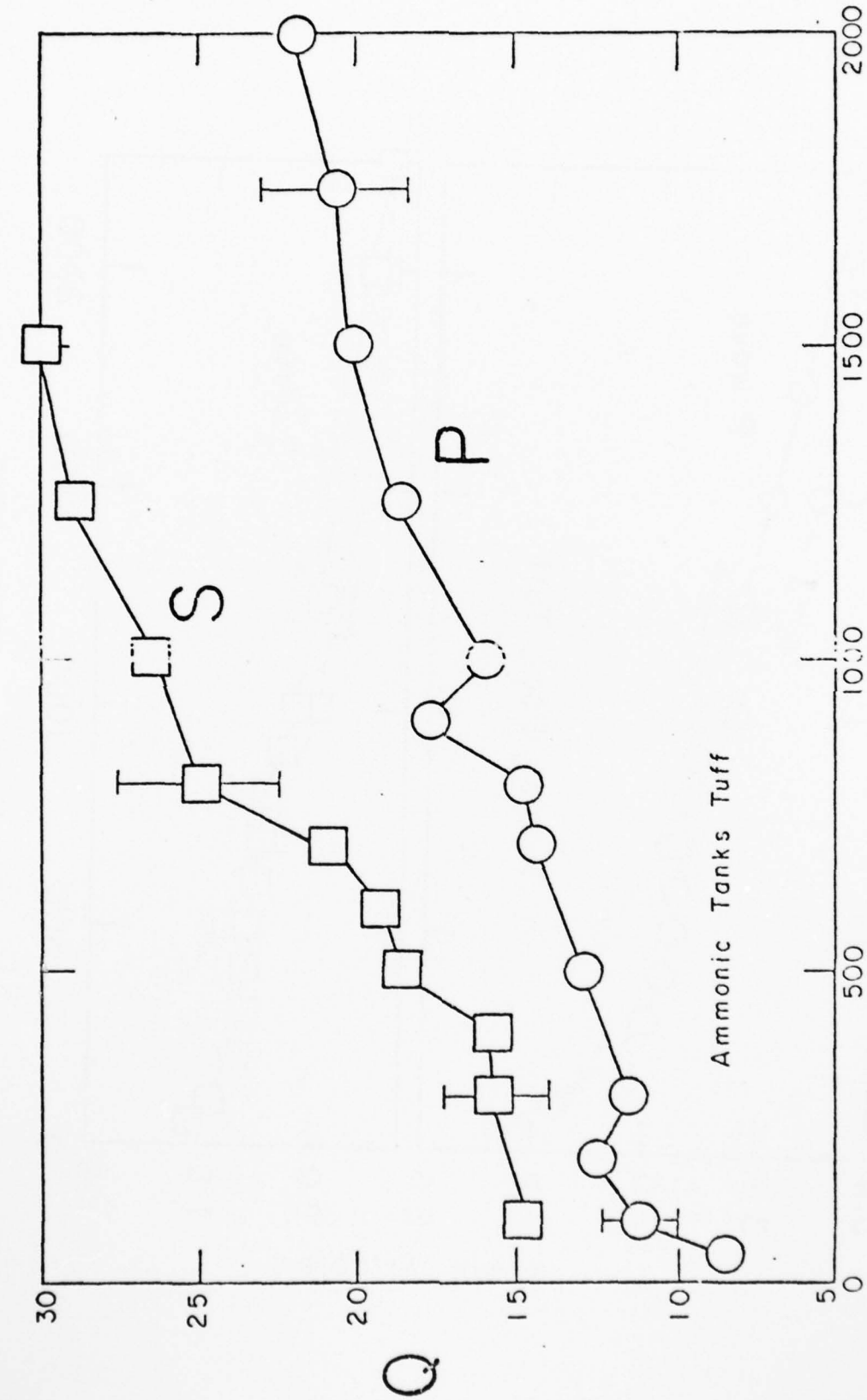
Q
30
25
20
15
10
5
0
500
1000
1500
2000
Confining Pressure, bars
Ammonic Tanks Tuff
S
P

Figure 21

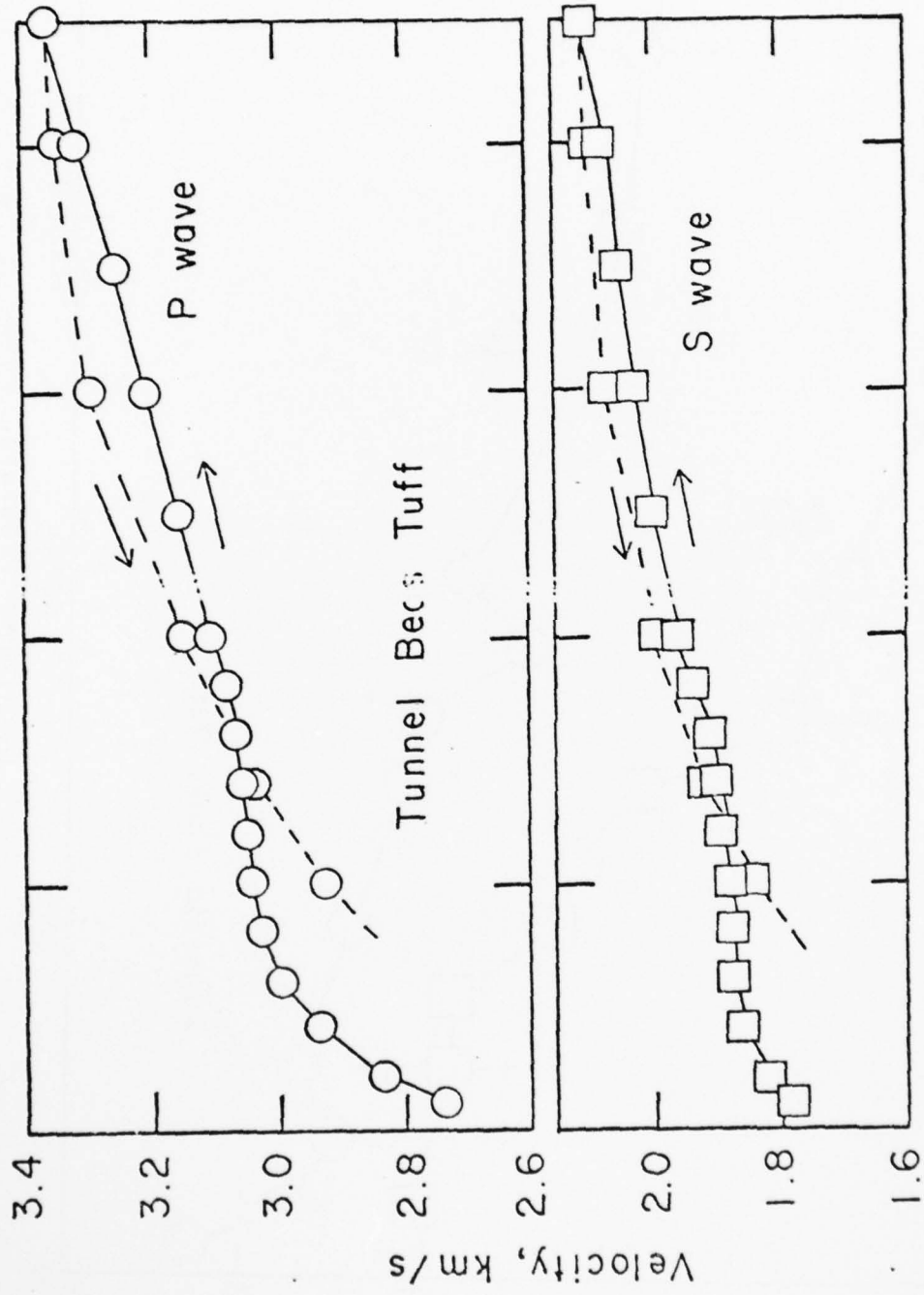
P wave
S wave
Tunnel Bed 3 Tuff
Velocity, km/s
3.4
3.2
3.0
2.8
2.6
2.0
1.8
1.6
0
500
1000
1500
2000
Confining Pressure, bars

Figure 22

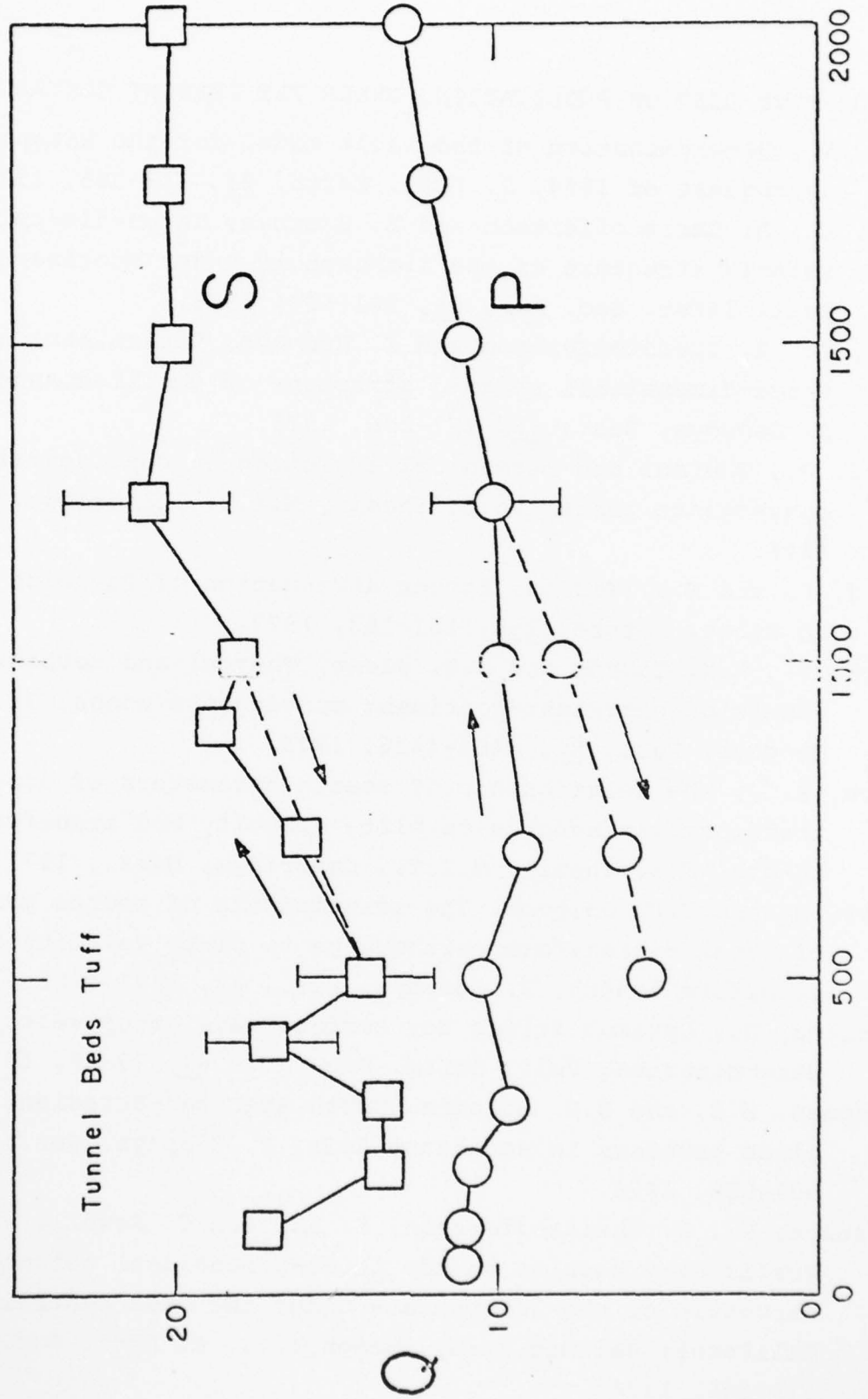
Tunnel Beds Tuff
S
P
Q
20
10
0
0
500
1000
1500
2000
Confining Pressure, bars

Figure 23

4. CUMULATIVE LIST OF PUBLICATIONS UNDER THE PRESENT CONTRACT

Abe, K., Re-examination of the fault model for the Niigata earthquake of 1964, J. Phys. Earth, 23, 349-366, 1975.

Aki, K., A. Christoffersson and E. Husebye, Three-dimensional seismic structure of the lithosphere under Montana LASA, Bull. Seism. Soc. Am., 66, 501-524, 1976.

Aki, K., A. Christoffersson and E. Husebye, Determination of the three-dimensional seismic structure of the lithosphere, J. Geophys. Res., 82, 277-296, 1977.

Bird, P., Thermal and mechanical evolution of continental convergence zones, Ph.D. Thesis, M.I.T., Cambridge, Mass., 1976.

Bird, P. and M.N. Toksöz, Strong attenuation of Rayleigh waves in Tibet, Nature, 266, 161-163, 1977.

Bird, P., M.N. Toksöz and N.H. Sleep, Thermal and mechanical models of continent-continent convergence zones, J. Geophys. Res., 80, 4405-4416, 1975.

Burr, N.C., The relationship of source parameters of oceanic transform earthquakes to plate velocity and transform length, M.S. Thesis, M.I.T., Cambridge, Mass., 1977.

Burr, N. and S.C. Solomon, The relationship of source parameters of oceanic transform earthquakes to plate velocity and transform length, J. Geophys. Res., 83, 1193-1205, 1978.

Canitez, N., Optimum filter for surface-wave group velocity determination, Bull. Seism. Soc. Am., 67, 79-85, 1977.

Chapman, M.E. and S.C. Solomon, North American-Eurasian plate boundary in northeast Asia, J. Geophys. Res., 81, 921-930, 1976.

Husebye, E., A. Christoffersson, K. Aki and C. Powell, Preliminary results on the three-dimensional seismic structure of the lithosphere under the USGS central California seismic array, Geophys. J. R. Astr. Soc., 46, 319-340, 1976.

Johnston, D.H., The attenuation of seismic waves in dry and saturated rocks, Ph.D. Thesis, M.I.T., Cambridge, Mass., 1978.

Johnston, D.H., M.N. Toksöz and A. Timur, Attenuation of seismic waves in dry and saturated rocks, II. Mechanisms, Geophysics, in press, 1979.

Johnston, D.H. and M.N. Toksöz, Thermal cracking and amplitude dependent attenuation, submitted to JGR, 1979.

Johnston, D.H. and M.N. Toksöz, Ultrasonic P and S wave attenuation in dry and saturated rocks under pressure, submitted to JGR, 1979.

Lee, W.B., Simultaneous inversion of surface wave phase velocity and attenuation for continental and oceanic paths, Ph.D. Thesis, M.I.T., Cambridge, Mass., 1977.

Lee, W.B. and S.C. Solomon, Inversion schemes for surface wave attenuation and Q in the crust and the mantle, Geophys. J. Roy. Astr. Soc., 43, 47-71, 1975.

Lee, W.B. and S.C. Solomon, Simultaneous inversion of surface wave phase velocity and attenuation: Love waves in western North America, J. Geophys. Res., 83, 3389-3400, 1978.

Lee, W.B. and S.C. Solomon, Simultaneous inversion of surface wave phase velocity and attenuation: Rayleigh and Love waves over continental and oceanic paths, Bull. Seism. Soc. Am., 69, 65-95, 1979.

Madariaga, R., Dynamics of an expanding circular fault, Bull. Seism. Soc. Am., 66, 639-666, 1976.

Patton, J.H., Source and propagation effects of Rayleigh waves from central Asian earthquakes, Ph.D. Thesis, M.I.T., Cambridge, Mass., 1978.

Sengupta, M.K. and B.R. Julian, P-wave travel times for deep earthquakes, Bull. Seism. Soc. Am., 66, 1555-1579, 1976.

Sengupta, M.K. and M.N. Toksöz, Three dimensional model of seismic velocity variation in the earth's mantle, Geophys. Res. Lett., 3, 84-86, 1976.

Sengupta, M.K. and M.N. Toksöz, The amplitudes of P waves and magnitude corrections for deep focus earthquakes, J. Geophys. Res., 82, 2971-2980, 1977.

Solomon, S.C., Geophysical constraints on radial and lateral temperature variations in the upper mantle, Am. Mineral., 61, 788-803, 1976.

Solomon, S.C. and K.T. Paw U, Elevation of the olivine-spinel transition in subducted lithosphere: seismic evidence, Phys. Earth Planet. Int., 11, 97-108, 1975.

Taylor, S.R., and M.N. Toksöz, Three-dimensional crust and upper mantle structure of the northeastern United States, submitted to JGR, 1978.

Toksöz, M.N., The subduction of the lithosphere, Sci. Amer., 233, 88-98, 1975.

Toksöz, M.N., E. Arpat and F. Saroglu, East Anatolian earthquake of 24 November 1976 - field observations, Nature, 270, 423-425, 1977.

Toksöz, M.N. and P. Bird, Formation and evolution of marginal basins and continental plateaus, in Island Arcs, Deep Sea Trenches and Back Arc Basins, eds. M. Talwani and W.C. Pitman III, Maurice Ewing Series, Vol. 1, 379-393, AGU, Washington, D.C., 1977.

Toksöz, M.N. and P. Bird, Modelling of temperatures in continental convergence zones, Tectonophysics, 41, 181-193, 1977.

Toksöz, M.N., J. Nabelek and E. Arpat, Source properties of the 1976 earthquake in E. Turkey: A comparison of field data and teleseismic results, Tectonophysics, 49, 199-205, 1978.

Ward, R.W. and K. Aki, Synthesis of teleseismic P waves from sources near sinking lithospheric slabs, Bull. Seism. Soc. Am., 65, 1667-1680, 1975.